POLYMERIC MICRONEEDLES FOR TRANSDERMAL DRUG DELIVERY

JASPREET SINGH KOCHHAR

NATIONAL UNIVERSITY OF SINGAPORE

2013

POLYMERIC MICRONEEDLES FOR TRANSDERMAL DRUG DELIVERY

JASPREET SINGH KOCHHAR

(B. Pharm., University of Delhi, India)

A THESIS SUBMITTED FOR THE DEGREE OF

DOCTOR OF PHILOSOPHY

DEPARTMENT OF PHARMACY

NATIONAL UNIVERSITY OF SINGAPORE

2013

Declaration

I hereby declare that this thesis is my original work and it has been written by me in its entirety. I have duly acknowledged all the sources of information which have been used in the thesis.

This thesis has also not been submitted for any degree in any university previously.

_____

Jaspreet Singh Kochhar

14 December 2013

Acknowledgements

I owe my subservience to The One, Primal, Omnipresent and Omniscient Lord, who manifested through various remarkable people, with whom I had an extraordinary time at NUS, filled with science, learning and fun. To these, I am forever grateful.

To my supervisor, Dr. Lifeng Kang for accepting me as his first graduate student. I'm grateful to you for exposing me to a new world, teaching me to be innovative and efficient, and being supportive always. I have learnt a lot from you and that has paved the tarmac for my career ahead.

To my co-supervisor, Prof. Sui Yung Chan, for being there to advise me whenever I needed, to help me improve my presentation skills and making me feel comfortable all this while that I have been away from home. You have impressed me with your ability to communicate optimism which has helped me grow both personally and professionally.

To the Department of Pharmacy at NUS, for providing me scholarship and this wonderful opportunity, to other faculty members who advised me and gave their insights at some point or the other.

To my lab mates, Jing Pan, Hairui Li and Sara Dana, with whom I spent numerous *fun-filled* hours at the lab.

To my mentees, who worked for their undergraduate and high school projects, each one of you was special and your questions made me think. You have made me a better teacher than I was before.

To other graduate students of our *Pharmily*, from whom I sought opinions on my research. Thank you for all your help.

To the lab-support and administrative staff of our *Pharmily*, my research wouldn't progress if not for your timely assistance.

To my best friend, Hardeep, who always encouraged me to think big.

To my wonderful parents, who sacrificed all their comforts and provided me with everything I wanted, so that I could pursue my goals. To my lovely brother, Pavneet, for guiding me on innumerable aspects of my life. To my other relatives, who helped whenever I had a need. I have got the most extraordinary family; you are the true abode of My Lord.

Finally am indebted to most amazing person of my life, Aparna, for being by my side for the past six years and sharing with me some really awesome times outside the lab. You put everything in perspective in my life.

To my grandfather, Prithipal Singh,

Without you I would be nothing today

Table of Contents

Summary

Transdermal drug delivery has gained importance in the past three decades, with several drugs being approved by FDA. Cosmetic science, has also gained prevalence with the development of novel molecules. However, the outermost layer of skin, *stratum corneum*, only allows the passage of molecules smaller than 500 Da to passively diffuse to the underlying vascular tissues. Molecules larger than this size, majorly proteins, peptides and vaccines have thus been delivered using painful injections, which significantly reduce compliance among users. Delivering these macromolecules through skin by reversibly modifying the permeability of stratum corneum is an attractive alternative. Techniques such as iontophoresis, ultrasound, laser and thermal ablation have been used to alter the membrane properties and enhance drug delivery. Concerns have been raised about the safety of these techniques and researchers have looked to develop safer alternatives. Microneedles are miniaturized needles supported on a flat base, intended to be applied on skin in a manner similar to transdermal patch, to create micron sized channels that enable the macromolecules to diffuse to the underlying vascular tissues for improved drug absorption. Previously, microneedles have been fabricated from silicon, metals, glass and various polymers. The needles from non-biodegradable materials pose biohazard concerns, as well as the risk of breakage in the skin. On the other hand polymeric needles developed previously utilized complex multi-step procedures involving long exposure to ultraviolet (UV) light, high temperature, vacuum, solvents and other strenuous procedures, which may compromise the stability of fragile protein molecules. Most of these methods require the preparation of reverse molds, which may interact with the drugs and affect drug stability.

In this thesis, a simple method of fabricating polymeric microneedles using a simple photolithographical approach, using short exposure to ultraviolet light, in a mold and solvent free process was developed. The influence of various parameters such as UV intensity, time of exposure, and distance from UV light source on microneedle geometry was evaluated. The process was capable of

controlling the microneedle length and tip diameter for specific control of drug delivery at various depths in the skin. The needles were shown to be robust enough to penetrate the skin, using trypan blue staining and histological sectioning of the skin. They were shown to deliver a range of drugs/cosmetics, including chemicals rhodamine B and lidocaine and proteins like bovine serum albumin and collagen, at much higher rates and amount as well as greater depths in the skin, as compared to passive diffusion through the skin using solutions. The encapsulated proteins were shown to remain stable post UV exposure, by analyzing the primary, secondary and tertiary structural characteristics. Microneedles were also shown to be non toxic by assessing in vitro cytotoxicity using mitochondrial succinate dehydrogenase and lactate dehydrogenase activity in three different cell lines, representing epidermal and dermal skin cells as well as normal human embryonic kidney cells. Conclusively, the prepared microneedles are expected to serve as a potentially useful delivery system to deliver biological drugs and cosmeceuticals.

In another part of this thesis, a miniaturized flow through cell (MFtC) for testing the skin permeation of drugs was fabricated. During the development of new transdermal dosage forms/cosmetics, it is imperative to carry out preformulation studies to test the permeation capability of drug/cosmetic compounds across the skin. However, currently available models for testing skin permeation consist of a donor (contains compound) and a receptor chamber (contains buffer), require large amounts of compounds as well as the high receptor flow rates, owing to their inherent design, causes excessive dilution of permeated compounds, making subsequent analysis difficult. This is particularly important for new drug entities, which are available in limited amounts and are prohibitively expensive. The cells also require larger human skin samples, which are scarce due to lack of donors. Moreover, the commercial versions of diffusion cells are expensive, too. In light of these shortcomings, a prototype miniaturized flow through cell (MFtC) on the concept of microfluidics has been developed. The MFtC utilizes minimal amount of compound and the low flow rate achievable prevents excessive dilution of permeated compound. The device is carved out of polydimethylsiloxane (PDMS) and hence is easily adaptable to the various

sizes. The low cost of fabrication and material used make the device single-use, disposable entity, potentially avoiding contamination issues that arise from repeated use of commercial models for different compounds, making MFtC adaptable for a GMP environment.

In addition, these miniaturized platforms for drug delivery and drug testing, provide suitable alternative to macroscopic systems, both with respect to materials as well as the amount of pharmaceutical ingredients used. This in turn, opens up possibilities to reduce the environmental load due to non recyclable materials used in conventional systems, together with a significant reduction in the use of chemicals and solvents, thereby reducing waste generation.

List of Tables

List of Figures

List of symbols & abbreviations

Abbreviation	Full name
°C	degree Celsius
µm	micro meter
µg	micro gram
µL	micro liter
λ_{em}	emission wavelength
λ_{ex}	excitation wavelength
®	registered
™	trademark
$A_{polymer}$	absorbance measurements of the wells containing polymeric extracts
$A_{control}$	absorbance measurements of the wells containing control
ANOVA	Analysis of variance
BSA	bovine serum albumin
$CaCl_2$	calcium chloride
cm	centimeter
cm^{-2}	square centimeter
CMC	critical micelle concentration
CO_2	carbon dioxide
Da	daltons
$dmol^{-1}$	1/decimole
EI	enhancement index
FDA	Food and drug administration
FITC	fluorescein isothiocyanate
FTIR-ATR	fourier transformed infrared - attenuated total reflectance
GI	gastrointestinal
H1N1	influenza A
HaCaT	human adult low calcium high temperature
HDC	horizontal diffusion cell
HDF	human dermal fibroblasts
HEK293	human embryonic kidney
HIV	human innumodeficiency virus
HMP	2-hydroxy-2-methyl-propiophenone
HPLC	high performance liquid chromatography
hr	hour

IACUC	Institutional Animal Care and Use Committee
J	Joules
J_{ss}	steady state flux
kDa	kilo daltons
kHz	kilo hertz
KOH	potassium hydroxide
kV	kilo volts
LDH	lactate dehydrogenase
LOD	limit of detection
Log P	partition coefficient
LOQ	limit of quantification
LPCVD	low pressure chemical vapour deposition
M	molar
mA	milli amperes
MEMS	micro electro mechanical systems
MFtC	miniaturized flow-through cells
mg	milli grams
MhZ	milli hertz
min	minutes
MITP	microneedle integrated transdermal patch
mL	milli liter
mm	milli meter
MN	microneedle
Mn	number average molecular weight for polymers
MTT	3-(4,5-dimethylthiazol-2-yl)-2,5-diphenyl tetrazolium bromide
MW	molecular weight
N	newtons
NaCl	sodium chloride
nm	nano meter
NUS	National University of Singapore
ODS	octadecyl silane
PBS	phosphate buffered saline
PDMS	poly (dimethyl siloxane)
PEGDA	poly (ethylene glycol) diacrylate
PEs	permeation enhancers
PG	propylene glycol
pKa	negative base -10 logarithm of the acid dissociation constant of a solution
PMMA	poly (methyl methacrylate)
PVA	poly (vinyl alcohol)
rpm	rotations per minute

SC	stratum corneum
SDS-PAGE	sodium dodecyl sulfate-polyacrylamide gel electrophoresis
sec	seconds
SEPA	2-n-nonyl-1,3 –dioxolane
shRNA	short hairpin ribonucleic acid
sMTS	solid microstructured transdermal system
SPE	Skin Permeation Enhancer
TMSPMA	3-(trimethoxysilyl) propyl methacrylate
TR	Texas red
US	United States of America
UV	ultraviolet light
v	volume
W	watts

List of publications

The projects highlighted in this thesis are the subject of two patent applications:

1. **Kochhar JS**, Goh WJ, Chan SY, Kang L. A novel method to fabricate polymeric microneedles. WO 2013/137831.

2. **Kochhar JS,** Mah CS, Kang L. A miniaturized flow-through cell (MFtC) for testing the permeation of drugs across biological membranes. US Patent application no 14/051720.

The presented thesis is based on the following international reviewed journal papers:

1. **Kochhar JS**, Goh WJ, Chan SY, Kang L. A simple method of microneedle array fabrication for transdermal drug delivery. *Drug Development and Industrial Pharmacy*. 2013; 39 (2): 299-309.
2. Mah CS*, **Kochhar JS***, Ong PS, Kang L. A miniaturized flow-through cell to evaluate skin permeation of endoxifen. *International Journal of Pharmaceutics*. 2013; 441 (1-2): 433-440. *Equal contribution.
3. **Kochhar JS**, Lim WXS, Zou S, Foo WY, Pan J, Kang L. Microneedle integrated transdermal patch for fast onset and sustained delivery of lidocaine. *Molecular Pharmaceutics*. 2013; 10 (11): 4272-4280.
4. **Kochhar JS**, Quek TC, Soon WJ, Choi J, Zou S, Kang L. Effect of microneedle geometry and supporting substrate on microneedle array penetration into skin. *Journal of Pharmaceutical Sciences*. 2013; 102 (11): 4100-4108.
5. **Kochhar JS**, Zou S, Chan SY, Kang L. Protein encapsulation in polymeric microneedles by photolithography. *International Journal of Nanomedicine*. 2012; 7: 3143-3154.

6. **Kochhar JS**, Parthiban A, Shelar SB, Neo JK, Iliescu C, Kang L. Direct microneedle array fabrication off a photomask to deliver collagen through skin. *Pharmaceutical Research*. 2013, In Press.

The contribution of *Jaspreet Singh Kochhar* to different publications:

1. Major part of design, fabrication, all experiments and writing
2. Equal contribution to design, part of fabrication, experiments and writing.
3. Major part of design, fabrication, experiments and writing
4. Major part of design, part of fabrication, experiments and writing.
5. Major part of design, fabrication, experiments and writing.
6. Some part of design, fabrication, experiments and writing.

The author also contributed to the following publications:

7. Dana SF, Duc VN, **Kochhar JS**, Liu XY, Kang L. UV-curable pressure sensitive adhesive films: synergistic effects of biocompatible plasticizers on mechanical and adhesion properties. *Soft Matter*. 2013; 9: 6270-6281.
8. **Kochhar JS**, Chan SY, Ong PS, Kang L. Clinical therapeutics for phenylketonuria. *Drug Delivery and Translational Research.* 2012; 2: 223-237.
9. Li H, **Kochhar JS**, Pan J, Chan SY, Kang L. Nano/micro-scale technologies for drug delivery. *Journal of Mechanics in Medicine and Biology*. 2011; 11: 337-367.

The author also wrote a book chapter:

10. **Kochhar JS**, Chan SY, Ong PS, Lee WG, Kang L. Microfluidic systems for drug discovery and analysis. In: *Microfluidic devices for biomedical applications*. Eds. Li XJ and Yu Z, Woodhead Publishing Limited, Cambridge, UK. (2013)

The author is also writing a book:

11. Kwan YH, Tung YK, **Kochhar JS**, Poh AL, Kang L. Handbook of cosmeceutical excipients. Woodhead Publishing Limited, Cambridge, UK. (2014)

The work presented in the thesis has also been presented at the podium or as posters at the following conferences:

12. **Kochhar JS**, Chan SY, Kang L. Microneedles for painless delivery of drugs and cosmetics. *Biomedical Engineering Society 7th Scientific Meeting, Singapore*. May 18, 2013. (Oral)

13. **Kochhar JS,** Chan SY, Kang L. Polymeric microneedles for transdermal drug delivery. *YLLSoM 3rd Annual Graduate Scientific Congress, Singapore*. January 30, 2013. (Oral)

14. **Kochhar JS**, Chan SY, Kang L. Polymeric microneedles for transdermal delivery in clinical and cosmeceutical applications. *8th PharmSci@Asia Symposium, Nanjing, China*. May 29-31, 2013. (Oral)

15. Kang L, **Kochhar JS**, Chan SY. Polymeric microneedles for transdermal drug delivery. *Microneedles 2012, Cork, Ireland*. May 13-15, 2012. (Oral)

16. Lim WXS, **Kochhar JS,** Zou S, Kang L. Integrated microneedle transdermal patch for delivering lidocaine in the management of peripheral neuropathic pain. *UK-Singapore Materials Workshop 2012, Singapore*. December 6-7, 2012. (Poster)

17. **Kochhar JS**, Chan SY, Kang L. A novel method of fabricating polymeric microneedles for transdermal delivery of chemical and biological drugs. *7th AAPS-NUS PharmSci@Asia Symposium, Singapore*. June 6-8, 2012. (Poster)

18. **Kochhar JS**, Zou S, Chan SY, Kang L. Microneedle-mediated transdermal delivery of lidocaine hydrochloride for the management of

neuropathic pain. *BES 6th Scientific Meeting, Singapore*. May 19, 2012. (Poster)

19. Mah CS, **Kochhar JS**, Ong PS, Kang L. Transdermal drug delivery of endoxifen for the treatment of estrogen receptor positive breast cancer. *Annual Pharmacy Research Symposium, Singapore*. April 4, 2012. (Poster)

20. Quek TC, **Kochhar JS**, Kang L. Optimization of novel polymer microneedles for transdermal drug delivery. *Singapore Science and Engineering Fair, Singapore.* March 7-8, 2012. (Poster)

21. Quek TC, **Kochhar JS**, Kang L. Novel polymeric microneedles – optimization of design and geometry. *7th International Student Science Fair, Thailand.* October 11-14, 2011. (Poster)

List of awards

The author won following awards during his candidature as a PhD student:

1. Best Graduate Researcher Award, 6 August 2013
2. Best podium presentation award, 8th PharmSci@Asia Symposium, Nanjing, China. May 29-30, 2013.
3. Oral Presentation Silver award, Biomedical Engineering Society 7th Scientific Meeting, Singapore. May 18, 2013.
4. Oral Presentation 1st runner-up award**,** YLLSoM 3rd Annual Graduate Scientific Congress, Singapore. January 30, 2013.
5. Best poster award + Royal Society of Chemistry Book Prize**,** UK-Singapore Materials Workshop 2012, Singapore. December 6-7, 2012.
6. Represented Singapore at the Annual Young Persons' World Lecture Competition, organized by Institute of Materials, Minerals and Mining, London, 5 July, 2012.
7. Rank 1 at Annual Young Persons' Lecture Competition organized by Institute of Materials (East Asia), 10-11 May, 2012.
8. Innovation and Entrepreneurship Practicum Grant (SGD 10,000) by NUS under National Research Foundation's University Innovation Fund (UIF), June 2012
9. NUS Research Scholarship, 2009 – 2013.

CHAPTER 1

Introduction & Literature Review

1.1. Transdermal drug delivery – an introduction

Anticipating the need for patient friendly technologies which deliver the drug reliably at their intended site of action, researchers have looked for alternatives to conventional oral and parenteral route based dosage forms. Skin, which forms a major part of our integumentary system, is the largest organ of the body and has been utilized as a drug delivery route to achieve both local (dermal) as well as systemic (transdermal) pharmacological effects. Local application of plant extracts and herbal drugs to treat topical conditions such as eczema, dermatitis and psoriasis has been in practice for hundreds of years now. The potential of skin as an effective route to deliver drugs to systemic sites has gained importance in the past four decades and has evolved as an appealing alternative to the conventional dosage forms. This can be testified by the number of drugs that have been approved by FDA for transdermal use since the first transdermal patch was approved in 1979 (**Figure 1**) [1].

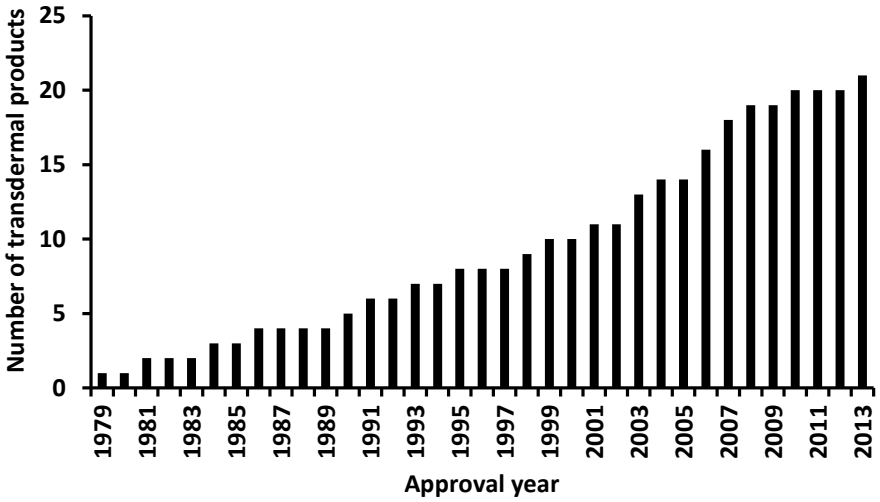

Figure 1 Cumulative number of transdermal products approved by FDA since 1979 when scopolamine patch was approved. Currently 21 drugs and their combinations are approved by FDA for transdermal use. Data has been derived from FDA Orange Book [1].

1.2. Skin as a route for drug delivery: anatomy and challenges

The primary function of the skin is to provide a rigid structural barrier protecting the underlying tissues rather than being an amenable passage for chemicals to permeate. The skin has three basic layers: epidermis, dermis and hypodermis (**Figure 2**) [2]. Epidermis, which is the outermost layer,

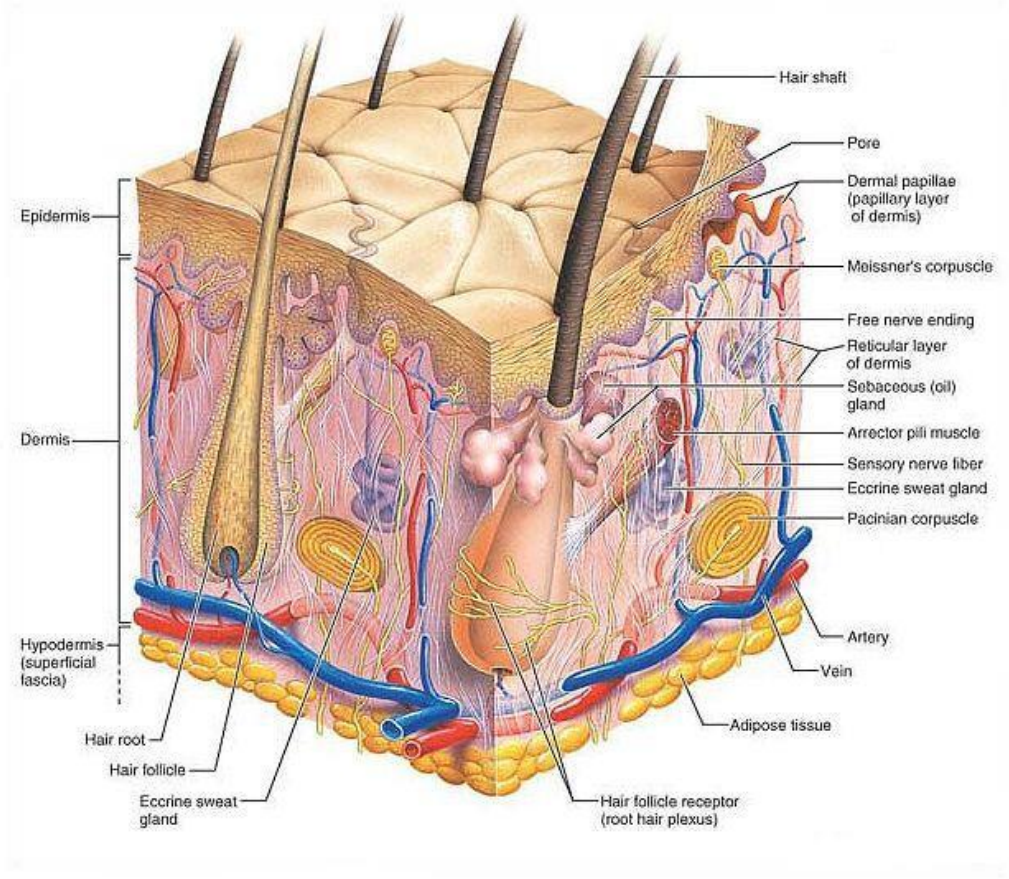

Figure 2 A three dimensional view of the skin and underlying subcutaneous tissue. Adapted with permission from [2].

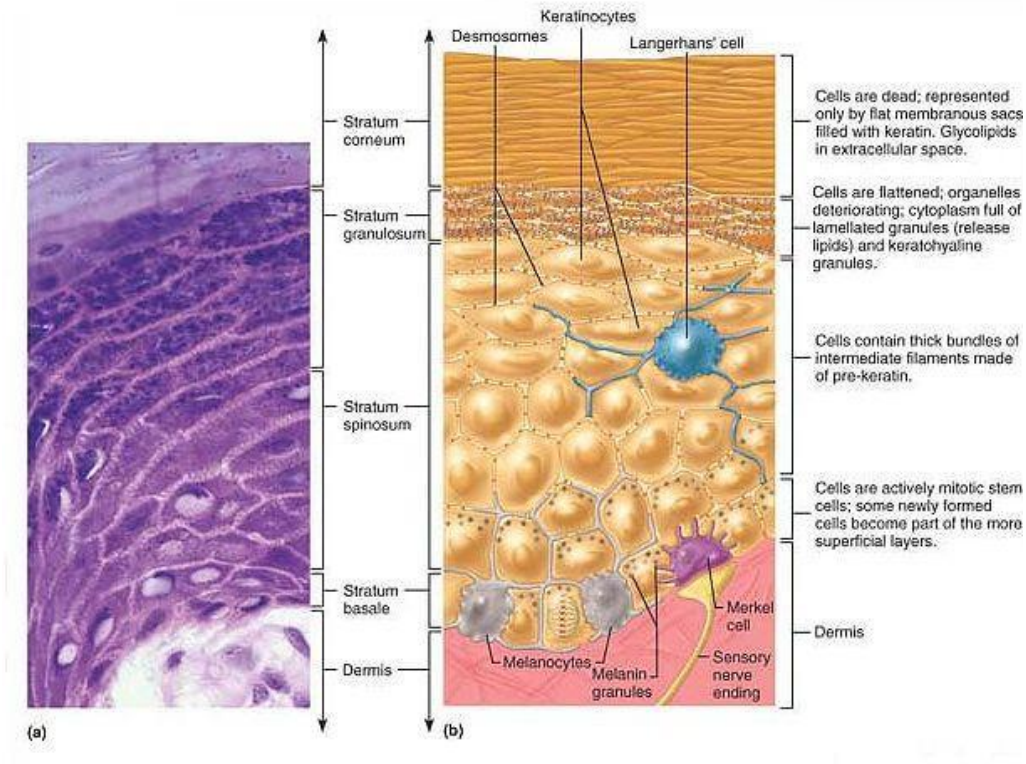

Figure 3 Structural features of epidermis (a) Photomicrograph of four epidermal layers (b) Epidermal layers with distribution of cells. Adapted from [2].

comprised of five layers which from top to bottom are as follows: *stratum corneum, stratum lucidum (present only in thick skin), stratum granulosum, stratum spinosum and stratum basale* (**Figure 3**) [2]. The outermost layer of epidermis, *stratum corneum*, also called as the horny layer, presents a strong permeation barrier. The barrier properties of stratum corneum were proved as early as in 1924 by Rein [3] and supported by several subsequent studies [4-6]. It offers mechanical, anatomical and chemical barrier due to its highly organized multi layer overlapping cells which are sealed by tightly packed intercellular lipid multi–lamellae [7]. This compacted mass of dead corneocytes interspersed with a lipid rich matrix resembles a "brick and mortar" architecture and is primarily essential to prevent the transepidermal water loss, egress of other endogenous substances and ingress of foreign particles (chemicals and drugs) [8], maintaining the internal homeostasis of the body. This complex organization of cells and lipids offers resistance to most pharmacological agents, making it a hurdle for topically administered

products to be systemically absorbed. This formidable barrier function of stratum corneum has limited the number of drug candidates that can be delivered through this route and the commercial transdermal products that are available for human use. **Table 1** and **2** summarize the advantages and limitations of transdermal drug delivery.

Table 1 Advantages of transdermal drug delivery

Benefits
• The avoidance of hepatic first pass effect and other variables associated with the GI tract, such as pH, gastric emptying time **[9, 10].**
• Sustained and controlled delivery over a prolonged period of time **[11].**
• Reduction in side effects associated with systemic toxicity, i.e. minimization of peaks and troughs in blood-drug concentration **[12].**
• Improved patient acceptance and compliance **[13-15].**
• Direct access to target or diseased site, e.g. treatment of skin disorders such as psoriasis, eczema and fungal infections **[16].**
• Ease of dose termination in the event of any adverse reactions, either systemic or local **[8].**
• Convenient and painless administration **[9].**
• Ease of use may reduce overall healthcare treatment costs **[17].**
• Provides an alternative in circumstances where oral dosing is not possible (in unconscious or nauseated patients) **[12].**
• Effective drug delivery system for drugs with short biological half-lives and narrow therapeutic indices **[8].**

Table 2 Limitations of transdermal drug delivery

Limitations
• A molecular weight less than 500 Da is essential to ensure ease of diffusion across the SC **[18]**, since solute diffusivity is inversely related to its size.
• Sufficient aqueous and lipid solubility, a log P (octanol/water) between 1 and 3 is required for the permeant to successfully traverse the SC and its underlying aqueous layers for systemic delivery to occur **[19].**
• Intra- and inter-variability associated with the permeability of intact and diseased human skin. This implies that there will be fast, slow and normal skin absorption profiles, resulting in varying biological responses **[20]**. The barrier nature of intact SC ensures that this route is applicable only for very potent drugs that require only minute concentrations (e.g. 10–30 ng mL^{-1} for nicotine) in the blood for a therapeutic effect **[10].**
• Pre-systemic metabolism; the presence of enzymes, such as peptidases, esterases, in the skin might metabolise the drug into its therapeutically inactive form **[21].**
• Skin irritation and sensitization, referred to as the "Achilles heel" of dermal and transdermal delivery. The skin as an immunological barrier may be provoked by exposure to certain stimuli; this may include drugs, excipients or components of delivery devices, resulting in erythema, oedema, etc. **[22-25].**

This thesis describes two major areas of transdermal drug delivery, viz. drug delivery platforms and permeation testing apparatus. Since skin with its natural barrier properties does not allow diffusion of many therapeutic molecules, scientists have worked to develop dosage forms and delivery devices that minimally disrupt the skin while enhancing delivery rates. On this aspect, this thesis describes a novel method of microneedle fabrication and its efficiency in delivering a range of drugs and cosmetics. On the other hand, many platforms for preformulation testing of transdermal dosage forms have been developed to suit the needs of novel drug delivery systems and efforts are needed to further enhance their applicability to sophisticated platforms like

electroporation, iontophoresis or microneedles. This thesis describes the development of a novel miniaturized flow through cell, with potential to reduce drug and skin sample consumption, a critical necessity, especially for new drug molecules.

1.3. Literature Review

1.3.1. Drug delivery systems

A drug delivery system is a formulation or a device that enables the placement of a therapeutic substance in the body and improves its efficacy and safety by controlling the rate, time and place of its release in the body. It is an interface between a patient and a drug. If a device is introduced into a patient's body for functions other than or in addition to delivering a drug, for example, a drug eluting stent, it is strictly classified as a device. Drug delivery systems have been further classified as per the route of administration as described below.

1.3.2. Routes of drug delivery

Table 3 summarizes various routes of drug delivery. *Oral* route of delivery is most commonly used simply because of ease of administration and patient acceptance. However due to variable absorption through the gut wall, enzymatic and acidic degradation of several drugs (particularly biomolecules), first pass metabolism, solubility of drugs in gastric fluid and irritation of gastric mucosa are some of the limitations of this route. Also, since the route involves systemic absorption, targeted drug delivery is seldom achieved and may lead to toxicity of non target organs as well.

Parenteral drug delivery, which stands for routes other than gastrointestinal tract, but has been majorly used to refer injection based routes such as subcutaneous, intravenous, intra-arterial or intramuscular routes of drug delivery. This route of drug delivery is often used when an immediate effect of the drug is desired and almost 100% bioavailability can be achieved. These injections can be used in comatose and unresponsive patients or those who cannot swallow pills, particularly paediatrics and geriatrics. However, always trained personnel are required to administer injections and they are associated with pain. Moreover, they are the biggest risk behind spread of infections if

misused. Achieving a sustained release of the drug may be a concern and it is difficult to reverse an overdose.

Intranasal route is used for drugs required in small doses and often required to act quickly, through the nasal epithelium drugs could bypass the blood brain barrier and hence delivery to the brain could be achieved. Since absorption of drug through nasal mucosa occurs through the aqueous channels of the membrane, it most often depends on the molecular weight of the compound and its ability to hydrogen bond with membrane components. However compounds with molecular weight more than 300 Da do not cross the membrane in significant proportions. Greater nasal secretions and ciliary movements also reduce bioavailability.

Colorectal drug delivery dates back to 1500 B.C., however is not very popular among consumers as it not very aesthetically pleasing. Nonetheless, it is an important route for delivering drugs to the intestines and systemically. The drugs can be slowly absorbed for a prolonged action and are not affected by the conditions in the gastrointestinal tract. Hydrophilic drugs are absorved to a lower extent than hydrophobic drugs. There is significantly lower first pass metabolism involved via this route.

Pulmonary route of drug delivery has been used since the middle of the 20^{th} century since aerosols were first developed. Recently the route has been studied for its ability to deliver drugs systemically due to large surface area that lungs offer for exchange of drug between lungs and systemic circulation. However large molecules such as proteins and peptides do not readily cross the pulmonary mucosa because it is thick, ciliated and covered with mucus lining.

Transdermal drug delivery as has been described earlier provides an alternative to delivery of both small and large molecular weight drugs, due to development various passive and active drug delivery systems being developed. These will be described in greater detail in the next section.

Table 3 Advantages and Disadvantages of other routes of administration for systemic drug delivery apart from transdermal

Route of administration	Advantages	Disadvantages
Oral	convenient (portable, easy, painless), economical to the patients (non-sterile, compact), variety (tablets, capsules, liquid, fast, slow release), high dose possible, high surface of absorption, good permeability of GI barrier	may be inefficient (high dose, low solubility), first pass effect (the concentration of a drug is greatly reduced before reaching the systemic circulation), food interaction, local effect (GI flora), not suitable for unconscious patients
Intravenous	direct access to blood central compartment, bypasses the digestive system, does not harm the lungs or mucous membranes, rapid onset of action	increased risk of infection and overdose, risk of the peripheral vein or arterial damage, limited to highly soluble drugs, fear, trained personnel is needed, sustained/controlled action not possible
Subcutaneous	can be self-administered, slow, but generally complete absorption	painful, tissue damage from irritant drugs, max. 2 ml injection
Intramuscular	depot or sustained effect is possible	unpredictable or incomplete absorption, trained personnel is needed
Inhalation	bypasses liver, large surface of absorption	difficulties in regulating the exact amount of dosage, difficulties administering the drug via inhaler
Rectal	bypasses liver, useful for children or older people, drug released at slow, steady state	unpredictable absorption, not well accepted by patients
Sublingual	avoid first pass effect, rapid absorption, drug stability, can be administered for local effect	small dose limit, inconvenience for some patients

1.3.3. Mechanisms of drug absorption through skin

Delivery of drugs across the skin has been achieved either by passive diffusion or by active disruption of the horny layer. These strategies have been able to increase the efficiency of drug delivery across the stratum corneum, in their

own capacity. **Figure 4** describes the various routes of transdermal diffusion employed by different techniques [26].

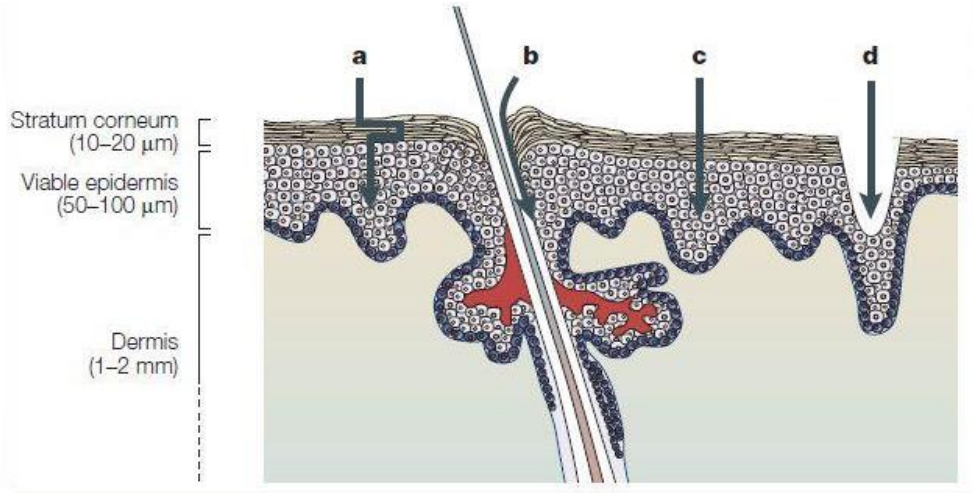

Figure 4 Mechanisms of transdermal delivery (a) Transdermal diffusion, passive and with chemical enhancer, follows a tortuous route across the stratum corneum (b) Low-voltage electrical enhancement by iontophoresis can make transport pathways through hair follicles and sweat ducts more accessible. (c) High-voltage enhancement by electroporation has been shown to occur via transcellular pathways made accessible by disrupting lipid bilayers. The application of ultrasound seems to make pathways (a) and (c) more permeable by disorganizing lipid bilayer structure. (d) Microneedles and thermal poration create micron-scale holes in skin. Adapted with permission from [26].

a) Passive methods of transdermal delivery: mechanism, evolution and limitations

The transport mechanisms by which drugs cross the intact skin have not yet been completely elucidated yet several pathways have been suggested. Drug transport through intercellular lipids follows a complex path around corenocytes, where hydrophilic molecules travel through the polar region (head group) of the intercellular lipids and the lipophilic molecules traverse through the lipid chains (lipid tails) [8, 27]. The appendageal route has also been implicated in passive diffusion of small polar molecules [8].

The passive diffusion of molecules through these routes depends on several factors including the time scale of permeation, the physico-chemical properties of the permeant (e.g. pKa, stability, molecular size, solubility, partition coefficient, etc.), integrity and thickness of stratum corneum, density of sweat glands and follicles, skin hydration and vehicle properties [8].

Conventionally, gels, creams and ointments have been used for passive diffusion of drugs across the stratum corneum. Michaels et. al. [28] studied the permeation characteristics of several drugs and low molecular weight compounds and proved that compounds with high water and oil solubility and sufficient potency can be delivered though the skin at effective rates through a small area. This spurred the revolution in the field of transdermal drug delivery and active research with several potent drugs led to development of transdermal patches. Creams and gels have long existed but are difficult to retain on skin for longer periods, together with non-uniform dosing. In 1979, US FDA approved the first patch to deliver scopolamine for motion sickness [26]. Transdermal patches have since been developed and marketed for fentanyl, clonidine, nitroglycerin, estrogens, lidocaine, testosterone and the blockbuster nicotine patch, which substantiated the role that transdermal drug delivery, played in public health. The success of transdermal patches can be judged from the fact that between 2003 - 2007 a new patch was approved every 7.5 months by FDA. The annual market for patches in US is more than US$ 3 billion [26].

Despite achieving this success, the amount of drugs that can be delivered using these conventional passive methods is limited. This can be attributed to the fact that for passive diffusion, drugs should possess the following characteristics: a molecular weight of < 500 Da, sufficient lipid solubility and a small therapeutic dose. This is exemplified further as the smallest drug currently incorporated in a commercial transdermal patch is nicotine (162 Da) and the largest is oxybutynin (359 Da) [26]. Drugs with molecular weight larger than 500 Da and low lipophilicity have failed to achieve the desired bioavailability when delivered passively through the skin. The success of transdermal patches has thus relied on the judicious selection of drugs which can passively cross the skin at therapeutic rates without the aid of physical or chemical disruption of the horny layer. Mark Prausnitz and Robert Langer have categorized these as the first generation of transdermal drug delivery systems [27].

Numerous active penetration techniques have been tried to chemically or physically alter the permeability of stratum corneum and drive the hydrophilic

molecules as well as macromolecules (proteins, peptides, nucleic acids) and vaccines across the skin to targeted sites or systemic circulation. These come under the scope of active methods of transdermal drug delivery and aim to broaden the horizon for this novel route for therapeutic application.

b) Active methods of transdermal drug delivery: mechanism, evolution, and potential

The advent of biotechnology and recombinant technologies in the latter half of the twentieth century has presented novel and potent biotherapeutics including proteins, peptides and vaccines [29]. These molecules are usually large molecular weight (> 500 Da) polar hydrophilic molecules. Drug delivery scientists have looked for alternatives to oral route which presents harsh acidic and enzymatic environment not conducive for the stability of these drugs [30]. Current administration relies on the hypodermic injection which is painful, needs trained personnel, poses a high risk of infection and requires careful disposal of biohazardous sharps. These issues have invoked a need for an efficient drug delivery system which circumvents the problems faced with oral and hypodermic routes for delivering novel biomolecules.

Active disruption of stratum corneum provides an ideal alternative route. These active penetration enhancement methods involve the use of external energy to drive large and hydrophilic molecules across the stratum corneum by reducing its barrier properties utilizing an array of mechanisms. Prausnitz and Langer have classified active permeation enhancers into two categories: second and third generation of transdermal drug delivery systems. These systems are based on their physico-chemical properties and their mechanism of enhancing drug permeability.

Chemical enhancers, which belong to the second generation, act by either enhancing drug solubility and/or partitioning in the stratum corneum or by reversibly disrupting the lipid structures of stratum corneum by fluidizing the lipid bilayers [31, 32]. This leads to creation of defects in the lipid packing structure [33-39] resulting in increased permeability of stratum corneum. Extensive research in screening and testing has resulted in identification of various classes of penetration enhancers, including surfactants (Tweens and

spans) [40], fatty acids/esters (oleic acid) [41], terpenes [42, 43] and solvents (ethanol, decanol) [44]. Although these penetration enhancers offer design flexibility in formulation and ease of application over a larger area, a challenge posed by them is the accompanying skin irritation. An increase in the enhancer concentration has resulted in increased permeability, but with increased skin irritancy [26, 27]. Fatty alcohols like decanol, undecanol and lauryl alcohol have shown to increase transepidermal water loss with resultant erythema and increased skin blood flow, all of which are markers of skin irritation [44]. A few non irritant penetration enhancers such as laurocapram (Azone) [45, 46] and 2-n-nonyl-1,3 –dioxolane (SEPA) [47] have been used, but they have been limited in use due to their inability to deliver macromolecules. Lack of convincing permeation enhancing properties for large hydrophilic molecules has led researchers to look for other efficient alternatives.

Technological advancements in bioengineering, computing, chemical and material sciences, microfabrication techniques have provided an array of miniature, powerful and efficient transdermal drug delivery systems which actively disrupt the barrier properties to deliver large molecules. These include iontophoresis, ultrasound (non-cavitational and cavitational), electroporation, thermal ablation, microdermabrasion and microneedles. They vary in their mechanism of increasing stratum corneum permeability to hydrophilic drugs and have been reported to be more effective than conventional chemical enhancers [8].

Iontophoresis, classified as a second generation transdermal drug delivery system, involves application of a small voltage electric current to the skin directly or indirectly using an electrically activated dosage form. This technique has been practiced for more than a century [48, 49] and employs a combination of methodologies, electrorepulsion (for charged molecules), electroosmosis (for uncharged molecules) and electroperturbation (for both charged and uncharged molecules) for drug transport across the skin. FDA has approved the use of iontophoresis for anti-inflammatory agents for their local effects [50], pilocarpine to induce sweating as a diagnostic tool for cystic fibrosis [51], tap-water delivery to treat hyperhidrosis [52], lidocaine

anaesthesia prior to venipuncture [53] and extraction of interstitial fluid for determining glucose levels in diabetics [54]. Research has also shown improved iontophoretic permeation of dexamethasone, ketorolac, luteinizing hormone-releasing hormone and calcitonin. An asset of significant impact in iontophoresis is the rate of drug delivery which could be modulated with a microprocessor to control the application of current. However, in this attempt to increase the rate of drug delivery, considerable skin irritation and pain resulted due to significant inflammation of underlying nerve innervated tissues [55]. The use of microprocessors for control and batteries to generate current involves complicated fabrication methods which accrue the cost of therapy for the end user. Regulatory constraint on the amount of current that can be applied (0.5 mA cm^{-2}) on human skin is another limitation for this technique. Iontophoresis doesn't primarily change skin's barrier properties and hence has been applicable to a small fraction of molecules which are either charged or low molecular weight, weighing up to few thousand Daltons (7 kDa) [56].

Non cavitational ultrasound comes under the class of second generation systems as well. Ultrasound is oscillating pressure wave whose frequency is higher than what human ear can hear. Use of ultrasound to increase transdermal permeability has been referred to as *sonophoresis* or *phonophoresis*. Ultrasonic energy has been used simultaneously or as a pre treatment before drug application on skin. Frequency between 20 kHz-16 MHz has been used to increase the permeability of stratum corneum but frequencies lower than 100 kHz have shown to more efficient in breaching barrier properties of stratum corneum with molecules up to 48 kDa effectively delivered transdermally [57]. Heating and subsequent lipid solubilisation has been hypothesized to disrupt the lipid architecture as a mechanism for penetration enhancement. Similar to iontophoresis, use of aggressive methods with the aim of increasing skin permeability and deliver larger molecules has resulted in irritation of deeper tissues and has thus limited its use to deliver small, lipophilic molecules.

The quest for development of transdermal drug delivery systems with stronger disruption of stratum corneum yet conferring minimal insult to the deeper tissues has led scientists to the third generation of transdermal drug delivery

systems. These techniques have shown the potential to deliver macromolecules including proteins, peptides and vaccines at therapeutic rates. Emanation of suitable supporting technologies from other disciplines has provided an impetus for the development of these systems, which has been made stronger by the desire to make these systems with agreeable clinical benefits. Techniques such as electroporation, cavitational ultrasound, thermal ablation, microdermabrasion and micron-scale needles have been used in an attempt to develop an ideal transdermal drug delivery system for macromolecules.

Electroporation, which involves use of electric fields for providing short, high voltage pulses to increase transdermal permeability of macromolecules acts by disrupting the lipid bilayer structure [58]. High voltages in excess of 100 volts for short duration of milliseconds has been applied frequently and molecules greater than 7 kDa (limit for iontophoresis) have been delivered [8]. Larger molecules like heparin [59], insulin [60], vaccines [61, 62], oligonucleotides [63], etc., have also been delivered in conjunction with chemical penetration enhancers. The electric field applied to skin is initially concentrated in the stratum corneum owing to the higher resistance offered by it. But as liquidation of stratum corneum lipids ensues, this resistance drops exposing the lower sensory organs to the electric field causing pain and muscle stimulation, limiting the scope of this efficient approach for human applications. Moreover, the complex design and the high fabrication and usage cost has curbed research initiatives and scientists have looked for other convenient and economical alternatives.

Cavitational ultrasound is known to increase skin permeability by formation, oscillation and collapse of bubble in ultrasonic pressure fields [64]. The formation and collapse of bubbles concentrates the energy of ultrasound on the skin surface, which is thought to generate shock waves. Generation of cavities and bubble collapse at high pressures is expected to create fallacies in the lipid arrangement leading to increased permeability of large molecular weight drugs [65]. This effect is observed at low ultrasound frequencies (< 100 MHz) and is distinct from high frequency (non cavitational) ultrasound which is thought to increase permeability by heating and solubilising stratum corneum

lipids. Cavitational ultrasound has been approved by FDA for delivery of lidocaine [66] and several animal studies have demonstrated the efficiency to deliver insulin, heparin, tetanus vaccine and other drugs [64]. However, the complicated equipment design and operation, high cost of fabrication preclude this technique from being a successful drug delivery system for the masses.

Thermal ablation involves selective heating of the skin surface to breach the stratum corneum. *In vitro* studies have demonstrated 2-3 fold increase in skin permeability for 7- 8˚C rise in skin temperature [67, 68]. Vasodilation which resulted as a homeostatic response of the body further increased systemic absorption of drugs [69]. Earlier studies employed a temperature of 40-42˚C which could be tolerated for longer periods (> 1hr). These methods caused dermal tissue damage and did not significantly improve enhancement for drugs greater than 500 Da. Newer thermal ablation methods involve heating of the skin surface to a very high temperature (> 100˚C) for a very short time (milliseconds or microseconds). The mechanism may involve vaporization of epidermal water resulting in creation of micron sized openings in the stratum corneum [70]. Skin heating could be achieved using ohmic micro-heaters and radio-frequency ablation [27]. Some animal studies have shown to increase the permeability of human growth hormone and interferon α-2b [71]. There are however several concerns with the applicability of this technique. Individual variance in tolerability to high temperatures may not make this technique widely acceptable. Another prime consideration is the stability of drug molecules, intended for this application (proteins, peptides and vaccines) may not withstand high temperatures.

Microdermabrasion, which has been used primarily for cosmetic purposes, involves removing the stratum corneum by simple methods such as the use of sandpaper. Increase in permeability of lidocaine, vitamin C and 5-fluorouracil has been reported and some animal studies have demonstrated possibility for vaccine delivery using this method [72-74]. Development of specialized microdermabrasion tools may aid in gently abrading the dead keratinized stratum corneum without causing much damage to the underlying tissues [75].

Laser radiation [74, 76, 77], photomechanical waves [78-80], radio frequency [81], magnetophoresis [82, 83], suction ablation [84] and needleless injection [85] are some other techniques that have been tried to enhance transdermal permeability of hydrophilic drugs. Although they have all shown potential, the sophisticated fabrication and functional approach, significant investment involved in research and development, the final cost of the delivery system and elaborate and inconvenient application methods have impeded their widespread clinical use. **Table 4** highlights the advantages and disadvantages of various passive and active transdermal drug delivery systems.

Successful transdermal drug delivery relies on the balance between efficiency of drug delivery and safety of the skin, coupled with the ease of application and economical nature of the system. Creation of micron scale perforations in the dead cells of stratum corneum, which do not significantly affect the living cells in the viable epidermis and dermis, is the goal of an ideal physical penetration enhancement technique. Micron scale needles, which consist of an array of projections, supported on a flat base present a pragmatic approach. They were first proposed in the 1976 [86] but conceptualized and realized only in the last decade by Henry et. al. [87], when microfabrication techniques came to fore. The advancement in microfabrication techniques and application of technology from the semiconductor industry to the biomedical arena has led to the innovation of microneedles.

Table 4 Advantages and Disadvantages of various passive and active transdermal drug delivery systems apart from microneedles

Delivery system	Advantages	Disadvantages
Liquids and semisolids	convenient (portable, easy, painless), economical to the patients (non-sterile, compact	limited absorption for molecular weight above 500 Da, short duration of action, may soil clothes
Patches	convenient, ease of application	only applicable for low molecular weight drugs, slow absorption of drugs
Chemical enhancers	increased permeability	Skin irritation, permeation enhancement not very high
Iontophoresis	increased permeation, suitable for peptides, FDA approved for some drugs	skin irritation, pain, for molecules up to 7 kDa, expensive
Non-cavitational ultrasound	milder than iontophoresis, molecules up to 48 kDa can be delivered	skin irritation at high frequencies
Electroporation	molecules > 7 kDa can be delivered, combined with chemical enhancers,	pain and muscle stimulation, complex design, high fabrication cost
Cavitational ultrasound	FDA approved for lidocaine delivery	high equipment fabrication cost, complex operation,
Thermal ablation	2-3 fold increase permeability	individual tolerance to high temperature, drug stability
Microdermabrasion	increase in permeability with minor injury, ideal for cosmetics	specialized tools not available

1.3.4. Microneedles as a transdermal drug delivery system

The revolution in microelectronics industry has knocked the doors of drug delivery. The advent of microelectromechanical systems (MEMS) has provided an impetus for fabrication of biomedical and drug delivery devices that offer the convenience of use as well as advantage of affordability as they can be mass produced. They can be specifically designed to be minimally invasive and the drug release can be specifically programmed using special tools. Amalgamation of concepts from several disciplines offers the specific benefits of optimization of design and functional parameters to best suit the clinical requisites.

Microneedles have been one such innovative present from the microelectronics industry, which provides a potential and promising alternative to hypodermic injection for delivering the plethora of biomolecules that are being synthesised as a result of the surge in biotechnology industry. Microneedles can be thought to be a hybrid offering the convenience and safe application of transdermal patches and efficiency of hypodermic injections. Microneedles exhibiting variations in their geometrical aspects of length, tip diameter, base diameter, needle to needle spacing and array dimensions have been fabricated. As such they can be tailor-made to be long enough to breach the stratum corneum, but short enough to avoid stimulation of the nerves in the underlying dermis. They have been proven to be painless in human volunteers by Kaushik et al. [88]. Microneedle length can also be tuned to deliver the drug to specific sites in the skin, especially vaccines which utilize skin's immune system, housing a large population of langerhans cells and dermal dendritic cells. They have been proved to show higher immunogenicity than intramuscular injection at a lower immunogenic dose of the influenza vaccine [89]. **Table 5** details the advantages of microneedle based transdermal drug delivery systems.

Table 5 Advantages of microneedles

Advantages of microneedles
• Painless alternative to hypodermic injections, which are invasive and stimulate the nerve endings in the dermal tissues. Microneedles deliver the drug in epidermal tissues, causing less pain and hence increased patient compliance **[88].**
• Potential risk of infection from hypodermic injection is obviated with the use of polymeric microneedles, which are biocompatible and generate no hazardous biological waste.
• Novel microfabrication techniques result in good reproducibility, high accuracy and moderate fabrication cost, which results in economy of therapy **[90].**
• Drug can either be coated on the needles, encapsulated within the polymeric matrix or a patch maybe subsequently applied to aid in drug permeation.
• Immunization and vaccination in developing nations such as in Asia and Africa can be easily achieved using microneedles with minimal patient education. They avoid the risk of infection prevalent in these countries due to needle re-use.
• Targeted drug delivery to specific cells in the skin, e.g. langerhans cells and dermal dendritic cells.
• Hollow microneedles can be used to deliver liquids and withdraw tissue fluids for analysis **[91].**
• Microneedles can be fabricated to achieve complex release patterns (bolus/sustained) **[92].**
• Dose delivered can be terminated immediately by removing the microneedle patch from the skin.

1.3.5. Microneedles: development and current status

The concept of micron scale arrays to transiently breach the stratum corneum was conceived by Gerstel et al. [86] in 1976. However, it was not possible to fabricate and commercialize these microneedles at that time due to lack of mass fabrication techniques. The advent of microelectronic tools, first employed to fabricate three dimensional microstructures for the semiconductor industry in the 1990s, renewed the interest of drug delivery scientists for fabrication of microneedles. Microneedles have since been fabricated from a variety of materials including, silicon, metal, glass, zeolite and more recently polymers and sugars. The mode of transdermal delivery is dependent on the design of microneedles (**Figure 5**). Microneedles displaying four distinct modes have been fabricated to increase skin permeability, including (a) solid microneedles, which are used to pre-treat the skin before application of dosage form, (b) coated microneedles that release the coatings once applied to skin, (c) polymeric microneedles which encapsulate the drug and may or may not dissolve in the skin upon application and (d) hollow microneedles that provide a channel for infusing liquids into the skin [93]. With nearly 400 research papers and 2 dedicated conferences organized, microneedles are a fast growing field [93, 94].

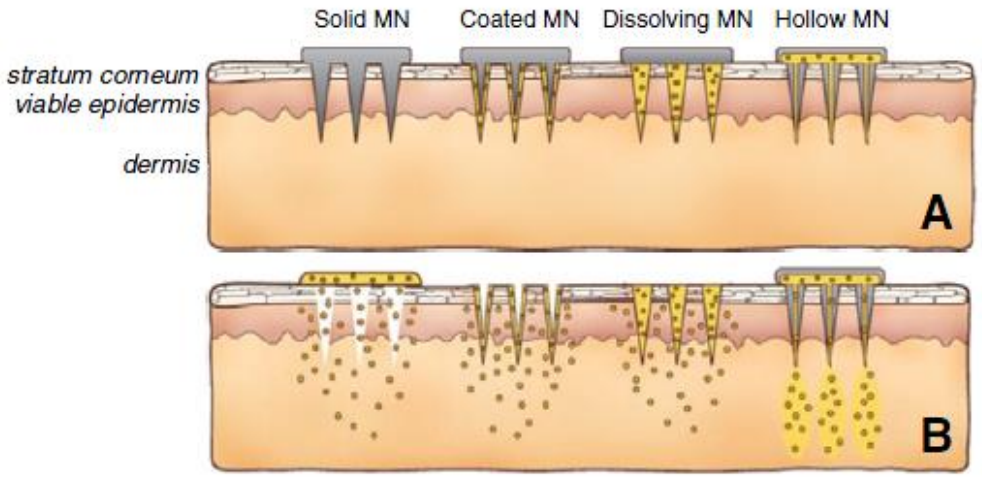

Figure 5 Methods of drug delivery to the skin using microneedles (MN). Microneedles are first applied to the skin (A) and then used for drug delivery (B). Solid microneedles are used as a pretreatment, after which drug can diffuse through residual holes in skin from a topical formulation (solid MN). After insertion of drug-coated microneedles into the skin, the drug coating dissolves off the microneedles in the aqueous environment of the skin (coated MN). Drug-loaded microneedles are made of water-soluble or biodegradable materials encapsulating drug that is released in the skin upon microneedle dissolution (dissolving MN). Hollow microneedles are used to inject liquid formulations into the skin (hollow MN). Adapted with permission from [93].

a) Silicon microneedles

Henry et al. fabricated microneedles from silicon wafer using a reactive ion etching technique [87]. In this process a silicon wafer was masked with chromium dots using lithographic patterning and the microneedles were further developed using a deep reactive ion etcher in plasma of SF_6 and O_2. The regions protected by chromium remained and formed the needles. The needles formed had extremely sharp tips and were approximately 150 µm long. These needles had sufficient strength to penetrate the stratum corneum without breaking and were successful in achieving a 1000 fold increase in calcein permeability [87]. However, materials such as single crystal silicon are brittle and hence are prone to breakage in the skin. Other materials such as meso porous silicon offer better biocompatibility and reduce the risk in case of inadvertent breakage in the skin [95].

With a vast amount of processing knowledge and experience in silicon micromechanics, it came as a natural choice for scientists as a material for

microneedle fabrication. Microfabrication of a device using silicon involves photolithographic patterning as the key process. Lithography (lithos means ‘stone’ and graphein means ‘to write’) [96] is the transfer of a specific pattern on to a substrate. Most of the initial microneedle fabrication processes revolved around these principles of lithographic patterning, film deposition and etching (wet and dry) to generate the required microstructure. Silicon microneedles have been fabricated of varying heights, shapes and densities of silicon. Several modifications of film deposition and etching processes have been adapted to reduce the number of processing steps, increase the efficiency of the process or to reduce the fabrication cost [90, 97-100].

Paik and co workers designed in-plane single-crystal silicon microneedles using the processes of anisotropic dry etching, isotropic dry etching and trench-refilling. The needles were integrated with a PDMS microfluidic chip which was used to deliver Rhodamine B and black ink in *in vitro* and *ex vivo* models [97]. Wilke et al. devised a wet etching technique using potassium hydroxide to fabricate silicon microneedles [90]. Similar technique was used by Wei-Ze et al. to fabricate super short microneedles measuring 70-80 µm in length, which were able to penetrate the skin as was observed with Evans Blue application as an array of blue spots on pierced human skin. Plasma based process such as those described above are very expensive and need elaborate equipments. Shikida and co workers devised a novel anisotropic wet etching and dicing based process which did not use any photolithography or the plasma based equipment. They proposed two different procedures, in first, the process involved the formation on an etching mass followed by dicing and an anisotropic wet etching process and the second process involved just dicing and wet etching processes [100]. These novel methods were suitable for fabricating solid microneedles. To make an adaptation of the process for fabrication of hollow microneedles, Shikida et al. proposed an enhancement of the previous processes by application of metal plating and minimizing the number of photolithography steps to fabricate hollow microneedles. The process involved mechanical grinding of a silicon substrate followed by anisotropic etching of a single silicon crystal to form the required molds. A thin metal film was deposited on the silicon molds by physical deposition,

vacuum evaporation or sputtering and further the hardness was increased by metal plating. The hollow microneedles were obtained by etching the silicon substrate [99]. Other techniques including Bosch deep reactive ion etching and isotropic etching have been used to fabricate tapered hollow microneedles [101] and microneedles with sharp tips [102], while chemical and deep reactive ion etching has been used to create sharp tipped hollow microneedles, with the help of a dicing saw [103].

Combination of sonophoresis and hollow silicon microneedles has been demonstrated by Chen et al. to deliver higher amounts of calcein and bovine serum albumin [104]. Similarly, Tao and Das demonstrated 10 × enhanced delivery of BSA using a combination of 1.5 mm long microneedles and 15 W ultrasound output device, as opposed to passive diffusion [105].

Although silicon offered the advantage of adaptability to a wide range of fabrication procedures and the knowledge exchanged from the microelectronics industry made the processing of microneedles easier, the complexity of the processes is not ideal for mass production of dosage forms. Silicon as a raw material, too, is expensive. The extensive hi-tech processing and the need for clean room facilities further adds to the cost and makes it less attractive for commercial use. However, during mass production cost is not the issue; the biocompatibility of silicon is questionable and it is a non approved material. Metals and glass have been shown to effectively penetrate the skin.

b) Metal microneedles

Some metals like stainless steel have already been used for medical devices and are approved. Microneedles have been fabricated from stainless steel [106, 107], palladium [108], titanium [109] and nickel [110] using approaches such as electroplating, photochemical etching and laser cutting.

Martanto et al. fabricated stainless steel microneedles from 75 µm thick sheets using an infra red laser which was operated at 1000 Hz for 4 minutes at energy density of 20 J/cm^2. The needles thus formed were bent 90˚ out of plane manually and electropolished [107]. Gill and co-workers successfully demonstrated the use of steel microneedles for the transdermal delivery of various compounds like vitamin B and calcein. They also devised a method to

seclude or ‘pocket’ microparticles within the holes of the microneedles to deliver particles of small dimensions like barium sulphate without wiping off on the skin [106, 111].

Microneedles have also been fabricated from materials like glass and ceramic. Adaptations from conventional glass micropipette drawing techniques were used to fabricate hollow microneedles [112]. Ceramic microneedles were prepared by sintering alumina slurry in PDMS moulds [113]. A two-photon polymerization method using a polymer-ceramic mixture has also been used to make ceramic microneedles [114].

Albeit the fast progress in fabrication techniques for silicon and metallic microneedles across academia and industry and the proof of their applicability in increasing permeability of skin, their clinical usefulness still remains ambiguous. Both, metals and silicon are non biodegradable and concerns over their breakage in the skin have been expressed. Silicon, unlike some metals (titanium) is not an FDA approved material and regulatory issues might pose a stumbling block in its path. Metals, being undoubtedly cheaper than silicon, present the concern of generating biohazardous sharps whose disposal is a global concern and houses the risk of transmission of diseases such as HIV AIDS, if the needles are accidently or incidentally reused. Cases of immune-inflammatory responses have also been reported with stainless steel and titanium implants [96]. Also, the drug dose that can be delivered using these solid microneedles is limited as the drugs can only be coated on the microneedle shafts, which is usually less than 1 mg for small microneedle arrays [115]. Hollow microneedles, on the other hand, are fabricated using complicated techniques and require a secondary drug delivery system. Polymeric microneedles have since drawn the attention of many researchers as they obviate the problems inherent with their predecessors. The needles are biocompatible and biodegradable and have been shown to be strong enough to penetrate the skin [92, 116, 117].

c) Polymeric microneedles

Various polymers including poly (vinyl pyrrolidone) [116], its co-polymer with methacrylic acid [116] and poly-lactide-co-glycolide [118] have been

used. Sugars and sugar derivatives like dextrose [119], maltose [120], galactose [121], carboxymethylcellulose [92] and amylopectin [92] have also been used for fabricating microneedles. These materials are biocompatible, cost effective and generate no biohazardous waste. Park et al. were the first to fabricate polymeric microneedles from polylactic acid, polyglycolic acid and their copolymers using PDMS micromolds. Beveled, chisel-tip and tapered cone shapes were obtained using techniques of MEMS masking and etching [122]. They reported 2-3 times increase in skin permeability for calcein and BSA. Deep X ray lithography techniques have been used by Moon et al. [123] and Perennes et al. [124] to fabricate hollow microneedle arrays from poly methyl methacrylate. Aoyagi et al. have used excimer laser to fabricate microneedles from polylactic acid [125]. Lee et al. fabricated microneedles from carboxymethylcellulose, albumin and amylopectin. The model drugs sulforhodamine B, albumin and lysozyme were either incorporated in the needles or in the backing for bolus or sustained release respectively [92]. Sullivan et al. designed a novel room temperature molding technique especially for biomolecules [116]. The process involved in situ polymerization of using monomer vinyl pyrrolidone, encapsulating albumin. The fabrication process involved use of PDMS molds and UV exposure for 30 minutes at room temperature to effect polymerization. Microneedles from sugars have also offered cheaper alternatives to silicon and metals with ease of fabrication. Ito et al. used another simple process to fabricate microneedles from dextrin [126]. Microneedles were fabricated with dextrin glue using polypropylene tip dipping method. Individual tips were dipped in the viscous glue followed by drying at room temperature and scrapping off to get the microneedle. Kolli et al. used maltose microneedles to study the permeation characteristics of nicardipine hydrochloride across hairless rat skin and observed an increase as compared to passive diffusion [127]. **Appendix 1** provides an overview of polymeric microneedles fabricated by different procedures using different polymer/s and sugar.

d) Polymeric microneedles: fabrication issues with current methods

Microneedles developed from sugars [128, 129] pose processing difficulties as the melting points of these sugars are usually very high (140-160˚C). Most of

the protein drugs cannot withstand these high temperatures and substantial losses in the drug content have been observed [129]. Fabrication from other sugars such as dextrin or dextran using a thread forming process with polypropylene [119, 126] or polyethylene tips [130], although avoids high temperature melting but is not suitable for large scale fabrication of microneedles. Casting method used by Prausnitz et al. [92, 118] utilizes polymers or sugar derivatives requiring the concentration of hydrogel using high temperature and vacuum which may have their deleterious effects on the fragile protein molecules. A microneedle roller device recently developed by Prausnitz et al. also involves the use of elevated temperatures [131]. Other methods for polymeric microneedle fabrication using techniques such as deep x-ray lithography [123], ultraviolet lithography [122], wet silicon etching and reactive ion etching [122], lens based lithographic patterning [122], photopolymerization with longer exposure to UV light [116] and laser based fabrication [125, 132] involve complex multistep procedures which accrue the overall cost of the process and make it inaccessible to many researchers. At the same time, such strenuous processes may not be suitable for encapsulation of biomolecular drugs and cosmetic molecules, which are inherently fragile and sensitive to solvents, ultraviolet light, x-rays and laser radiation.

e) Commercial microneedle products

A number of microneedle based products are available around the world, primarily for cosmetic purposes. Dermaroller®, was the first microneedle product, sold in Europe in 1999, and is now available the world over (http://www.dermaroller.com/). It consists of a cylindrical roller which holds an array of solid, metal microneedles measuring 0.2 – 2.5 mm in length and has been used for a variety of purposes, including improvement of skin texture at home by small microneedles to specific skin care treatments in clinics to treat scars and hyperpigmentation using longer microneedles. Similar products are also available from other companies (http://www.hansderma.net/, http://www.whitelotus.com.au/). The companies also provide training on use of these microneedle products. Nanomed Skincare (www.nanomed-devices.com) launched silicon microneedles devices called as SPE™ (Skin Permeation Enhancer) for cosmetic and medical applications. The devices consist of an array of nanopins with a diameter of 80 µm. LiteClear® , is a pen shaped device based on SPE™ technology, that consist of a pen shaped device holding a microneedle array at the end and a tube dispenser for delivering actives. These devices are intended for applications in acne treatment as well as wrinkles and blemish management. 3M™ Microchannel Skin System (http://solutions.3m.com/wps/portal/3M/en_US/Microchannel/Skin_Systems/) consists of an array of 351 microneedles / cm^2 , each measuring 650 µm in length and made from medical grade polymer. The device comprises of a microneedle patch and a snap-on handle. The device is intended for pretreatment of skin in dermatological and cosmetic applications, with needles expected to penetrate 100 µm into the skin with application of little force.

While these solid microneedle products do not containing any drug/cosmetics, a Japanese firm (http://www.cosmed-pharm.co.jp/) has designed a microneedle patch containing hyaluronic acid (MicroHyala®), which is intended for anti-wrinkle and whitening effect and is claimed to release active ingredients in 90 minutes. The patch was launched in 2008 is currently sold in Japan. Another Japanese cosmetics giant, Sheiseido (www.shiseido.co.jp), developed an eye patch containing hyaluronic acid. The patch consisting of 1200 microneedles was launched as Navision® in March 2011.

BD Soluvia™ prefillable microinjection system (http://www.bd.com/pharmaceuticals/products/microinjection.asp) consists of a hollow microneedle attached to a syringe that can be prefilled with drug/vaccines. The microneedle which is 1.5 mm in length is aimed to deliver drugs/vaccines intradermally. The device has been used widely for administration of first approved intradermal influenza vaccine Intanza® or IDflu®, marketed by Sanofi-Pasteur, the vaccines division of Sanofi-Aventis (http://www.sanofi.com/).

MicronJet600™ is an FDA registered medical device, which has completed world's first intradermal H1N1 flu vaccination study, demonstrating superior immunogenicity to intramuscular administration, at only 20% of the dose (http://www.nanopass.com/content-c.asp?cid=22). The device consists of a row of hollow silicon microneedles and is adaptable to any conventional syringe.

f) Microneedles in clinical trials

There are about 26 clinical trials, some of which have been completed, while others are currently underway, using microneedles for delivering vaccines, proteins, small molecular weight drugs, to carry out diagnostic tests or to study allergic reactions of skin to microneedles (http://www.clinicaltrials.gov, Keyword: Microneedle). MicronJet600™ is being tested for development of intradermal injection of lidocaine for local anaesthesia [133] insulin [134] and vaccine for influenza [135]. Lidocaine application for rapid anaesthesia has been the subject of other microneedle studies too [136]. BD Soluvia™ has been used to administer tuberculin intradermally in diagnosis of tuberculosis [137]. 3M™ Microchannel Skin System was tested for its skin irritation properties in a phase I clinical trial in 54 healthy volunteers [138]. While the results have not been made public yet, the company's website claims the system to be safe for all age and skin types and erythema formed upon application usually resolves in 1-2 minutes. Many other studies have primarily focused on vaccines like influenza and polio while others have looked at small molecules for management of osteoporosis and local skin conditions like actinic keratoses (http://www.clinicaltrials.gov).

1.3.6. In vitro skin permeation testing

Experimental evaluation of transdermal diffusion is mostly carried out using diffusion cells that have been fabricated in a variety of designs, but have a certain commonality in their elements, including a donor and a receptor chamber, having a piece of excised skin or equivalent membrane sandwiched between the two. Such studies are important in highlighting the behaviour of a dosage form *in vitro* or *ex vivo* and its likely performance *in vivo*. These devices are essential in pre-formulation studies, in assessment of extent of absorption of a particular compound from a dosage form, which helps in establishing dosing and safety profiles for a drug delivery system. Such profiles also enable cosmetic formulators to design safe products, minimizing the potential for allergic skin reactions as well as systemic side effects.

Transdermal diffusion cells have been the mainstay of *in vitro* cutaneous permeation studies since they were first conceptualized four decades ago. Apart from their major contribution in studying transdermal flux to predict possible *in vivo* absorption, they have also been used to monitor batch to batch variations, assessment of product quality and in several pre-formulation studies guiding product development [139]. Although several designs have been developed over the years, these systems, in principle, are of two major types: the static, non-flowing cells with stagnant receptor solution or the continuous flow through cells, with continual replenishment of receptor fluid also called as *in vivo* mimic diffusion systems [140, 141]. Most other features remain the same, including the donor and receptor compartments, which hold the skin tissue or an equivalent membrane in between themselves. A schematic of various types of diffusion cells in presented in **Figure 6**.

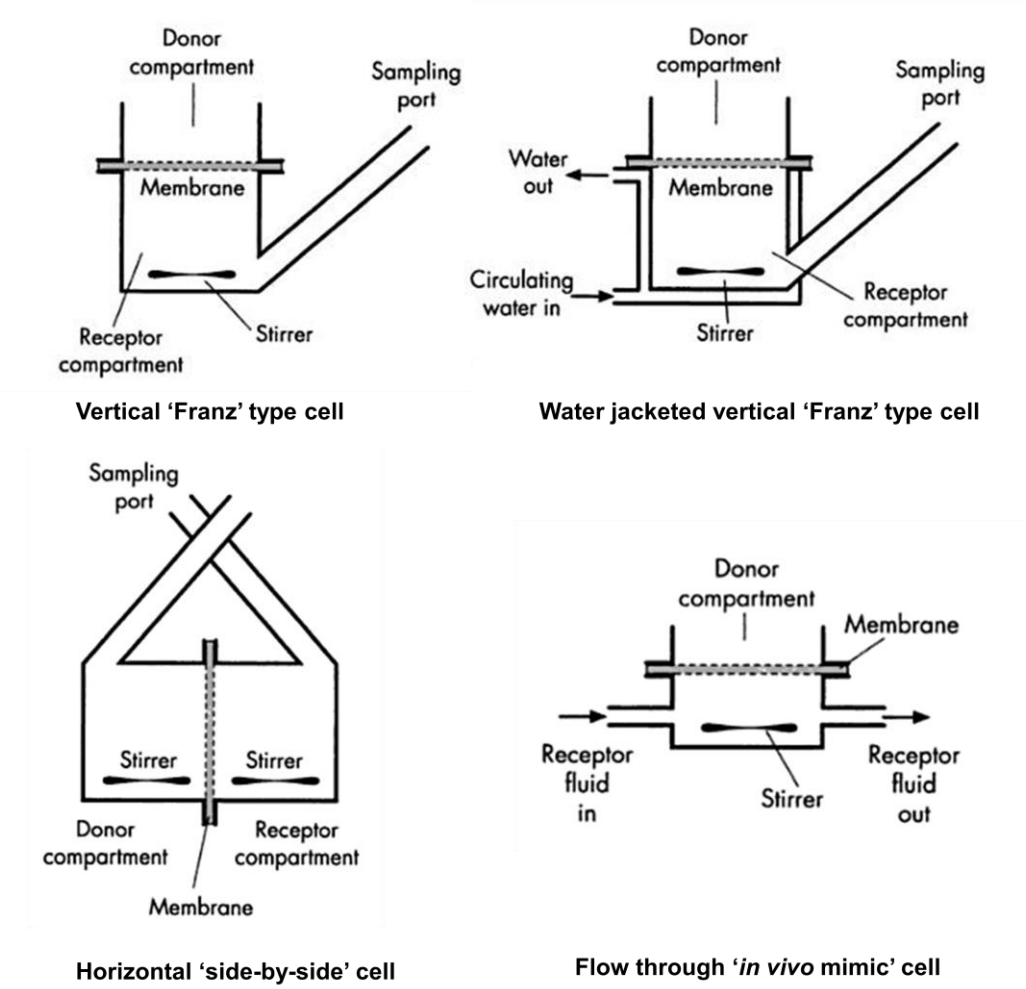

Figure 6 Schematic representations of various types of *in vitro* skin permeation systems. Adapted with permission from [141].

As temperature plays a critical role in transdermal absorption, water jackets are usually incorporated into the cell designs to maintain the temperature close to *in vivo* environment, although in some conventional designs, complete submersion of receptor compartments in a temperature controlled water bath has been practiced. A provision for agitation or constant mixing of receptor solution is incorporated, mostly by the use of magnetic stirrers. This is to avoid the formation of static diffusion boundary layers that may affect the permeation by reducing the sink conditions [142]. Since current regulatory guidelines offer only partial standardisation of *in vitro* permeation studies, a variety of diffusion cell designs with varying dimensions following laboratory customized/specific protocols have been used [143].

a) Static diffusion cells

Static diffusion cells are usually designed in two orientations, vertical (Franz) cells or horizontal (side-by-side) cells. Horizontal diffusion cells usually contain two parallel oriented cells sandwiching skin in between, tightly clamped together to prevent donor and receptor solutions from leaking. Made of glass, the donor and receptor compartments have been fabricated in various shapes and designs [144-147]. Earliest design of this shape was fabricated using brass chambers that had complicated screw threaded assembly for fixing donor and receptor chambers [148]. Large Teflon stirrers were mounted on the shafts and skin was mounted on O-rings placed on the chambers. The design required motors to turn the stirrers and the bulky design necessitated the use of large skin sample. Wurster et al. developed a modified conical flask shaped design that was used to test the permeation of model drug, sarin. The design was complicated and had no provision for temperature control. The whole assembly had to be submerged in a temperature controlled water bath and occasional shaking was required to uniformly disperse the permeated drug [149]. Further reduction in size and complexity was achieved by Southwell et al. who designed small glass chambers which can be placed over a small magnetic stirrer to allow for Teflon coated magnetic bars to be used within the diffusion cells [150]. Chien and Valia developed a water jacketed version of the horizontal cells to obviate the need to immerse the cells in a water bath. The cells had an effective skin exposure area of 0.64 cm^2, making them amenable to use with scarce human skin samples [145]. Over the years, horizontal cells have undergone several design manipulations and many of them can be easily purchased commercially as they offer the ease of operation and more intimate contact of receptor fluids with the skin, eliminating the formation of static boundary layers to a large extent. However, setting up the cell and preventing the leakage of donor and receptor compounds can be a challenging task and needs to be performed with care.

Franz type diffusion cells are the most commonly used type of *in vitro* diffusion apparatus that include a vertically oriented donor chamber and separated from a lower receptor chamber by a membrane, usually skin. A variety of donor formulations can be used with this design, allowing for

flexibility of operation. Also, as the cells are sealed by clamps in a vertical orientation, leakage of donor formulation is less often encountered. The receptor chamber is provided with a side arm as a sampling port and a mechanism to continually stir the receptor liquid is incorporated by using magnetic stirrers underneath. However, one of the main concerns with this design is the built-up of air bubbles below the skin surface, thus preventing intimate contact between receptor liquid and skin. This has to be carefully removed by tipping the cells before starting the experiment.

One of the earliest designs of this type called the skin cell was developed by Coldman et al. [151]. The device consisted of glass receptor containing 10 mL of receptor solution with a side arm for sampling. The receptor was mixed using a Teflon coated magnetic stirrer attached to a polyethylene sail. The skin was spread on a flat ground glass surface and held in place by Teflon clamps, leaving an exposed zone measuring 0.62 cm diameter. A modified design of vertical diffusion cell was developed by Southwell et al. [150]. The design had a stainless steel mesh screen to hold the skin samples above the receptor chamber. A drawback with these cells is the poorly stirred receptor liquid located in the side arm, which was undesirable.

Franz diffusion cells were first introduced by Thomas J. Franz [152]. Most of the design specifications pertaining to receptor solution, stirring mechanism and sampling remained similar to the earlier models. But, these cells were better than previously developed models as they allowed temperature control by providing in built water circulation jacket, an O-ring for effective sealing of donor and receptor together with a small donor compartment that could be sealed from the top. The design of receptor chamber, mimicking a dumbbell shaped tube with a narrow bottom and a wider top also suffered from similar drawbacks of poor mixing hydrodynamics as there was significant resistance to mixing from the constricted bottom to the stationary boundary layer in the wider top portion holding the skin [153]. Newer designs have tried to address this issue by using a spherical receptor chamber [154].

Franz diffusion cells were the first to be marketed *in vitro* permeation testing device and have undergone several design modification over the years. Several other designs have been developed since and commercialized.

A common shortcoming amongst all the static diffusion cells is their significant deviation from the dynamic *in vivo* environment where sink conditions are continually maintained underneath the skin, owing to flushing away of the absorbed drug molecules by blood flowing through the capillaries or lymph in the lymphatic circulation and lymph nodes. Hence, with greater appreciation of skin as a novel route for drug delivery, it was imperative to use *in vitro* systems that mimic the permeation conditions *in vivo*. These cells circumvent the mixing problems encountered in static cells by providing a continual replenishment of receptor solution that carries the drug across to a sampling tube. These devices are also amenable to automation, providing for minimal human involvement.

b) Flow-through diffusion cells

The first of its kind flow through diffusion cell was reported even before static diffusion cells were made. The device made from stainless steel had provision for holding skin and continuous passage of receptor fluid at a flow rate of 10-20 mL/hour [155]. The device had an effective surface area of skin exposure of 0.2 cm^2; however there was no mechanism for receptor stirring. Years later, several designs were made, most drawing their principles from the Franz static diffusion cells, in terms of design [153, 156] as well features such as automated sample collection [157] and similar permeation coefficients when compared to static versions [158]. Although most of the designs for flow-through cells are based on vertical orientation of donor and receptor chambers, horizontal orientations have also been reported [159].

It is noteworthy that flow through cells result in better prediction of *in vitro* permeation as compared to static diffusion cells, due to the dynamic flow pattern of receptor solution. Albeit, a concern with these flow-through cells is their inherent designs being in the macroscale range, requires large volumes of donor liquids. This is particularly difficult to manage during the pre-formulation studies in early drug/cosmetic development phases, where new

molecules might not be available in large quantities and may be prohibitively expensive to carry out extensive studies. Particularly with the development of new biotechnology based products, majority of which are macromolecular, hydrophilic, with low permeability coefficients, large receptor flow rates achieved in the conventional models, cause excessive dilution of permeated drug, making subsequent analysis a challenge. The large interface between donor and receptor chamber needs large skin samples, which are extremely scarce due to lack of donors and ever increasing stringency in guidelines for testing on human subjects. This calls for development of newer *in vitro* testing systems, which utilize a low volume of the reagent as well as have minimal surface area at the interface, requiring smaller skin samples.

1.4. Specific aims and objectives

Microneedle research has made rapid strides in the past few years, going from non-biocompatible materials like silicon, glass and metals to polymeric alternatives. While many microneedle products are available commercially, most of them are made of non biodegradable, potentially hazardous metals or plastics which may break off in the skin and necessitate a subsequent surgery to be removed. On the other hand some intradermal hollow microneedles require a secondary drug delivery system like syringes to deliver liquids to the dermis. These microneedles are long and may cause some amount of pain or discomfort to the users. Polymeric microneedles are hence the way forward. With the current fabrication techniques being strenuous for drug encapsulation, there is a need to develop simple microneedle fabrication method that is easily adaptable, scalable and innocuous to drug stability.

On the other hand, plethora of transdermal permeation testing platforms has been developed. However, their non suitability in case of limited drug and skin availability presents an opportunity to leverage the benefits of microfabrication to develop a miniaturized platform that utilizes minimal amounts of scarce, yet precious drug and skin samples. This thesis investigates the development of a simple lab scale photolithography based microneedle fabrication method as well as development of a miniaturized flow-through cell to test the permeation of transdermally applied drugs.

The following specific aims and objectives are outlined to realize the above mentioned goals:

1. To develop a simple photolithography based microneedle fabrication method, without the use of solvents or pre-formed moulds.
2. To determine the factors affecting microneedle geometrical properties
3. To demonstrate the ability of microneedles to penetrate animal skin models, *in vitro*.
4. To encapsulate model chemical and biological drugs in microneedles and test for their *in vitro* release and permeation through rat skin.
5. To evaluate the stability of protein molecules encapsulated in microneedles by an array of structural characterization tests.
6. To investigate the *in vitro* toxicity of microneedles by testing polymeric extracts on a variety of cell lines.
7. To evaluate the possibility of encapsulation of higher doses of a drug by integrating microneedles to a transdermal patch system.
8. To investigate the possibility of delivering cosmeceuticals using microneedles.
9. To develop a novel miniaturized transdermal permeation testing device to minimize the utilization of compounds as well as skin samples

Addressing these specific aims, this thesis is presented in **five parts** as mentioned below.

In the **first part (chapter 3)** of the thesis, the focus is to develop a simple photolithographical approach to fabricate polymeric microneedles in a mould free process. Photolithographic methods have been used previously to fabricate polymeric microneedles. However, most of the methods required fabrication of reverse moulds in the first step; followed by subsequent fabrication of microneedles in the moulds. The new method is intended to allow microneedle fabrication in a single step procedure, without the need to prefabricate the moulds, or to use any solvent to dissolve the polymers. The **second part (chapter 4)** of the thesis deals with an important application that microneedles are chiefly intended for: delivering protein drugs. Proteins, peptides and vaccines form a big group of biotherapeutics, whose

development has seen a surge in the past two decades. The surge has not been matched by the development of drug delivery systems; hence most of these compounds are still not in the market. Methods to fabricate polymeric microneedles in the past involved long exposure to UV light, melting of sugars at high temperatures and application of high vacuum to fill the moulds that may be deleterious to protein stability. The method developed in this thesis is expected to be adapted for delivering protein and peptide drugs as well as vaccines. Assessment of protein stability upon encapsulation in polymeric microneedle matrix is critical to prove the viability of photolithography as a safe method. The **third part (chapter 5)** of the thesis examines the possible clinical applications of microneedles. A shortcoming of the microneedle based transdermal systems, particularly for less potent small molecular weight drugs, is their inherent low encapsulation efficiency, as not enough drug can be encapsulated within the microstructures. This limits their use in conditions that require large dose of a drug, particularly conditions such as pain. Most transdermal delivery systems to treat conditions such as pain use conventional dosage forms such as gels, creams, ointments or transdermal patches. These however are not as effective due to differences in skin thickness and skin anatomy among individuals, leading to large variations in therapy. Integration of a transdermal patch to microneedle array could provide the advantage of active disruption of skin barrier to provide rapid delivery of drug as well as act as a source of drug reservoir for continued, sustained release over a long period of time. In this part, photolithography and ultraviolet curing were used as tools to create a microneedle integrated transdermal patch to encapsulate large doses of lidocaine to be potentially used for pain management. In the **fourth part (chapter 6)** of the thesis, an improved microneedle fabrication method is developed, to produce sharper microneedles. The conventional soft lithographic technique previously developed in part one used a planar photomask, which did not alter the path of UV light and hence had minimal effect on microneedle geometry, apart from its role in forming microstructures in a particular pattern. In an amended approach, embedded convex lenses in the photomask causing the light rays to converge to a point when they travel in the polymeric solution, was aspired to form sharp microneedles. These sharp microneedles are then investigated for

their ability to deliver cosmeceuticals. The **fifth part (chapter 7)** of this thesis deals with the development of a novel skin permeation testing device is developed based on the concepts of microfabrication. Due to the inherent design properties of the current set-ups, it is difficult to do exhaustive pre-formulation testing, without employing a large amount of the drug/cosmetic compound as well as skin samples. The idea here is to miniaturize all the components, without compromising on the testing protocol especially skin's morphology as well as maintenance of sink conditions during the permeation experiments.

CHAPTER 2

Materials and Methods

2.1. Materials

The following chemicals were purchased from Sigma-Aldrich (St. Louis, MO, USA): poly (ethylene glycol) diacrylate (PEGDA, Mn = 258), 2-hydroxy-2-methyl-propiophenone, (HMP), 3-(trimethoxysilyl) propyl methacrylate (TMSPMA), trypan blue solution (0.4 %), bovine serum albumin, lidocaine, bovine collagen type I – fluorescein isothiocyanate (FITC) conjugate, endoxifen hydrochloride and (R)-(+)-limonene and oleic acid.

Rhodamine B and sodium azide were purchased from Alfa Aesar (Lancaster, UK). 3-(4,5-dimethylthiazol-2-yl)-2,5-diphenyl tetrazolium bromide (MTT) and dimethyl sulfoxide were purchased from MP Biomedicals (Cleveland, OH). A CytoTox-ONE™ homogeneous membrane integrity assay kit was bought from Promega (Madison, WI). Sodium azide was purchased from Alfa Aesar (Lancaster, UK). BSA Texas red conjugate was bought from Molecular Probes, Invitrogen (Orlando, FL, USA). HPLC-grade acetonitrile was purchased from Tedia, USA. Phosphate buffered saline (PBS, 10×) ultra pure grade was obtained from Vivantis, Malaysia. Propylene glycol was obtained from Chempure, Singapore. Polydimethylsiloxane (PDMS) (Sylgard 184 Silicone Elastomer Kit) was obtained from Sylgard, USA. Myristyl lactate was a gift from Chemic Laboratories, USA. α-mangostin standard was supplied by Dr. Prachya Kongtawelent from Chiang Mai University, Thailand. Ultrapure water (Millipore, USA) was used in the preparation of aqueous solutions. All chemicals and materials were of analytical grade and used as received.

2.2. A simple method of microneedle array fabrication for transdermal drug delivery

2.2.1. Coating of glass coverslips

Glass coverslips (Menzel Glaser, Germany, 190 micron thickness, 22 × 22 mm) were first rinsed with 70 % ethanol and air dried. Later, they were

immersed in 0.4 % TMSPMA solution overnight for coating. The coverslips were then washed with water and baked for 2 hours at 70 ºC. TMSPMA molecules attach to the silanol groups on the glass. The resultant chemical interaction is depicted in **Figure 7**.

2.2.2. Fabrication of microneedle backing layer

Two uncoated coverslips were supported on either side of a glass slide (Sail Brand, China) as 'spacers' as shown in **Figure 7 A**. A TMSPMA coated coverslip was placed on this setup to create a cavity in the centre, approximately 190 μm thick. PEGDA, containing 0.5% w/w HMP (referred as the prepolymer solution) was wicked by capillary action into the cavity. The set up was then irradiated with high intensity ultraviolet light (11.0 W/cm^2) for 1.5 sec using UV curing station with a UV filter range of 320–500 nm (OmniCure® S200-XL, EXFO Photonic Solutions Inc., Canada). The intensity of the UV light was measured with the OmniCure® R2000 radiometer. A collimating adaptor (EXFO 810-00042) was used with the UV light probe. TMSPMA molecules bonded to the glass coverslips are covalently linked to the acrylate groups of PEGDA via free-radical polymerization (**Figure 7**, within dashed ellipses) [160, 161]. The backing layer approximately 190 μm thick was then easily removed from the setup.

2.2.3. Fabrication of microneedle shafts

The set up for fabrication of microneedles is similar to that for microneedle backing except for number of 'spacers'. Increased spacer thickness was achieved by increasing the number of coverslips stacked on either side of the glass slide as shown in **Figure 7 B**. The prepolymer solution was then similarly wicked by capillary action into the cavity. A plastic film (known as *photomask*) was inked specifically in the pattern of microneedle array. The background of this film was inked leaving small circles in an array pattern transparent to allow the UV light to pass through. The transparent circles govern the base diameter of the microneedles. Similarly, the center-to-center spacing between two microneedles can be controlled. Such a film was placed on the coverslip carrying the microneedle backing and the setup was irradiated with UV light. The use of photomask blocked the UV access in the inked

regions and allowed the UV light to pass through the transparent circles, which resulted in the formation of microneedles. The microneedles were covalently bonded with the PEGDA macromers in the backing layer to form an interpenetrating polymer network (**Figure 7 B**, within dashed rectangles) [160, 161]. The microneedle structures, attached to the coverslip, were carefully removed from the glass slide and washed with water to remove the un-crosslinked prepolymer solution. The prepared microneedles were imaged using Nikon SMZ 1500 stereomicroscope (Nikon, Japan), to quantify the microneedle geometric characteristics.

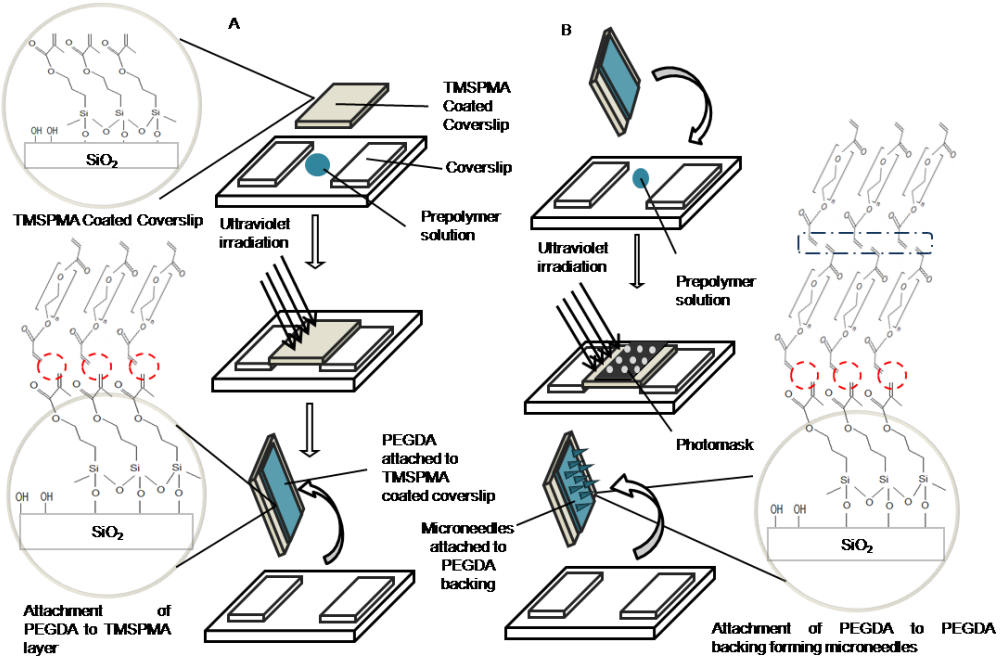

Figure 7 Schematic representation of the fabrication process. (A) PEGDA is attached to TMSPMA coated coverslip via free radical polymerisation using UV irradiation, forming the backing for microneedles. (B) Using glass slides as support, the PEGDA backing is mounted onto the set-up with PEDGA filled in the enclosed cavity. Subsequently, the set-up is irradiated with UV light. UV light is only able to pass through the clear regions on the photomask, forming microneedles.

2.2.4. Microneedle insertion in pig skin

To ascertain that microneedles penetrate the skin, PEGDA microneedles, in an 8 × 8 array were inserted into excised cadaver pig skin obtained (after the pig was sacrificed using CO_2 asphyxiation) from a local abattoir. The hair was first removed using an electric hair clipper (Philips, Hong Kong) followed by

hair removal cream *Veet*® (Reckitt Benckiser, Poland) to completely remove the hair [162]. The skin samples were cleaned and stored at −80 °C until use. Prior to use, the subcutaneous fat was removed using a scalpel. The skin was fixed fully stretched on a thin (7-8 mm) layer of modelling clay (Nikki, Malaysia), to mimic the tissue-like mechanical support. Microneedles were inserted using the force of a thumb on the backing layer for approximately 1 min. The arrays were then removed and the area of insertion was stained with trypan blue for 5 min, which specifically stains the perforated stratum corneum sites. The excess stain was washed away with water. The areas stained with the dye were viewed by brightfield microscopy using Eikona Image Soft Microscope (China). A positive control, which consisted of a 27 gauge hypodermic needle, was used to create perforations in the form of a 4 × 3 array. Intact skin stained with trypan blue was used as a negative control.

Histological examination of the skin was also carried out by the microneedle treated skin samples in to 10 μm sections using a microcryostat (Leica, Germany). The histological sections were stained with hematoxylin and eosin and imaged by stereomicroscopy. All animal experiments were approved by Institutional Animal Care and Use Committee (IACUC), National University of Singapore (NUS).

2.2.5. Encapsulation of a model drug: imaging and in vitro release

Rhodamine was dissolved in the prepolymer solution at a concentration of 0.09, 0.17 and 0.44 weight %, respectively. The drug-laden microneedle samples were imaged using a fluorescence stereomicroscope SMZ - 1500 (Nikon). The amount of drug encapsulated in the microneedles was calculated from the percent weight of the drugs in the prepolymer solution and the weight of fabricated microneedles. Selective incorporation of rhodamine B in the backing layer or microneedle shafts was made possible by using the prepolymer solutions containing the model drug to fabricate the backing layer or microneedles respectively. *In vitro* release of rhodamine B was tested by suspending fabricated microneedle arrays in 15 mL of 1 × PBS, at 37 °C and sampled at regular intervals. At each sampling point, the whole 15 mL of release medium was withdrawn and replaced with 15 mL of fresh 1 × PBS.

The samples were stored at 4 °C before analysis. The amount released was quantified by measuring rhodamine B fluorescence at excitation and emission wavelengths of 554 nm and 586 nm, respectively, with a Tecan 2000 microplate reader (Tecan, Germany) [122].

2.2.6. In vitro permeation through rat skin

To analyze the increase in skin permeability following microneedle application, cadaver rat skin was used. The subcutaneous fat was removed with a scalpel. Microneedles containing 50 μg of rhodamine B were applied to the skin samples. As a comparative control, a similar concentration of rhodamine B in propylene glycol solution in the donor compartment was used.

Skin was mounted on a side-by-side diffusion cell (TK- 6H1, Shanghai Kai Kai Science and Technology Co., Ltd, China) with receptor compartment containing 4.5 mL of 1 × PBS with 0.005% v/v sodium azide (Alfa Aesar). For each group, six replicates were used. Water was circulated at 37 °C and the donor and receptor solutions were continuously stirred at 250 rpm with magnetic stirrers. The samples were collected at regular intervals over a period of 48 hours. At each sampling point, 1 mL of receptor medium was withdrawn and replaced with 1 mL of fresh PBS. The samples were stored at 4°C before analysis. All the sample vials were centrifuged at 10,000 rpm and supernatant was analyzed by measuring rhodamine B fluorescence as previously mentioned. Cumulative amount of drug permeated against time and skin permeability was calculated by assuming a steady state flux.

2.3. Protein encapsulation in polymeric microneedles by photolithography

2.3.1. Fabrication and characterization of polymeric microneedles

The microneedles were fabricated by a photolithographic method, as described previously in section 2.2. The geometric characteristics of the microneedles (length, base, and tip diameter) were studied using an SMZ-1500 stereomicroscope (Nikon, Tokyo, Japan).

2.3.2. Incorporation and uniform protein distribution in microneedles

BSA Texas red conjugate was incorporated into the microneedle backing layer and shafts at a concentration of 0.045% w/w in the prepolymer solution to ascertain uniform distribution of drug in the polymerized microneedles. The fabricated microstructures were then imaged using a Nikon A-1R confocal microscope to observe the fluorescence intensity at various areas of the backing layer and various lengths of a microneedle shaft. The fluorescence intensity was calculated using Nikon NIS elements BR 3.1 analytical software. Microneedle arrays were also imaged with a Nikon SMZ-1500 stereomicroscope.

2.3.3. Stability tests for BSA in microneedles

a) Primary structure stability

Sodium dodecyl sulfate-polyacrylamide gel electrophoresis (SDS-PAGE) was carried out using Laemmli's method to assess the effect of ultraviolet-initiated photopolymerization on the conformational stability of BSA [163]. It was performed by casting 10% running gel and 5% stacking gel. Each formulation, containing 10 μg of protein sample as determined by bicinchoninic acid protein assay (Pierce, Rockford, IL), was mixed with an equal quantity of Laemmli sample buffer and 5% of β-mercaptoethanol. The solutions were heated at 100 °C for 2 minutes after which they were loaded onto a comb stacked on the gel cast in an electrophoresis cell. The gel was run at 100 volts for 2.5 hours. After removal from the electrophoresis cell, the gel was stained with Coomassie brilliant blue R-250 staining solution for 2 hours on an orbital shaker. The excess stain was removed by a destaining solution (20% methanol, 10% glacial acetic acid, 70% water) overnight and the gel was imaged using a Samsung ST-550 digital camera (Seoul, South Korea).

b) Secondary structure stability

Circular dichroism spectroscopy was performed on the samples to evaluate the secondary structural characteristics of BSA in the fabricated microneedles. The analysis was performed using a Jasco J-810 spectropolarimeter (Tokyo, Japan) with a 1 mm light path quartz cell (Hellma, Müllheim, Germany). Data

were acquired at a bandwidth of 0.1 nm with a scan speed of 50 nm per minute and a response time of 8 seconds. The samples and standard BSA solution were scanned over the wavelength range of 240–200 nm. The microneedle release samples were first filtered using microcentrifugal concentrators, (30 kDa cutoff, Vivaspin 20, General Electric, Addlestone, Surrey, UK) to separate the protein from the polymer. The samples were compared with a standard solution of BSA, and BSA degraded using heat (75°C) and acidic conditions (pH 2) was used as a control [164, 165]. The average value of triplicate measurements was used to plot the curve of mean residue ellipticity (in degrees cm^2 $dmol^{-1}$) to wavelength. The experimental data acquired from the spectropolarimeter were analyzed using the DichroWeb browser and a deconvolution algorithm (K2d) to calculate the mean residue ellipticity and percentage of alpha helix [166-168].

c) Tertiary structure stability

In order to evaluate tertiary structural changes in the protein conformation, their fluorescence spectra were analyzed. A standard BSA solution at a concentration of 0.026 mg/mL in purified water was prepared to compare the spectral data with the BSA released from the microneedle samples. The emission spectra were studied in the range of 300–400 nm at a fixed excitation wavelength of 280 nm using a Hitachi F-7000 fluorescence spectrophotometer (Hitachi, Japan). Similar to the circular dichroism experiments, heat-degraded and acid-degraded samples were used as a control. The fluorescence intensities were plotted against wavelength as an average of triplicate measurements.

2.3.4. In vitro release of BSA from microneedles

BSA was encapsulated in the microneedles at three different concentrations (0.5%, 0.8%, and 1.3% w/w BSA in prepolymer solution) to obtain microneedle arrays containing 0.4–1.6 mg of the protein. The *in vitro* release was determined by suspending the microneedle arrays in 15 mL of 1× phosphate buffered saline at 37 °C. Periodically, the release medium was withdrawn completely and replaced with 15 mL of fresh medium to maintain sink conditions. The collected samples were kept at 4 °C until analysis. The

protein concentration in the release samples was analyzed by a bicinchoninic acid protein assay kit. Each concentration was analyzed in triplicate and the mean value was used for analysis. The cumulative amount in mg and the percentage of BSA released were plotted against time.

2.3.5. In vitro permeation through rat skin

In vitro permeation studies were carried out in water jacketed horizontal diffusion cells as described in section 2.2.6. The skin was hydrated in the receptor solution (1× phosphate-buffered saline with 0.005% w/v sodium azide) overnight. The skin was placed stretched on ten layers of Kimwipes (Kimberly-Clark, Roswell, GA) to provide tissue-like mechanical support [122]. Microneedles containing 0.7%, 1.42%, and 1.85% w/w BSA were applied to abdominal rat skin after removing the subcutaneous fat. Microneedles containing no BSA were used to blank the inherent protein released from the skin. BSA dissolved in propylene glycol was used to compare the enhancement of BSA permeation by microneedles over passive diffusion. The microneedle array was secured on the skin using scotch tape and the skin was placed between the donor and receptor compartments. The receptor compartment was filled with 4.5 mL of receptor solution, which was continuously stirred at 250 rpm using a Teflon-coated magnetic stirrer. At each sampling point, 1 mL of receptor solution was withdrawn and replaced with fresh receptor solution. The collected samples were stored at 4°C until they were analyzed. All samples were centrifuged at 10,000 rpm for 5 minutes and the supernatant was collected for analysis. The concentration of permeated BSA was determined by the ultraviolet A_{215}–A_{225} method [169]. Each sample was analyzed in triplicate. The cumulative amount of drug permeated per unit area was plotted against time.

2.3.6. In vitro cytotoxicity of polymeric microneedles

Cytotoxicity of the microneedle materials was assessed by the viability of three different cell lines using colorimetric determination of mitochondrial succinate dehydrogenase activity using the MTT assay [170]. Human dermal fibroblasts, human adult low calcium high temperature (HaCaT) keratinocytes,

and human embryonic kidney (HEK293) cells were used to assess the toxicity of the polymer used in fabricating the microneedles. The cells were grown in Dulbecco's modified Eagle's medium (DMEM) supplemented by 10% fetal bovine serum and 1% penicillin-streptomycin solution. After the cells had achieved 80% – 90% confluency, they were trypsinized and counted. Cells (1×10^4 cells/well) were plated into 96-well microtiter plates (Corning, NY) in 200 μL of growth medium. After 24 hours of plating, 20 μL of polymer extracts (prepared by extracting the polymer from fabricated microneedles in 1× phosphate-buffered saline at 37 °C for 24 hours) were added to each well. Positive control consisted of wells containing 20 μL 1× phosphate-buffered saline. The plates were incubated at 37 °C in humidified 5% CO_2 for 24, 48, and 72 hours. The medium was aspirated at the respective analysis point, and 20 μL of MTT solution (5 mg/mL in phosphate-buffered saline) was added to each well, followed by 200 μL of growth medium. The plates were incubated for 4 hours at 37 °C. After 4 hours, the medium was aspirated again and 150 μL of dimethyl sulfoxide was added into each well to dissolve the formazan crystals formed, with the aid of a plate shaker operated at 100 rpm. The colorimetric assay was carried out by measuring the absorbance at 595 nm using a Tecan 2000 microplate reader (Tecan, Germany). The cell viabilities were calculated as a percentage of the control.

The toxicity of the polymer was also assessed by analyzing the amount of lactate dehydrogenase released from the membranes of damaged cells [171]. The cells were cultured in well plates in a similar manner as described above and treated with polymer extract and phosphate-buffered saline. Maximum lactate dehydrogenase release was achieved by treating the cells with the lysis solution (9% w/v Triton X-100) provided by the manufacturer. The assay was performed according to the manufacturer's protocol using the CytoTox-ONE™ Homogeneous Membrane Integrity Assay kit. The percentage toxicity was calculated using the following equation, where $Polymer_{LDH}$, $Vehicle_{LDH}$, and $Triton_{LDH}$ represent the respective fluorescence values obtained from wells treated with polymer, phosphate-buffered saline, and Triton X-100.

$$Cytotoxicity(\%) = \frac{Polymer_{LDH} - Vehicle_{LDH}}{Triton_{LDH} - Vehicle_{LDH}} \times 100$$

2.4. Microneedle integrated transdermal patch for fast onset and sustained delivery of lidocaine in acute and chronic analgesic applications

2.4.1. Fabrication of microneedle integrated transdermal patch (MITP)

Fabrication of MITP consists of two phases. In the phase one, a microneedle array was fabricated as described previously in section 2.2 [117]. Briefly, PEGDA containing 0.5% v/v of HMP (called as 'prepolymer' solution) was filled into a 190 µm high preformed cavity made from glass slides and coverslips The solution was then exposed to a high power (12.9 W/cm^2) ultraviolet (UV) light source (Exfo®, Canada) for 2 seconds. This resulted in the formation of a thin film (microneedle backing) that acts as a support for subsequently fabricated microneedle shafts. Following this, the thin film was removed from the fabrication set-up and placed on another similar set-up scaffold, 950 µm in height. The cavity formed was filled with prepolymer solution and exposed to UV (12.9 W/cm^2) through a specially patterned photomask, for a duration of 4.3 seconds, forming the microneedle shafts. The remaining prepolymer solution was pipetted out and microneedles were rinsed with water to remove any un-crosslinked polymer and left to air dry.

In the second phase of fabrication, low power ultraviolet curing was used to fabricate a thick patch for enhanced drug loading capacity. A cavity measuring 1.2 mm in height was created using glass slides as base and spacers and a coverslip as a lid shown in **Figure 8 A**. Prepolymer solution was wicked in to this cavity and a thick patch of polymer was cured using a low intensity (5.8 mW/cm^2) ultraviolet radiation source (Single-side Mask Aligner, H94-25, Sichuan Nanguang Vacuum Technology Co. Ltd, China) for a duration of 15 seconds. The patch was then removed from the set-up using a blade and placed on another glass slide as shown in **Figure 8 B**. At this stage, the microneedle array fabricated in phase I was integrated to the thick patch fabricated in phase II. A drop of prepolymer solution was spread evenly over the surface of the thick patch and microneedle array was placed over it. The integrated set-up was exposed to a high power (12.9 W/cm^2) UV radiation for

a period of 3 seconds, to facilitate the binding between the two layers through formation of interpenetrating polymer networks [160].

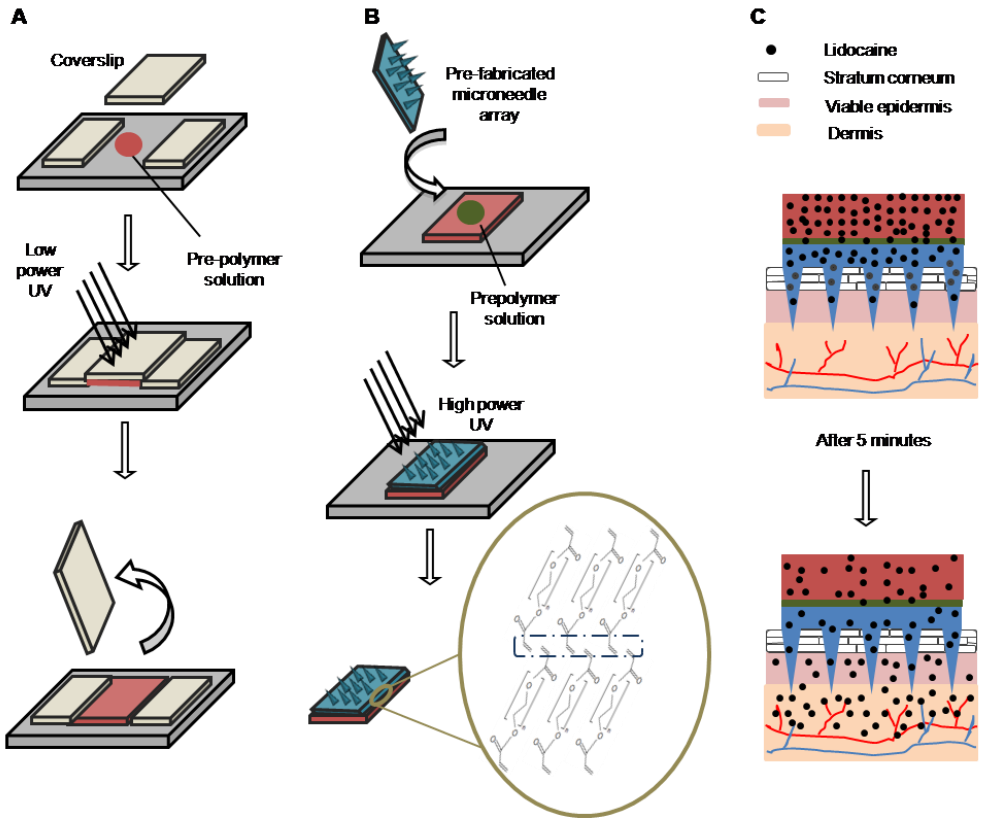

Figure 8 Schematic showing fabrication of microneedle integrated transdermal patch (MITP) using ultraviolet curing. (A) Fabrication of thick transdermal patch using low intensity UV irradiation, (B) conjugation of pre-fabricated microneedle array from [117] to the thick patch by ultraviolet curing forming interpenetrating polymer networks and (C) rapid release (within 5 minutes) of lidocaine from MITP, potentially providing rapid pain relief.

2.4.2. Drug encapsulation in MITP

Incorporation of lidocaine in the MITP was achieved by dissolution of the drug in the prepolymer solution prior to UV curing. Various concentrations (2.2%, 15% and 21% w/w) of lidocaine were dissolved in prepolymer solution followed by fabrication of MITP. As all the liquid prepolymer was converted to solid polymer, the amount of lidocaine encapsulated in MITP was determined by weighing the MITP specimens and calculating the amount on weight by weight basis. Selective incorporation of drugs in a specific layer of MITP could be possible by using the drug containing prepolymer solutions to specifically fabricate that layer, while other components can be fabricated

using drug free prepolymer solution. **Figure 8 C** demonstrates a schematic showing rapid release of lidocaine from MITP and its subsequent diffusion through skin's layers upon application. Rhodamine B was encapsulated at 0.075 % w/v in prepolymer solution to image the drug distribution using a Nikon AZ 100 microscope (Nikon, Japan).

2.4.3. Mechanical strength of MITP

To determine the mechanical strength of the microneedles on the integrated patch, an electronic force gauge (Dillon Model GL, USA) held on a test stand (Dillon CT manual test stand) was used. The fracture force of the microneedles was first determined by placing the microneedles on a flat block of aluminium [172] and rotating the hand wheel of the test stand slowly till the force probe contacts the top of the patch. Successive increase in application force caused the microneedles to break, with a sudden decrease in the amount of force exerted. This point was taken to be the fracture force of the microneedle [173]. As a comparative control, force of a thumb was obtained from 5 individuals, males and females, aged 21-25, by pressing the thumb of the stronger hand against the force gauge probe.

The effect of varying the amount of force exerted on the microneedle patch was also investigated for studying the degree of skin penetration. De-fatted rat skin was placed on top of 10 layers of Kimwipes® to provide a tissue like mechanical support [122]. Varying forces (10N, 30N, 50N, 70N) were exerted on the microneedles placed on rat skin for 1 minute. The extent of needle penetration into the rat skin was determined by the trypan blue staining method [117]. Trypan blue was placed on the microneedle treated skin with a dropper for 5 minutes and removed gently using Kimwipes® and 70% ethanol. Skin samples were then viewed under the hand-held microscope (Eikona Image Soft, China).

2.4.4. In vitro release test

In order to ensure that lidocaine could diffuse out of the integrated patch, an *in vitro* release test was conducted. First, the upper surface of the integrated patch was covered with a waterproof vinyl tape (3M® Vinyl Tape) to prevent

diffusion of lidocaine from the upper surface (which will be in contact with the air during *in vivo* application) of the integrated patch. After which, the integrated patch was immersed in 15 mL of 1× phosphate buffered saline (PBS) in a falcon tube incubated at 37°C and sampled at regular intervals. At each sampling point, all 15 mL of the release solution was withdrawn and replaced with fresh PBS. A positive control to determine the release of lidocaine from Lignopad® was done as well. The amount of lidocaine released into PBS was determined by high performance liquid chromatography (HPLC) method described in section 2.4.6.

To characterize the surface properties of microneedles before and after the release test, samples with different concentrations of lidocaine were imaged using a JSM - 6701F field emission scanning electron microscope (JEOL, Japan) at an acceleration voltage of 5 kV. The microneedles samples were first platinum sputter coated using a JFC – 1600 autofine coater (JEOL, Japan) at a current of 20 mA for 30 seconds to provide a coating of 5 nm thickness

2.4.5. In vitro rat skin permeation study

To determine the enhancement of rate of delivery of lidocaine by MITP, an *in vitro* skin permeation study was carried out. Cadaver rat skin was used to determine the comparative rate and extent of permeation of lidocaine through the skin between the fabricated MITP and commercial lidocaine patch, Lignopad®. The skin from the same rat was divided into 6 portions in order to minimize inter-animal variation: 3 replicates with Lignopad® placed on intact skin and 3 replicates using the fabricated MITP. For the application of MITP, 10 layers of Kimwipes® which mimic underlying skin tissues was used to support the rat skin. The integrated patch was applied on the skin for 1 minute with the force of a thumb. The array was then secured onto the skin using Scotch® tape.

The rat skins with the patches were mounted on horizontal diffusion cells with an effective exposed area of 1.131 cm^2. The diffusion cells were maintained at 37 °C by a circulating water jacket and the solutions were continuously stirred at 250 rpm. The receptor cells were filled with 4.5 mL of PBS with 0.005 %w /v sodium azide as an anti microbial agent and samples were taken at regular

intervals [174]. 4 mL of receptor solution was withdrawn at each time interval and replaced with the same amount of fresh receptor solution. The samples were stored at 4 °C upon collection and they were centrifuged at 10,000 rpm for 5 minutes before the supernatant was withdrawn for HPLC analysis.

2.4.6. HPLC analysis of lidocaine

The amount of lidocaine released/permeated is analyzed using Hitachi L2000 LaChrome Elite HPLC system with a Hypersil ODS C_{18} reverse column (ODS hypersil, Thermo Scientific; 4.6 × 250 mm, 5 μm). The mobile phase used was acetonitrile : water (70:30 v/v) with 5.5% v/v triethylamine, which was filtered through a nylon membrane filter (Whatman®, Germany) and sonicated before use. The flow rate of the pump was maintained at 0.7 mL/min and each run was 8.0 min long. 20 μL of sample was injected during each run and UV detection was performed at a wavelength of 254 nm [175].

Before analyzing the samples, standard lidocaine curves were plotted by preparing standard lidocaine solutions of 0.2, 1.0, 10.0 mg/mL. Injection volumes of 2, 5, 10, 15 and 20 μL were drawn from the standard solutions to obtain 3 calibration curves. The peaks obtained from the samples were then compared to the calibration curves and the amount of lidocaine present in the injected sample was extrapolated.

2.4.7. Interaction between polymer and lidocaine: FTIR-ATR spectroscopy

To verify the interactions between the PEGDA and lidocaine, fourier transformed infrared attenuated total reflectance (FTIR-ATR) spectroscopy using Spotlight 400 FTIR Imaging System (PerkinElmer, CT, USA) with an ATR accessory having a diamond crystal, was carried out. The spectra of the pre-polymer solution with and without lidocaine, and that of the polymerized film with and without lidocaine were obtained. The films (190 μm thick) were fabricated under identical conditions as used for MITP fabrication, to expose the polymer and drug to same extent of UV radiation. To analyze liquid samples, a drop of liquid was placed on top of and covering the crystal. For solid samples, the solid was placed on top of the crystal and a pressure arm

was positioned over the sample to exert a force of ~80 N on the sample. No additional sample preparation was required for IR analysis.

2.5. Direct Microneedle Array Fabrication off a Photomask to Deliver Collagen through Skin

2.5.1. Fabrication of photomask with embedded microlenses

A 4" Pyrex glass wafer (Corning 7740) was first cleaned in piranha (H_2SO_4/ H_2O_2) for 20 minutes at 120 °C as shown in **Figure 9 A**. Later an e-beam evaporator was used to deposit a Chromium/Gold (Cr/Au) layer (30 nm/1 µm) [176] on the glass wafer. A classical photolithographic process using an AZ7220 positive photoresist was utilized to create patterns in the Cr/Au layer using Cr/Au etchant. In order to increase the quality of the Cr/Au/photoresist masking layer, a hard baking process was performed on a hot plate at 120 °C for 30 minutes [177]. The opposite surface of the glass wafer was temporary bonded using wax on a dummy silicon wafer in order to conserve the quality of the surface during the wet etching process. Isotropic etching of the lens was performed using an optimized hydrofluoric acid (49%) / hydrochloric acid (37%) in 10/1 volumetric ratio [178] using magnetic stirring for 8.5 minutes (having an etching rate of 7 µm/min). Separation of glass wafer from the dummy silicon wafer was performed by placing on a hot plate (at 100 °C). Over-hanging photoresist and Cr/Au layers at the edges of the lenses were removed by ultrasonication. Finally, removal of the photoresist mask and residual wax was done by cleaning in *N*-Methyl-2-pyrrolidone at 80 °C in an ultrasonic tank. Microscopic analysis of the photomask dimensions were performed by directly imaging the photomask and the PDMS mold replicas copied from the microlenses with a scanning electron microscope and Nikon SMZ 1500 stereomicroscope (Nikon, Japan) respectively.

2.5.2. Fabrication of microneedle shafts

A photomask (1 × 1 cm) consisting of an array of 7 × 7 embedded lenses was used for the fabrication process. A cavity, measuring 2.5 × 0.9 cm, was created using glass slides as shown in **Figure 9 B**. The number of glass sides used determines the height of the cavity (referred to as spacer thickness).

Increased spacer thickness was achieved by increasing the number of glass slides stacked on either side of the glass. The photomask was positioned to ensure that the chromium coated surface faced the interior of the cavity with none of the lenses being obscured by the sides of the cavity walls. PEGDA, containing 0.5% w/w HMP (referred as prepolymer solution) was filled into the cavity until the chromium coated surface was in contact with the solution without any visible bubble. The setup was then irradiated with high intensity ultraviolet light of the desired intensity for 1 sec at the distance of 3.5 cm from the UV source using UV curing station with a UV filter range of 320-500 nm (OmniCure S200-XL, EXFO Photonic Solutions Inc., Canada). The intensity of the UV light was measured with the OmniCure R2000 radiometer. A collimating adaptor (EXFO 810-00042) was used with the UV light probe. After exposure to UV light, the photomask with the array of needles was removed and the remaining prepolymer solution could be reused. The use of the photomask blocked the UV access in the chromium-coated regions and allowed UV light to pass through the embedded lenses followed by subsequent refraction of light rays to a focal point that determines the height of the microneedles formed. The prepared microneedles were then imaged using Nikon SMZ 1500 stereomicroscope (Nikon, Japan), to quantify the microneedle length and tip diameter.

2.5.3. Fabrication of microneedle backing layer

The photomask with needles was placed in a well of a 24-well plate (Thermo Fisher Scientific, USA) as shown in **Figure 9 C**. A specified volume (300 and 400 µL) of prepolymer solution was added to the well until the needles were submerged to a desired height. The volume of prepolymer solution used determines the thickness of the backing layer. The set up was then irradiated with high intensity ultraviolet light (15.1 W/cm^2) from a distance of 10.5 cm from the UV source for a duration of 1 second. After polymerization, the microneedle with the backing layer was separated from the photomask. Microneedles of two different lengths with minimal differences in tip diameter could be achieved via this method. The prepared microneedles with the backing layer were then imaged using Nikon AZ100 stereomicroscope

(Nikon, Japan), to quantify the microneedle length, tip diameter and base diameter.

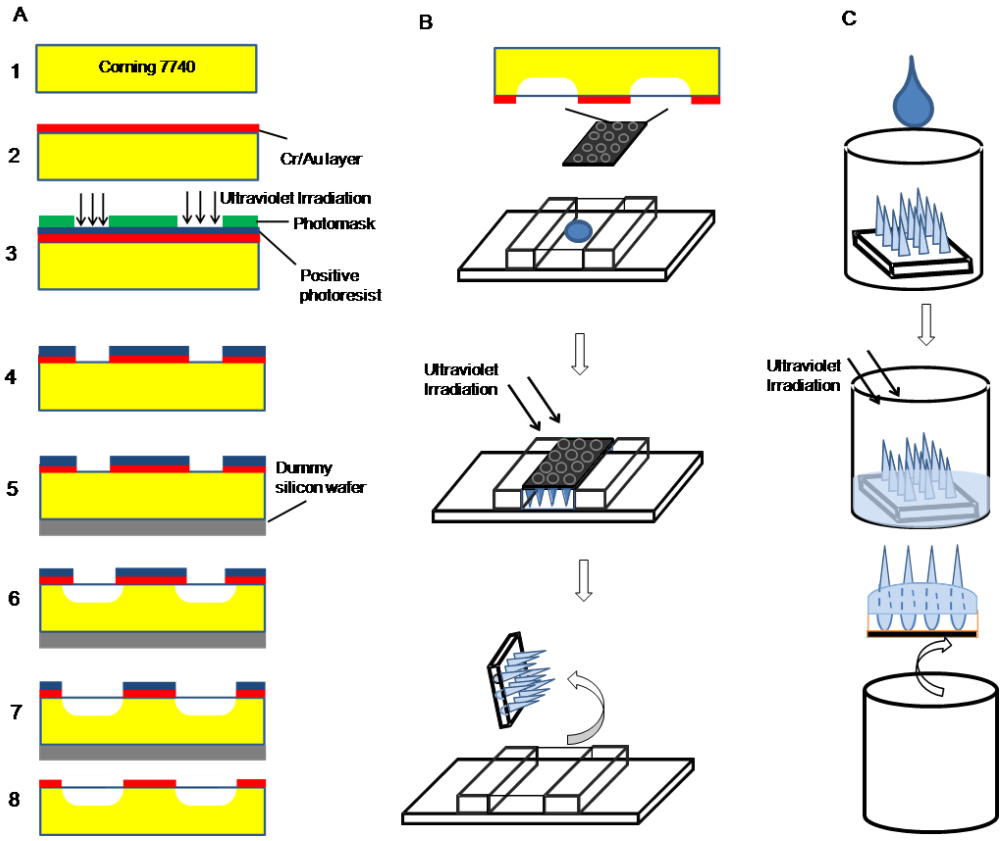

Figure 9 (A) Schematic representation of the fabrication process of lenses-embedded photomask. (1) 4" glass wafer. (2) Cr/Au layer deposited using an e-beam evaporator. (3) Exposure of Cr/Au/photoresist masking layer to UV light with photomask. (4) Formation of pattern on layer using Cr/Au etchant. (5) Temporary bonding of glass on a dummy silicon wafer. (6) – (7) Wet etching (isotropic) process using HF/HCl etchants followed by ultra-sonication. (8) Debonding of dummy silicon wafer and removal of photoresist layer. (B) Schematic representation of the fabrication process of needles. Chromium coated photomask (7 × 7 array), is placed over a cavity containing pre-polymer solution and exposed to UV irradiation. (C) Schematic representation of the fabrication process of the backing layer. Photomask, with microneedles attached, is placed in a well filled with pre-polymer and exposed to UV irradiation.

2.5.4. Microneedle fracture force testing

Microneedles of two different lengths were pressed against an aluminium plate with a force applied by a Dillon GL-500 digital force gauge (Dillon, USA) [172]. The applied force was increased until maximum resistance was observed. The force at which microneedles start to break (fracture force) was recorded after which microneedles were imaged using Leica M205FA

stereomicroscope (Leica, Germany), to assess the changes in the microneedle geometric characteristics.

2.5.5. Sharper microneedle penetration in cadaver human skin

Microneedles of two different average lengths were inserted into cadaver human back skin obtained through posthumous organ donation by a 75 year old, white female. The skin was laid stretched on a board and microneedle shafts of both lengths were inserted using the force of a thumb for 1 min. The microneedles were then removed and the area of insertion was stained with trypan blue for 12 minutes. The excess stain was wiped away using Kimwipes and ethanol (70%). The areas stained with the dye were viewed by brightfield microscopy using Eikona Image Soft Microscope (China).

2.5.6. Collagen permeation through rat skin

Microneedles of the two different lengths were inserted into excised rat abdominal skin after removal of hair and fat as mentioned previously in section 2.26 and 2.3.5. A force of 10 Newton (N) [179] was applied using the Dillon GL-500 digital force gauge [172] for 2 minutes. Bovine skin collagen type 1, FITC conjugate (MW= 300 kDa) of concentrations 0.025, 0.050 and 0.075% w/v was obtained by diluting the stock collagen solution (0.1% w/v) with appropriate amount of 0.1M Tris-HCl buffer (pH 7.8) containing 0.4 M NaCl, 10 mM $CaCl_2$ and 0.25 M glucose [180]. NaCl and $CaCl_2$ aid in stabilizing the collagen molecules and glucose is added to prevent gelation of the collagen fibers [180]. Each collagen concentration was applied to separate skin samples at the area of insertion. The time of contact between the collagen solution and the skin was kept constant at 4 hours [181] at room temperature, after which excess collagen on the skin surface was removed using Kimwipes®. The degree of permeation of collagen through the skin was quantified by using the A-1R confocal microscope (Nikon, Japan) to observe the fluorescence intensity of collagen type 1, FITC conjugate at excitation and emission wavelengths of 490 nm and 520 nm respectively. Other parameters including high voltage (150), offset (-1), laser (7.2% of 150 mW), pinhole (1.2 A.U), optical sectioning (16.6 µm), scan size (512 × 512), scan speed (1

frame/sec), pixel dwell (2.2 µsec), lever average (4), zoom (5×), step size (5 µm) and intensity calculation (low = 300, high = 4095) were kept constant.

2.6. A Miniaturized Flow-through Cell (MFtC) for testing the permeation of drugs across biological membranes

2.6.1. Fabrication of miniaturized flow-through cell (MFtC)

The fabrication process involved two simple polydimethylsiloxane (PDMS) moulding steps. Firstly, for fabricating the receptor compartment (16 mm tall, 22 mm wide), a specially designed borosilicate glass mould (16 mm wide) was inserted into a single well of a 12-well plate, (Cellstar, Greiner Bio-One), carrying 0.9 mm poly vinyl chloride tubing, (B. Braun, Germany) bore through its axis. The borosilicate glass sits firmly in a small split created in the tubing. PDMS was then filled into the cavity between the glass mould and the well plate (**Figure 10 A**) and was subsequently cured at 70 °C for 2 hours. The glass mould was then removed to create a hollow cavity for donor compartment to sit in.

The donor compartment (13 mm tall, 16 mm wide) was fabricated with a similar process in a single well of a 24-well plate. A 6 mm hollow lumen was first created with a metal mold (**Figure 10 B**). The mold was placed in the well of the 24-well plate and PDMS was used to fill the space between the external wall of the mold and the 24-well plate and was similarly cured at 70 °C for 2 hours. The metal mold was removed to create a hollow cavity, to serve as the donor liquid compartment. As part of the property of MFtC, donor compartment was designed to hold up to 283 µL of drug solution with an area of 0.283 cm^2. The assembled donor and receptor compartments are shown in **Figure 10 C**.

2.6.2. Assembly and operation of MFtC

MFtC was assembled by connecting the tubing of the fabricated cell to an infusion pump system (Terufusion, UK) at one end and sampling tubes at the other end (**Figure 10 D**). The fabricated diffusion cell was then placed in a

water bath maintained at 37 °C using a hot plate. Drug solution is placed in donor compartment. Flow rate of the receptor solution through the fabricated diffusion cell was controlled by the infusion pump that delivers the solution from a syringe (**Figure 10 D**).

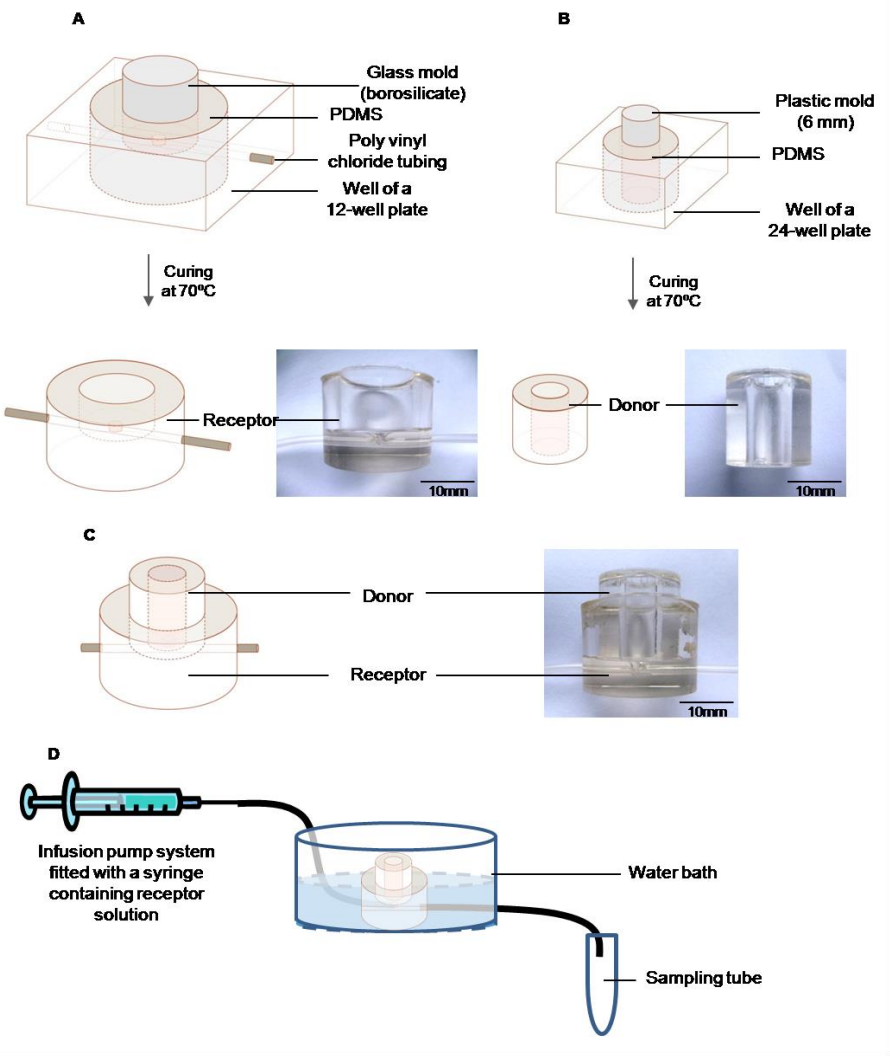

Figure 10 Schematic diagram of fabrication process of (A) donor compartment and (B) receptor compartment. (C) Full assembly of fabricated diffusion cell. (D) Schematic diagram of full assembly of Miniaturized Flow-through Cell (MFtC).

2.6.3. Validation of MFtC against horizontal diffusion cell

a) Skin permeation of model drugs using both diffusion cells

To evaluate the performance characteristics of the MFtC, permeation of model compounds rhodamine B and mangostin using a horizontal diffusion cell (TK-6H1, Shanghai Kai Kai Technology, China) and MFtC were compared.

Rat abdominal skins were obtained from National University of Singapore Animal Centre and kept at −80 °C until use. Prior to permeation studies, the skins were thawed and hair was completely removed with an electrical shaver and hair removal cream (Veet®). Subcutaneous fat and connective tissues were also lightly trimmed off.

Rat abdominal skin of 2.0 cm × 2.0 cm was mounted between the donor and receptor compartments of the horizontal diffusion cell, with stratum corneum side facing the donor compartment. The effective diffusion area was 1.13 cm^2. Each donor cell contained 4.5 mL of each model compound in propylene glycol (PG) and the receptor cell contained the same volume of PBS. Mangostin was used at a concentration of 2.3 mg/mL and rhodamine B at concentrations of 1 mg/mL and 5 mg/mL. Both compartments were thermostated at 37 °C by means of a surrounding temperature controlled water jacket. In order to minimize evaporation, all cell openings were occluded with parafilm. The fluids in both compartments were maintained in a stirred state by a Teflon coated magnetic stirrer at a speed of 250 ± 1.25 rpm. Samples (1 mL) were withdrawn from the receptor compartment for analysis at specific time intervals. Upon each sample withdrawal, the receptor compartment was immediately replaced by equal volume of fresh solution. The experiments were performed in triplicates or more.

Similar conditions were used in the MFtC setup. Rat abdominal skin of 1.0 cm × 1.0 cm was mounted between the donor compartment and the receptor compartment with the stratum corneum side facing the donor compartment of this apparatus. High vacuum grease (Dow Corning, USA) was applied to the donor compartment on unexposed stratum corneum side, in contact with receptor compartment, to minimize leakage from the donor compartment. Application of grease prevented the leakage of donor solution, even at the end of 48 hr study, which could be observed when no grease was applied. The effective diffusion area was 0.283 cm^2. 70 µL of the donor solution was added into the donor compartment. Degassed PBS solution constituted the receptor fluid. Flow rate of each diffusion cell was controlled by an infusion pump at 0.20 mL/hr. MFtC were placed in a water bath maintained at 37 °C using a hot plate. In order to minimize evaporation, the donor compartment and sampling

microfuge tubes were occluded with parafilm. The sampling tubes were collected at specific time intervals and replaced by empty tubes for subsequent collections. The experiments were performed in triplicates or more.

Skin samples from the same rat were used for comparisons between the horizontal diffusion cell and MFtC setups to minimise inter-animal variability. All experiments were performed at least three times. The samples were collected at the same time intervals and stored at 4 °C until analysis. During analysis, samples were first centrifuged at 13,000 rpm (Sorvall Biofuge Pico, UK) for 5 min. The supernatant was obtained and analyzed according to their respective assay methods as reported below.

b) Fluorimetric analysis of rhodamine B

Concentration of rhodamine B was determined by fluorescence spectroscopy with a microplate reader (Tecan, Switzerland) [182, 183] at an excitation wavelength (λ_{ex}) = 554 nm and an emission wavelength (λ_{em}) = 586 nm at ambient temperature. All samples were protected from light to prevent possible light quenching of fluorescence during the assay [184].

c) HPLC analysis of mangostin

Mangostin concentration was determined with a reversed phase HPLC (Hitachi, Japan) using a C18 column (5 µm, 4.6 mm × 250 mm; ODS Hypersil, Thermo Scientific) maintained at ambient temperature. The mobile phase comprised of methanol and ultrapure water (90:10, v/v) delivered at a flow rate of 1 mL/min. The UV detector (L-2400, Hitachi, Japan) was operated at a λ = 320 nm. Under these conditions, the mangostin peak appeared at a retention time of 6.8 min.

d) Histological analysis of skin from both diffusion cells

Comparison of change in skin's properties when applied on a diffusion cell for a particular period of time was done by histological examination of the skin applied to MFtC and horizontal diffusion cell. For this purpose, defatted rat skin was clamped in both the diffusion cells in a manner described above. PG was applied to the donor side and receptor comprised of PBS. Histological

examination of skin applied to both the diffusion cells was carried out at 0, 24 and 48 h post application by cutting the skin longitudinally into 20 µm sections using a microcryostat (Leica, Germany). Subsequently the sections were fixed in absolute ethanol and stained with hematoxylin and eosin and imaged using a Nikon AZ100 (Nikon, Japan) microscope.

2.6.4. Permeation testing of a novel anticancer drug, endoxifen

a) Endoxifen fluorescence assay

A fluorescence assay for endoxifen was established whereby endoxifen was converted to highly fluorescent phenanthrene derivatives following exposure to ultraviolet (UV) irradiation [185, 186]. A UV transilluminator (BioRad, USA) at a λ = 302 nm and an intensity of 866 µW/cm^2 was used for the conversion of endoxifen to its phenanthrene derivatives. The fluorescence emitted from the phenanthrene derivatives of endoxifen after various durations of UV exposure was determined with a microplate reader at a λ_{ex} = 260 nm and a λ_{em} = 380 nm. Fluorescence measurements from non-UV exposed samples served as a control. The optimum duration of UV irradiation was determined with 10 µg/mL solution of endoxifen. For all subsequent experiments, this duration of UV irradiation was fixed at the optimal time.

The linearity and sensitivity of the assay were determined by spiking endoxifen in PBS at eleven concentrations (0.78–25.00 µg/mL). The fluorescence, obtained post UV irradiation, was plotted against endoxifen concentrations. Linear regression was performed to obtain the slope and intercept. The limit of detection (LOD) and limit of quantification (LOQ) were set as three and ten times the standard deviation of the blank respectively [187].

The intra-day accuracy and precision of the assay method were determined by spiking receptor solution collected from a permeation study with PG as the donor solution with four concentrations (1.56–12.50 µg/mL) of endoxifen. Aliquots of these samples were analyzed on three occasions on the same day. Triplicates were prepared for each analysis.

b) Endoxifen permeation testing

The validated MFtC mounted with rat abdominal skin was employed to determine the permeation profile of endoxifen. Donor solutions consisting of endoxifen (2 mg/mL) in PG with and without permeation enhancers (PEs) namely limonene, myristyl lactate and oleic acid at 0.5% (w/v) were prepared. All solutions were sonicated for 3 min to ensure dissolution of endoxifen and PEs [185]. Each donor compartment was filled with 200 µL of donor solution. Endoxifen was allowed to permeate through the rat abdominal skin over 48 hr. The experiments were performed in triplicates. Samples of permeated solutions were collected at specific time intervals and stored at −20 °C until analysis. The flux at steady state (J_{ss}) and lag time were obtained from the cumulative plots. The effect of the PEs on the flux was evaluated by calculating the enhancement index (EI).

2.7. Statistical analysis

All experiments were carried out in triplicates, unless otherwise stated. Results were stated as mean ± standard deviation. One-way ANOVA was used, for analyzing multiple groups of data or statistical differences (IBM SPSS PASW Statistics 18). Independent sample t-test was used wherever applicable. Results with *p* value of less than 0.05 were considered to be statistically significant.

CHAPTER 3

A Simple Method of Microneedle Array Fabrication for Transdermal Drug Delivery

(Adapted from *Drug Development and Industrial Pharmacy*. 2013; 39 (2): 299-309)

3.1. Overview

Despite some special advantages over their silicon and metallic predecessors, microneedles fabricated from polymers and sugars present some processing concerns. Microneedles developed from sugars [128, 129] pose processing difficulties due to high melting points of sugars (140–160°C) and substantial losses in the drug content [129]. Similarly, high temperatures have been used for the casting methods used by other groups for fabricating polymeric microneedles [92, 118]. A microneedle roller device recently developed also involves the use of elevated temperatures [131]. Fabrication from other sugars such as dextrin using a thread forming process with polypropylene [119, 126] or polyethylene tips [130], has been adapted for single-needle/micropile fabrication, which may limit the amount of drug encapsulation [188].

Other methods involve techniques such as deep X-ray lithography, ultraviolet lithography, wet silicon etching and reactive ion etching, lens based lithographic patterning, photopolymerization with longer exposure to UV light and laser based fabrication involve sophisticated equipments which accrue the overall cost of the process and make it potentially inaccessible to many researchers.

In this chapter, a simple photo-polymerization method to fabricate microneedles with poly (ethylene glycol) diacrylate (PEGDA) is described. PEGDA was used owing to its known biocompatibility [189] and FDA approval for human use [190]. It has a long history as non toxic and non immunogenic polymer, widely used for several drug delivery applications [191]. Compared with the photo-crosslinkable monomer vinyl pyrrolidone [116, 192], the macromer PEGDA can be cross-linked in short time under UV

(a few seconds). In addition, PEGDA used in this study (Mn = 258) has a larger molecular weight than vinyl pyrrolidone (MW = 111), which may indicate better biocompatibility [193].

Moreover, its extensive use as a substrate for tissue engineering [194, 195] also makes it a potentially useful biomaterial for microneedle fabrication. The fabrication method is based on photolithography, involving exposure of the polymer to UV light through a patterned mask in a single step process. The method offers the advantage of short exposure to UV light. It is similar to the commercial manufacture of contact lenses, which also employs a mask based photolithography method to polymerize the monomers [196], suggesting that the process lends itself suitable to be scaled up commercially for industrial applications.

3.2. Results

3.2.1. Effect of varying UV light parameters on fabrication of microneedles

a) Effect of varying polymerization time

Microneedles were fabricated at different polymerization times ranging from 0.5 to 4 sec, keeping the UV light intensity (11.0 W/cm^2) and the distance from UV light source (3.5 cm) constant. Uniform microneedle arrays could not be formed at times below 1 sec. At polymerization times beyond 1 sec microneedles started to form with an average length of 1218 ± 18 μm until the exposure time of 2 sec ($p > 0.05$). Beyond that, the microneedle length increased to an average of 1268 ± 16 μm till a maximum exposure time of 4 sec ($p > 0.05$) (**Figure 11 A**). Similarly, for times up to 2 sec, the tip diameter averaged 131 ± 18 μm, which increased to 163 ± 17 μm with increase in exposure time between 2.5 and 4 sec (**Figure 11 B**). Higher polymerization times may have resulted in higher microneedle strength which is important for microneedle penetration in skin.

b) Effect of intensity of UV light

The intensity was varied between 1.15 and 11.0 W/cm^2 maintaining the polymerization time (3.5 sec) and distance from UV light source (3.5 cm) constant. Uniform microneedle arrays could not form below the strength of

2.21 W/cm^2. Microneedle length averaged at 1250 ± 4 μm and varying the intensity had insignificant effect on the microneedle length ($p > 0.05$) (**Figure 11 C**). Average tip diameter of microneedle tip was found to be 154 ± 8 μm ($p > 0.05$) (**Figure 11 D**). The microneedles fabricated at 11.0 W/cm^2 were observed to be strong enough to be used for subsequent penetration experiments.

c) Effect of varying distance from UV light source

Variation of intensity of UV light with increase in the distance from the light source was tested for its influence on the microneedle length and tip diameter. For this purpose, the fabrication stage was placed at a distance ranging, 3.5–9.5 cm from the light source. Microneedles were fabricated at several distances within this range, keeping other variables of polymerization time (3.5 sec) and ultraviolet light intensity (11.0 W/cm^2) constant. It was observed that as the distance was increased, the microneedle length decreased from 1256 ± 21 μm to 1190 ± 70 μm. However the difference was found to be statistically insignificant between the distances 3.5–6.5 cm and 3.5–9.5 cm (**Figure 11 E**). Increasing the distance of the fabrication stage beyond 9.5 cm resulted in the formation of non uniform arrays of microneedles with variable lengths. Tip diameter averaged at 156 ± 10 μm with the increase in distance from 3.5 cm to 9.5 cm (**Figure 11 F**).

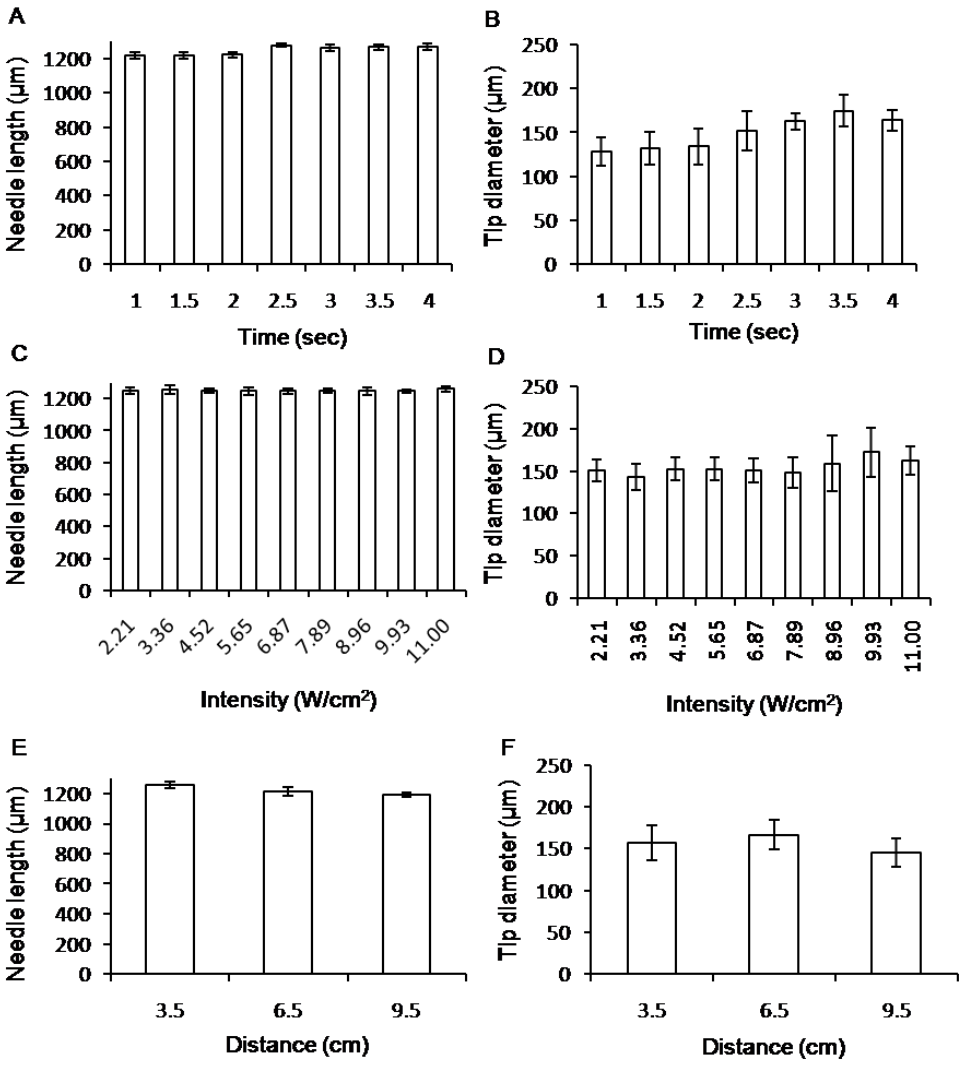

Figure 11 Effect of UV parameters on microneedle geometry. Effect of (A) polymerization time, (C) intensity and (E) distance from UV source on microneedle length. Effect of (B) polymerization time (D) intensity and (F) distance from UV source on tip diameter.

3.2.2. Effect of non UV light parameter (spacer distance)on fabrication of microneedles

For targeting the drugs to specific areas of the skin, it is essential to have a definite control over the microneedle length. The spacer thickness was manipulated by increasing the number of coverslips stacked on the base glass slide (**Figure 7**). Such a successive increase in the space between the base glass slide and the TMSPMA coated coverslip (which has PEGDA backing

fabricated on it), increases the microneedle length (**Figure 12 A - F**). At each step one coverslip was added to the stack increasing the spacer thickness by approximately 190 µm. The spacer thickness could be varied between 380 and 1330 µm. The UV parameters were kept constant at UV intensity (11.0 W/cm^2), polymerization time (3.5 sec) and distance from UV source (3.5 cm). In this manner, the microneedle length could be varied between 299 ± 8 µm and 1387 ± 35 µm (ANOVA, $p < 0.001$) which is corroborated by the average coverslip thickness of 190 µm each (**Figure 12 G**). An increase in the spacer thickness also resulted in a corresponding decrease in the tip diameter of the microneedles. The tip diameter ranged from 174 ± 22 µm to 260 ± 13 µm (**Figure 12 H**).

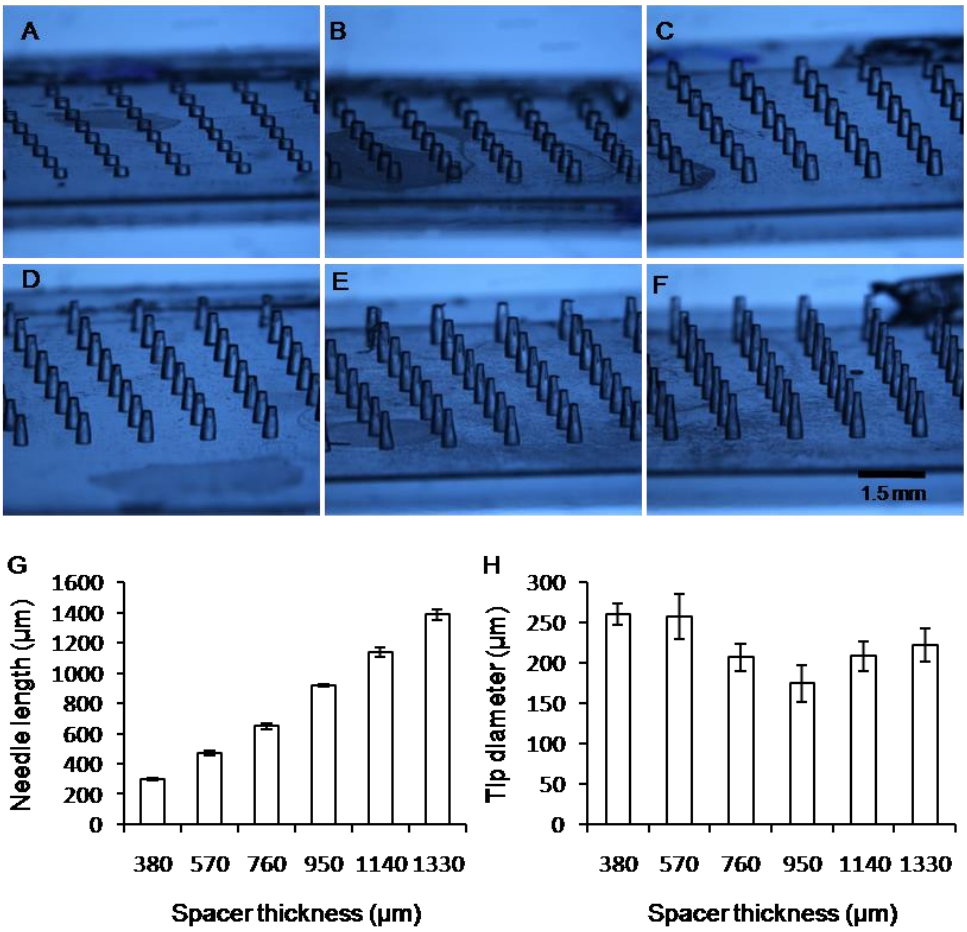

Figure 12 Effect of increasing spacer thickness. (A–F) Images at various spacer thickness, with microneedle length of 252, 441, 680, 820, 1044 and 1211 µm, respectively. (G) Increase in microneedle length with increase in spacer thickness. (H) Decrease in the tip diameter with increase in spacer thickness.

3.2.3. Microneedle penetration in pig skin

Microneedles measuring 921 ± 31 μm in length were inserted in cadaver pig skin. Penetration of microneedle arrays in the skin was demonstrated using the trypan blue staining method. **Figure 13 A** shows the image of a microneedle array penetration after staining. The blue spots are specifically stained at the points of microneedle insertion. Penetration with a hypodermic needle as a positive control and staining with trypan blue to ascertain the staining specificity and capability of the dye is displayed in **Figure 13 B**. As a negative control, the dye was applied on intact skin. After washing, the stain was removed, proving that the blue dye only stains the sites of stratum corneum perforation (**Figure 13 C**). The microneedles were not deformed upon removal from the skin suggesting that they were robust enough to penetrate the skin. **Figure 13 D** shows the histological section prepared after microneedles were inserted and removed subsequently. Hematoxylin and eosin staining to visualize the skin layers displays a clear indentation left by microneedle penetration. The microneedle penetrated almost completely into the skin suggesting that the encapsulated drug can be delivered efficiently. As these needles present a blunt tip, they are observed to pierce through the stratum corneum, a phenomenon also observed with hollow microneedles [112].

3.2.4. Encapsulation and in vitro release of encapsulated model drug

Figure 14 A shows the microneedles fabricated from PEGDA, in which no model drug has been incorporated. As observed from **Figure 14 B**, the microneedle shafts contain the red coloured rhodamine B, whereas there is no fluorescence observed from the backing layer. Conversely, in **Figure 14 C**, the microneedle shafts do not contain any rhodamine B dye and the fluorescence is only observed in the backing layer, which specifically contains the dye. The drug can also be incorporated in both microneedles as well as the backing, which were also fabricated during this study (**Figure 14 D**).

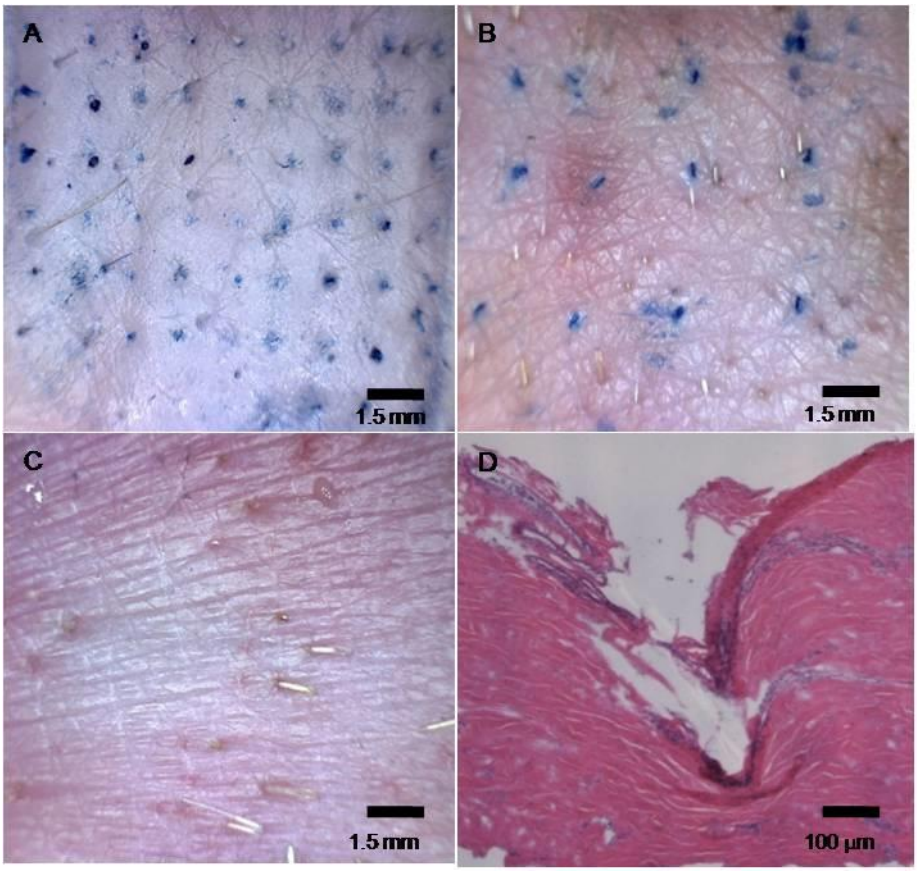

Figure 13 Penetration of microneedles in cadaver pig skin. (A) Area of microneedle penetration stained with trypan blue. (B) A positive control with skin penetrated using a 27 gauge hypodermic needle (4 × 3 array) and holes stained by trypan blue. (C) Negative control (no microneedles) applied on the skin, subsequently stained by trypan blue. (D) Histological section of skin stained with hematoxylin and eosin post microneedle application.

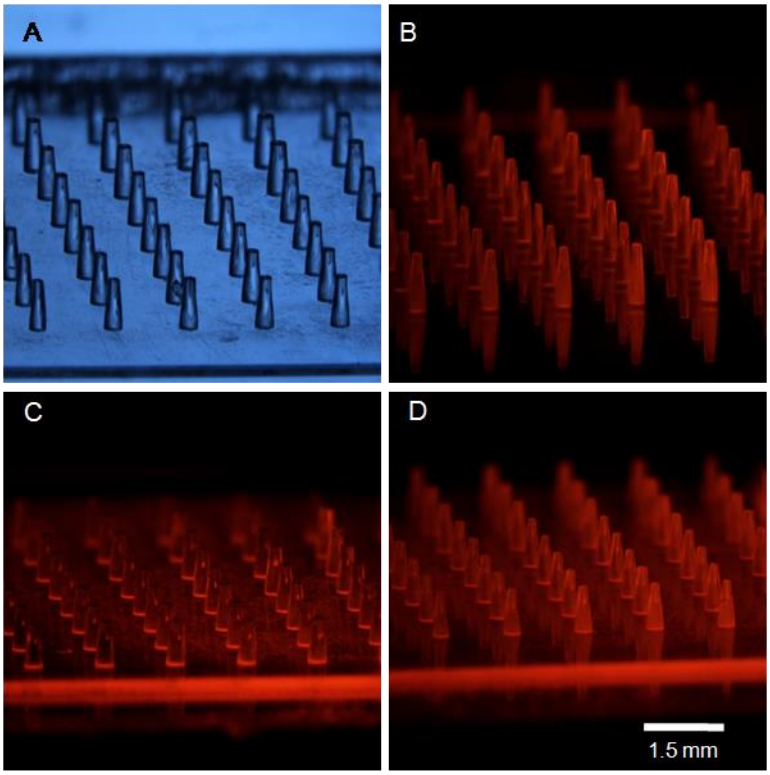

Figure 14 Incorporation of rhodamine B in microneedle arrays. (A) Without rhodamine B, (B) rhodamine B in microneedle shafts, (C) rhodamine B in backing layer and (D) rhodamine B in both microneedle shafts and backing.

The release of encapsulated rhodamine B was studied over a period of 1 week. It was observed that nearly 30% of the encapsulated drug was released within the first hour (**Figure 15 A**). The drug release continued as the drug loaded in the backing layer potentially serves as a reservoir. The percentage amount released was independent of the concentration of the drug in the microneedles and the backing layer. The actual amount released was shown in **Figure 15 B**.

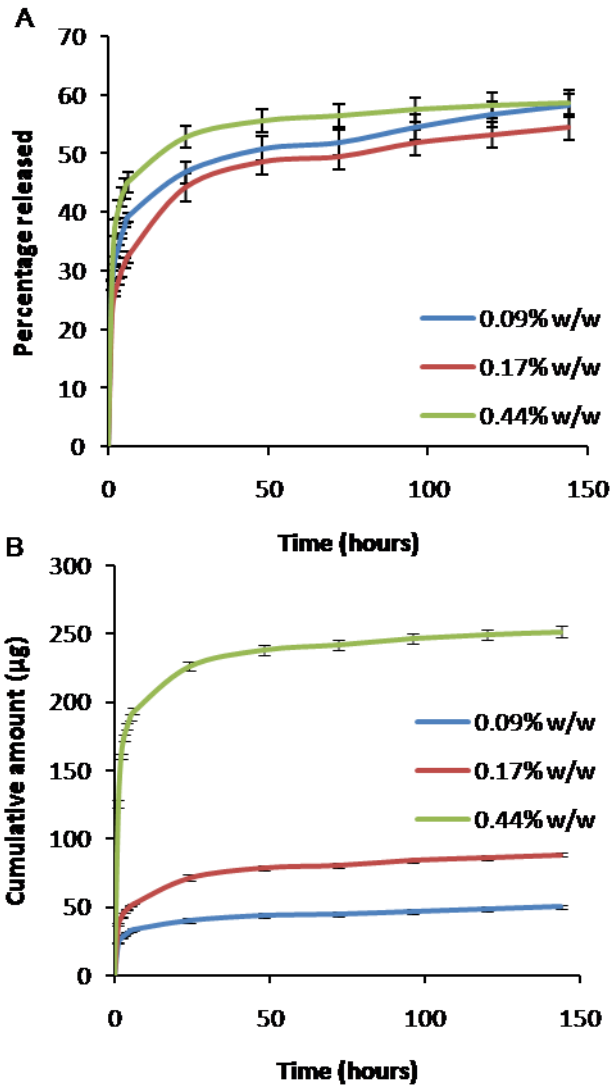

Figure 15 Release profile of rhodamine B encapsulated in microneedles over a period of 1 week. (A) percentage released (B) cumulative amount released.

3.2.5. In vitro permeation through rat skin

The ability of microneedles to increase skin permeability of rhodamine B was assessed. Microneedle increased the total amount permeated by 3.89-fold as compared to a propylene glycol solution of rhodamine B (**Figure 16**). The steady-state flux was 0.299 ± 0.1 µg/cm^2/hr for microneedle and 0.067 ± 0.01 µg/cm^2/hr for propylene glycol solution, which is 4.35 times lower ($p < 0.05$).

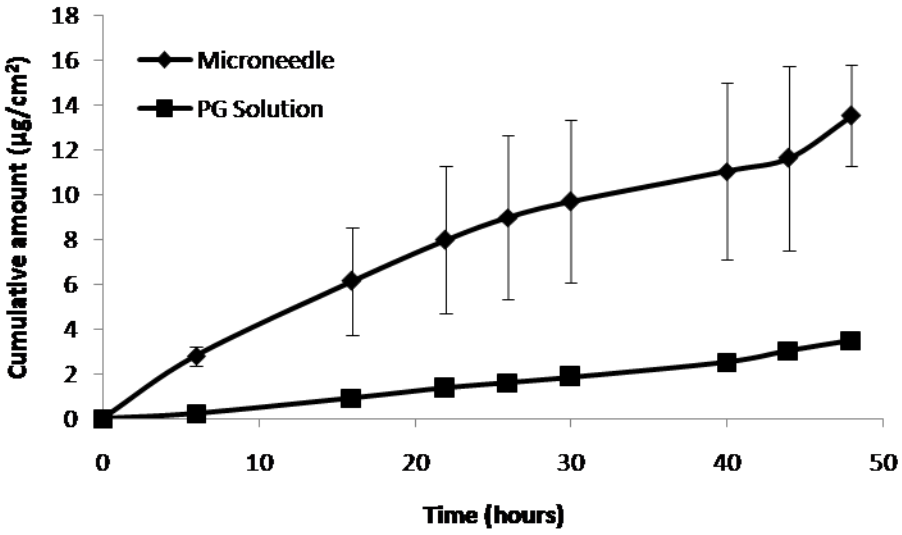

Figure 16 Cumulative amount of rhodamine B permeated through rat skin when microneedle patch and propylene glycol solution of rhodamine B were applied over a period of 48 hr.

3.3. Discussion

Development of a one-step lithographical method to fabricate microneedles was accomplished. The major equipment in this method is the UV curing station [194]. The fabrication process involved free radical polymerization using the photoinitiator HMP, which initiates the polymerization reaction in the presence of UV. Polymerization time ranging from 1 to 4 sec is not expected to compromise the stability of encapsulated drugs. The fabrication set up does not have specific requirements of vacuum or heating arrangements.

Fabrication of microneedles from PEGDA began with the process of optimization of fabrication conditions. As method to fabricate microneedles using ultraviolet light governed photo polymerization was being developed, several variables were studied. The polymerization time (time of exposure of polymer to ultraviolet light), ultraviolet light's intensity and the distance of the fabrication assembly from the ultraviolet light source was considered as factors influencing microneedle fabrication and were evaluated for their effect on microneedle geometry.

The time of exposure to UV light, defined as the polymerization time, is important with respect to the microneedle geometric properties as well the encapsulated drug stability. Ultraviolet light has been well known to cause primary photooxidation, which is the major contributor to drug degradation [197]. One of the aims of these experiments was to study the geometric properties and develop a method of fabricating microneedles in the shortest possible polymerization time. The photopolymerization methods used to date involved long exposure times to UV in the range of 30 min [116]. With the new approach, microneedle structures were obtained at low polymerization time of 1 – 4 sec. Although microstructures could be formed at lower polymerization times as well, but as the time was increased the microneedle strength increased. A polymerization time of 3.5 sec was used for microneedles fabricated in the current study as it resulted in robust microneedle arrays enabling penetration in skin. On the other hand, photopolymeric reactions can also be influenced by the intensity of the light source used [198]. Beyond a certain intensity of UV light, microneedle length was governed by the spacer thickness and intensity only affects the microneedle strength. The aim was to find the right combination of polymerization time and the UV intensity for fabricating robust microneedles. It was found that a combination of polymerization time of 3.5 sec and intensity of 11.0 W/cm^2 was suitable for this method.

Penetration of microneedles in cadaver pig skin revealed that microneedles penetrated the skin using a thumb with little force. Trypan blue is a hydrophobic dye and is known to specifically stain the sites of stratum corneum perforation, which is confirmed by histological sectioning of the skin. Microneedles are intended to create transient pores in the skin structure and release the drug through these pores. These pores have been previously shown to close within 72 hr upon microneedle removal [126] and microneedle application has been associated with a lower risk of microbial infection as compared to hypodermic needles [199].

Polymeric microneedles offer the advantage of incorporating the drugs in the polymeric matrix as compared to silicon or metallic counterparts where the drug can only be coated on pre-fabricated microneedles. Incorporation of

drugs in microneedles fabricated from PEGDA demonstrates the encapsulation efficiency of PEGDA microneedles. The drugs have been incorporated either in the microneedle shafts for bolus release or in the backing layer for sustained release or in both layers for a prolonged effect [92]. The drug release from the microneedles in the surrounding subcutaneous tissue is followed by release of the drug encapsulated in the backing layer, which continues to release the drug through the transient pores created by the microneedles. Since it is possible to incorporate a larger amount of drug in the backing layer as compared to the microneedles, it is useful to incorporate the drug both in the microneedles and the backing layer to increase drug loading. The drug encapsulated was released with a burst upfront in the first hour, which was followed by slower release over a period of 1 week of the study. This can be attributed to the reservoir capacity of the backing layer which can release the drugs through the microneedles inserted into the skin. The drug release properties, however, may be modified by coating the microneedles or incorporating varying amounts of release modifying polymers, such as chitosan, to control the release of the drug from the PEGDA matrix. Chitosan as a coating material for controlling the release rates has been previously investigated [169]. Other photo-crosslinkable polymers may also be used to alter the release profile of the drugs. Drug laden microneedles created transient pores which may have led to a higher flux as compared to a control, which included a propylene glycol solution containing the same amount of the drug as in one microneedle array. The microneedles increased the flux by over four times compared to passive diffusion of rhodamine B through the capillary intercellular pathways in the stratum corneum, which is the main mode of drug transport across the skin for a propylene glycol solution [8].

3.4. Summary

A simple photolithographical approach was developed to fabricate polymeric microneedles. Microneedles were found to be capable of penetrating cadaver pig skin when inserted with the force of a thumb. A model drug, rhodamine B could be encapsulated in the polymeric matrix of the microneedle shafts and the backing layer and released in an *in vitro* release medium. The microneedles, when applied to rat skin, increased the flux of encapsulated

rhodamine B by 4 times over passive diffusion of a solution. The approach is amenable to other photo cross linkable polymers and potentially useful for transdermal drug delivery. Moreover, the method may be potentially scaled up for mass production of microneedle arrays.

CHAPTER 4

Protein Encapsulation in Polymeric Microneedles by Photolithography

(Adapted from *International Journal of Nanomedicine*. 2012; 7: 3143-3154)

4.1. Overview

The growth of biotechnology has produced a surge in the number of protein and peptide drugs available for human use [29]. Transdermal delivery has evolved as an interesting alternative for protein drug therapy because it circumvents the inherent challenges associated with oral and parenteral routes. However, the skin's natural barrier prevents these macromolecules from diffusing through the skin. Microneedles have been shown to disrupt the stratum corneum actively by creating micron-sized pores and hence enhancing the flux of macromolecules. They offer the advantage of delivering a drug without impinging on the underlying nerves.

Drugs, both small and macromolecular, have been delivered using microneedles by three different modes. Firstly, coating onto microneedle shafts, [200, 201] and secondly, pretreating the skin with microneedles to create pores, followed by application of conventional dosage forms [202, 203]. With the development of polymeric microneedles, a third approach was developed whereby drugs could be encapsulated in the polymeric matrix and released from the polymer upon application [192]. Encapsulation of drugs within the polymeric core offers the advantage of a higher drug loading in one convenient formulation, omitting multiple steps that would otherwise be required.

Encapsulation of proteins inside microscale and nanoscale particles has been studied previously using various approaches, such as double emulsion [204], electrospray [205], self-assembly [206], and microfabrication [207]. For example, lipid nanocarriers of the self-assembled type can be used to encapsulate proteins, peptides, and nucleic acids with tunable sizes and

morphologies [206, 208]. These three-dimensional nanostructures can be obtained by homogenizing a mixture of lipids hydrated with protein solutions.

Similarly, therapeutic proteins such as insulin and vaccines can be encapsulated in microneedles and proteins released from microneedles can form a depot from where they can be absorbed into the systemic circulation or lymphatic vessels.

However, previously reported fabrication approaches used for these protein-laden microneedles involve use of high temperatures, vacuum, or prolonged exposure to ultraviolet light which may be potentially harmful to biological drugs. High temperatures (140 °C–160 °C) used for micromoulding of sugar microneedles have resulted in a significant loss of drug content [129]. Casting methods used by other groups [92] utilize polymers or sugar derivatives requiring a concentration of hydrogel using high temperatures and vacuum which may have deleterious effects on fragile protein molecules. A newer process reported recently involves prefabrication of a female purple sand mould at high temperatures and subsequent fabrication of needles by vacuum suction and freeze-drying [209]. These challenging conditions may not be ideal for a drug delivery system aimed to encapsulate fragile molecules.

A novel photolithography-based method utilizing low exposure to ultraviolet light developed in chapter 3 [117] can be potentially applied for protein encapsulation. In this chapter, bovine serum albumin (BSA) was selected as a model protein. To ensure that the encapsulated material retains its structure and activity, the stability of the encapsulated BSA was tested by analyzing its primary, secondary, and tertiary structural features. This is relevant for therapeutic proteins and peptide drugs like insulin, desmopressin, and vaccines, such as influenza vaccine. This chapter is the first report in literature for exhaustive stability testing for protein encapsulation in microneedles. The *in vitro* release of the BSA protein was tested in phosphate-buffered saline. *In vitro* permeation of the encapsulated BSA through rat skin was also tested. In addition, the *in vitro* biocompatibility of microneedles was also reported using three different cell lines to assess the toxicity of the polymeric microneedles for skin applications.

4.2. Results

4.2.1. Fabrication and characterization of microneedles

The microneedles were found to have an average length of 820 μm, a base diameter of 300 μm, a center to center spacing between the needles of 1500 μm, and an average tip diameter of 140 μm. The microneedle patch consisted of an array of 8 × 8 needles spread over an area of 1.44 cm^2.

4.2.2. Incorporation and uniform drug distribution in microneedles

Drug incorporation in the polymeric matrix prior to microneedle formation allows for higher drug loading as opposed to coating the drug molecules on the fabricated microneedles. In this study, drug loading up to 1.6 mg of BSA per microneedle array could be achieved. Confocal imaging was used as a tool to image the microneedle samples to assess the fluorescence distribution at different areas and depths of the microstructure. As observed from **Figure 17 A and D**, fluorescence is distributed across different areas of the backing layer in a uniform pattern ($p > 0.05$). However, as the microneedle length increased from the bottom of the array (length 10 μm) to the microneedle tip (length 700 μm), the fluorescence intensity was observed to decrease gradually from 377 to 3.1 (**Figure 17 B and E**). Drug distribution among different microneedles in an array varied in different areas, with microneedles at the edges having a lower intensity and those in the centre exhibiting higher intensity. Approximately 60% of the microneedles were in the high intensity range. (**Figure 17 F**). Since needles contain much less drug than backing, this is expected to ensure uniform drug delivery over the patch area of 1.44 cm^2. **Figure 17 C** shows a stereomicroscope image of a complete microneedle array, showing that the drug is evenly distributed.

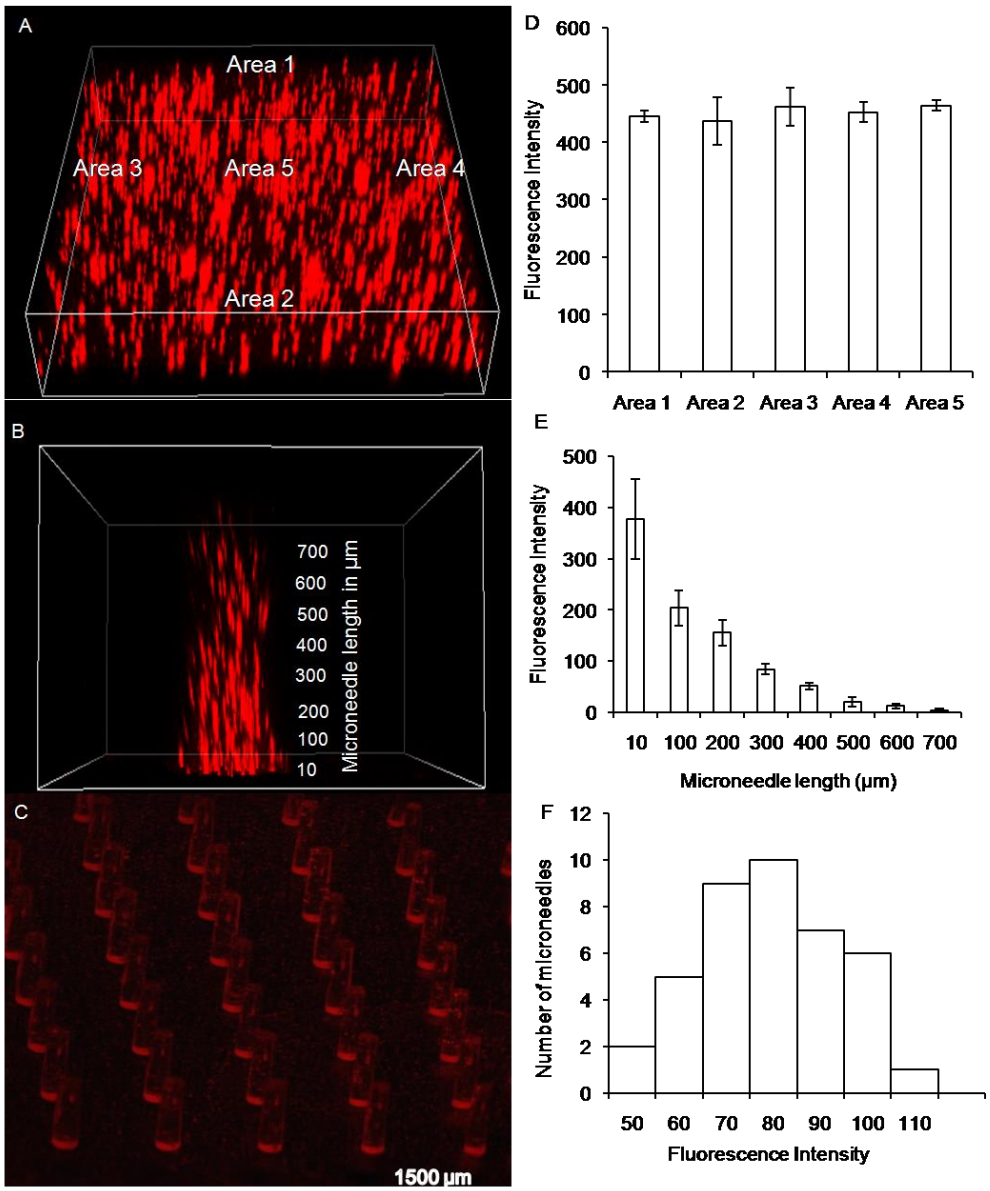

Figure 17 Encapsulation of bovine serum albumin Texas red conjugate (TR-BSA) in polymeric microstructures shows uniform distribution. Uniformly distributed TR-BSA in (A) microneedle backing and (B) microneedle shaft (C) microneedle array. Quantitative estimation of fluorescence intensity shows uniform distribution over (D) different areas of the backing layer (n = 3) and (E) different lengths on a microneedle shaft (n = 6). (F) Distribution of fluorescence intensity among different microneedles of an array shows a varied pattern.

4.2.3. Stability tests for BSA in microneedles

a) Primary structure stability

In this study, sodium dodecyl sulfate polyacrylamide gel electrophoresis was used to determine the amino acid sequence of BSA and analyze any

deleterious effect of ultraviolet radiation on the protein (**Figure 18**). BSA released from the formulation was compared with a freshly prepared solution and a protein standard marker. The single line of bands appearing at 66 kDa suggests that the protein was stable during the fabrication process and remained stable in the dosage form for a period of 72 hours.

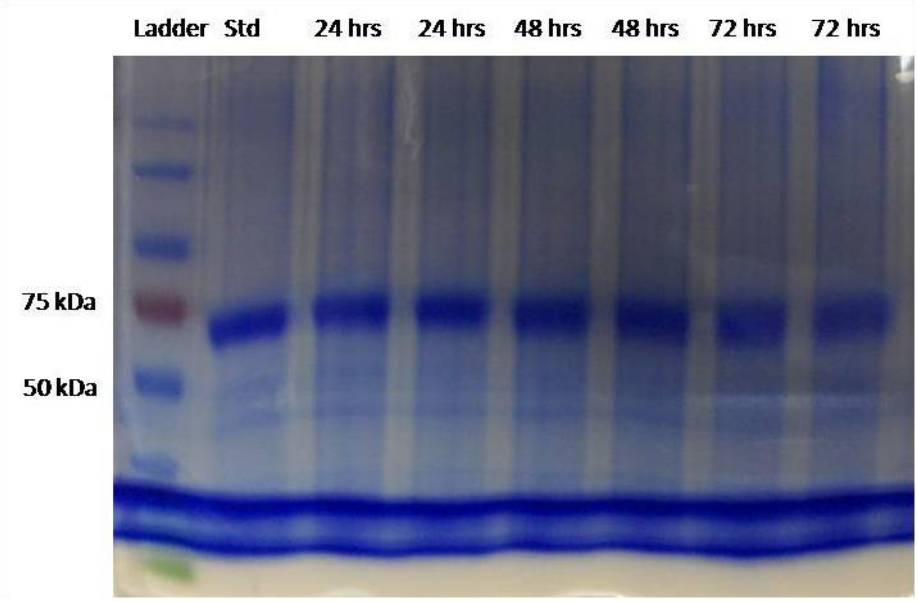

Figure 18 Sodium dodecyl sulphate-polyacrylamide gel electrophoresis images of protein standard marker, bovine serum albumin standard and bovine serum albumin released from microneedles after 24, 48, and 72 hours.

b) Secondary structure stability

The secondary structure of BSA was assessed by circular dichroism. It was observed that the secondary structure of BSA encapsulated in the microneedles was similar to a freshly prepared solution of BSA, as shown in **Figure 19 A**. The degraded BSA used as a control showed significantly lower ellipticity values than the standard BSA and microneedle release samples. The percentage of α-helix from the microneedle release samples was consistent with the reported amount of helix in the native BSA structure (about 67%) [210]. The percentage of α-helix in the BSA released from the microneedle samples was comparable with the standard ($p > 0.05$, **Figure 19 B**) and significantly different from heat-denatured and acid-denatured BSA samples ($p < 0.05$).

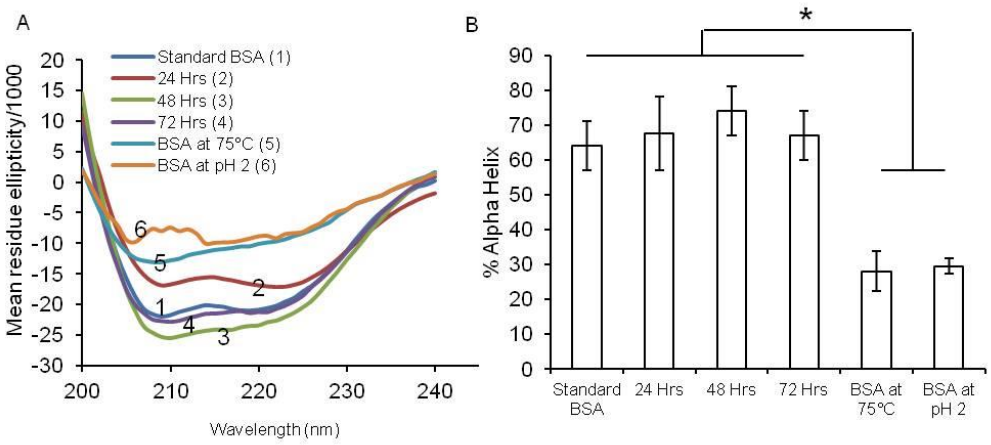

Figure 19 Circular dichroism analyses to assess the stability of encapsulated bovine serum albumin (BSA). Stability of BSA released from microneedles after storage for 3 days at 37 °C is compared with a freshly prepared BSA solution and BSA degraded by heating at 75 °C and under acidic conditions, pH2 (A) mean residue ellipticity and (B) percentage of alpha-helix. All results confirmed the alpha helix structure of BSA was preserved during encapsulation and release over a period of 3 days (* $p \leq 0.05$).

c) Tertiary structure stability

BSA emission spectra were scanned between 300 nm and 400 nm and an emission maximum was observed at 338 nm for all the release samples and a standard solution of BSA (**Figure 20**). This is in accordance with previously reported results [211] and demonstrates the feasibility of this fabrication process for retaining protein stability in the microneedles. On the other hand, BSA samples denatured using heat or acid did not show any fluorescence (excitation wavelength 280 nm and emission wavelength 300 – 400 nm).

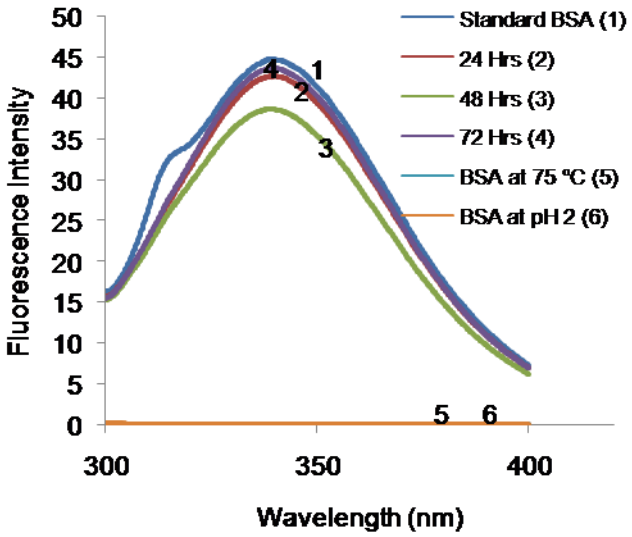

Figure 20 Fluorescence spectroscopic analysis to assess the tertiary structure of encapsulated bovine serum albumin (BSA). Stability of BSA released from microneedles after storage for 1-3 days at 37 °C is compared with freshly prepared BSA solution and BSA degraded by heating at 75°C and under acidic conditions, (pH2) by analyzing the emission spectra of BSA. Peak BSA emission wavelength was found to be similar for all samples. No fluorescence was observed in degraded BSA samples.

4.2.4. In vitro release of BSA from microneedles

The release profile of BSA is depicted in **Figure 21 A** (percentage release) and **Figure 21 B** (cumulative amount). Phosphate-buffered saline (pH 7.4) was used as a release medium because it closely resembles extracellular fluids and plasma. It was observed that 80 – 100% of the protein encapsulated in the microneedle array was released within a period of 6 hours. Most of the protein was encapsulated in the microneedle backing layer (about 90%) and the needles owing to their micron-scale geometry contain lesser drug.

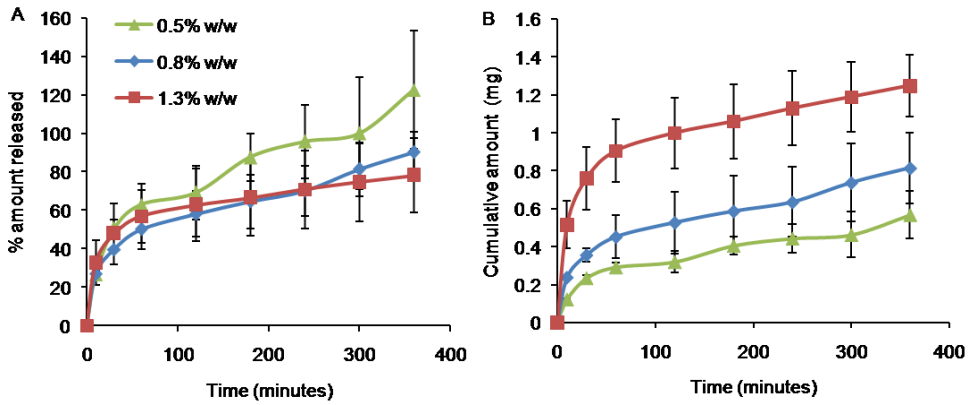

Figure 21 Release profile of bovine serum albumin encapsulated in microneedles over a period of 6 hours. (A) Percentage amount and (B) cumulative amount released.

4.2.5. In vitro permeation through rat skin

Microneedles increased the amount of BSA permeated as compared with passive diffusion of BSA. **Figure 22** shows the increase in the cumulative amount permeated per unit area on microneedle application as compared with a propylene glycol solution of BSA, which showed practically no permeation at the end of 48 hours. The amount permeated in the case of microneedles increased with the increase in the encapsulated amount of BSA. The permeation curve resembles the *in vitro* release profile observed in phosphate-buffered saline, with an initial burst-release followed by a slow-release phase.

The protein concentration was calculated using the following equation:

$$\text{BSA concentration } (\mu g/mL) = 144 \times (A_{215} - A_{225})$$

where, A_{215} and A_{225}, are the absorbance readings of BSA solutions at wavelength of 215 and 225 nm respectively.

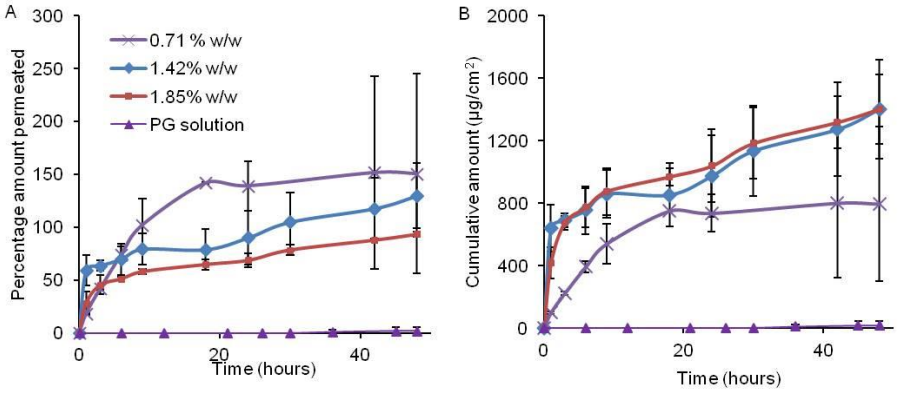

Figure 22 *In vitro* permeation through rat skin. (A) Percentage amount and (B) cumulative amount permeated through rat skin when applied with a microneedle patch (containing 0.71% – 1.85% w/w bovine serum albumin) or a propylene glycol solution of bovine serum albumin over a period of 48 hours.

Microneedles containing no BSA were used as a control to minimize any absorption from the dissolved polymer. When lower amounts of BSA were encapsulated, the permeation curve demonstrated a plateau at nearly 18 hours, because most of the drug was released. When higher amounts were encapsulated, the protein continued to be released for 2 days, suggesting that the microneedle array developed in the study is amenable to dose adjustment as per the requirements of the therapeutic regimen. As compared with microneedles, passive diffusion of BSA using a propylene glycol solution did not result in any significant amount of drug permeation through the skin.

4.2.6. In vitro biocompatibility of polymeric microneedles

Using three different cells, HDF, HaCaT and HEK 293, the local and systemic biocompatibility of polymeric microneedles was assessed. The MTT assay was used to assess the toxicity of microneedle extracts to these cells. Viable cells, possessing the active mitochondrial succinate-tetrazolium reductase system, reduce MTT to formazan crystals which were quantified by colorimetric determination [212]. The cell viabilities were calculated as $A_{polymer}/A_{control} \times 100$, where $A_{polymer}$ and $A_{control}$ were the absorbance measurements of the wells containing polymeric extracts and control

(phosphate-buffered saline), respectively. Each value was an average of six replicates.

High cell viabilities with respect to the control were found for human dermal fibroblasts and HaCaT cells for exposure of cells to polymeric extracts up to 72 hours (**Figure 23 A** and **B**), with cell survival numbers statistically insignificant between 24 and 72 hours ($p > 0.05$). This shows that the polymer used for fabricating the microneedles was safe to skin locally. HEK293 cell viability assays yielded similar viability for the first 24 hours, which subsequently decreased ($p < 0.05$, **Figure 23 C**).

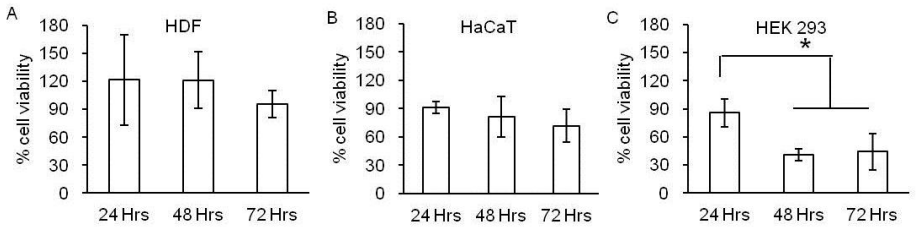

Figure 23 *In vitro* biocompatibility testing using MTT assay in (A) human dermal fibroblasts (HDF), (B) human adult low calcium high temperature (HaCaT) cells, and (C) human embryonic kidney 293 (HEK293) cells demonstrated high cell viability, indicating the biocompatibility of polymerized PEGDA microneedles.

Fluorometric determination of lactate dehydrogenase leaked out from damaged cell membranes into the supernatant medium was also used to assess the cytotoxicity of PEGDA microneedles. In this study, low cell toxicities were observed for HDF and HEK 293 cell lines, while slightly higher toxicity was observed for HaCaT cells treated with polymer extracts. The percentage cytotoxicity for cells treated from 24 – 72 hours did not vary significantly ($P > 0.05$), supporting the results from the MTT assay and further proving the non toxicity of polyethylene glycol diacrylate (**Figure 24 A–C**).

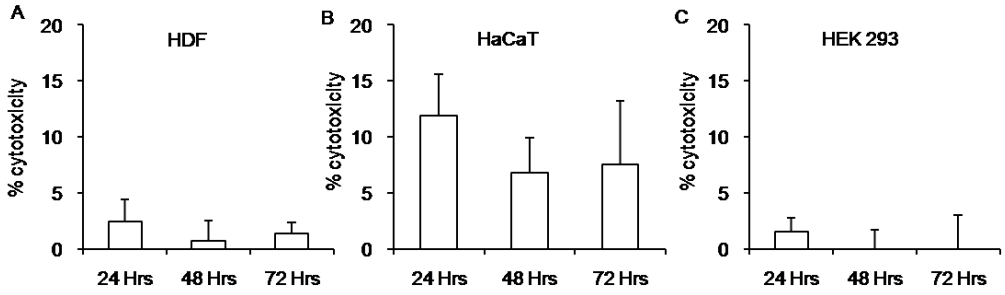

Figure 24 *In vitro* cytotoxicity testing using lactate dehydrogenase assay in (A) human dermal fibroblasts (HDF), (B) human adult low calcium high temperature (HaCaT) cells, and (C) human embryonic kidney 293 (HEK293) cells demonstrated low toxicity, indicating the biocompatibility of PEGDA microneedles.

4.3. Discussion

Microneedles have been considered as a useful drug delivery system to deliver therapeutic peptides, proteins, and vaccines [27]. Drug encapsulation in polymeric microneedles has been used previously with other polymers, namely, polyvinyl pyrrolidone and its copolymer with methacrylic acid [116], copolymer of methylvinylether and maleic anhydride [213], and polyvinyl alcohol [214]. However, the method developed in this thesis circumvents the long ultraviolet exposure and extensive preprocessing required for microneedle formation using the previous methods, which may impact protein stability. Moreover, the process does not involve any mold-based or template-based processing, potentially avoiding interactions between mold or template material and fragile protein molecules.

An important aspect of a drug delivery system is the uniform distribution of drug in the carrier matrices. To test for uniformity, BSA Texas red conjugate was encapsulated to visualize the distribution of the protein inside the backing and the shafts of the microneedle array. The BSA Texas red conjugate shows peak excitation wavelength (λ_{ex}) and emission wavelength (λ_{em}) at 596 nm and 615 nm, respectively [215], which was quantified using fluorescence microscopy and protein distribution was found to be uniform.

Because the biological function of a protein is dependent on its conformation, it is imperative to design a dosage form which does not adversely affect the stability of these fragile molecules. In this fabrication process, ultraviolet

light-based photo cross-linking method was used for creating polymeric microstructures. Ultraviolet light has been previously reported to cause protein denaturation and structural changes in the primary, secondary, and tertiary structure of proteins [197]. These three structural features were studied by investigating sodium dodecyl sulfate polyacrylamide gel electrophoresis, circular dichroism spectra, and fluorescence intensity measurements of BSA encapsulated in the microneedles. While the results here demonstrate that the conformation of BSA was maintained throughout the fabrication process and the subsequent release experiments, the structural and biological properties of proteins other than BSA will depend on individual protein characteristics.

Sodium dodecyl sulfate polyacrylamide gel electrophoresis has been the most common method used for the separation of proteins and determination of protein molecular weight [216, 217]. It has been used previously to determine the structural integrity of BSA in microspheres [218]. There were no other bands observed during the electrophoretic separation, except for BSA bands at 66 kDa providing evidence against any protein aggregation to form dimer or multimer or fragmentation to smaller subunits, indicating that the primary structure of BSA remained intact during the fabrication process.

Circular dichroism has been a common technique in assessment of secondary structure of proteins. BSA contains 67% of α-helix, 10% of turn, and no β-sheet [164]. The far ultraviolet circular dichroism spectrum (260 – 200 nm) has been used to characterize the structural stability of BSA [219]. The α-helix structure is indicated by two negative peaks at 208 nm and 222 nm with a minimum peak at 208 nm, which is attributed to $n \rightarrow \pi^*$ and $\pi \rightarrow \pi^*$ transition of the α-helix structure [220, 221]. BSA encapsulated in microneedles showed similar structural properties to a freshly prepared solution together with retention of α-helix structure. Circular dichroism analysis has been similarly reported for lysozyme [92]. These results demonstrated that secondary structural integrity of BSA was maintained during ultraviolet-dependent photopolymerization.

Because proteins contain aromatic amino acids like tyrosine, tryptophan, and phenylalanine, which are inherently fluorescent, fluorescence spectra and

intensity can be used as a marker of protein structural stability. Tryptophan is the most dominant fluorophore and displays the largest extinction coefficient. Thus, the emission spectra of proteins can be measured at a fixed excitation wavelength of 280 nm [222]. The emission maximum of tryptophan in water is observed around 350 nm and is dependent on the polarity of the solvent. BSA showed an emission maximum at 338 nm, which is a characteristic of its tertiary structure.

The analysis of primary, secondary, and tertiary structural stability of BSA demonstrated the microneedles to be a potentially useful carrier for protein drugs. The ultraviolet photo cross-linking did not significantly alter the structural properties of BSA, possibly due to the short time of exposure.

The transient pores created by microneedles and diffusion of the protein through the polymeric layer to the epidermal and dermal regions to create a depot of protein drugs have been reported [118]. The drugs can be subsequently absorbed into the blood stream or lymphatic circulation [223]. It is expected that the protein released will accumulate in the subepidermal tissues and be rapidly absorbed from the highly vascularized regions lying underneath. The initial burst of the drug from the microneedle array intends to form a depot which slowly gets absorbed. This drug concentration is also supplemented by the protein continuously released from the backing layer. Similar release kinetics was observed in previous reports [118].

Microneedles enhanced the permeation of BSA as compared to passive diffusion of BSA solution which resulted in negligible permeation even at the end of 48 hour study period. A similar BSA permeation pattern has been reported previously [169]. Other protein molecules, like fluorescein isothiocyanate-labeled BSA and insulin, incorporated in polymeric microneedles have also shown such burst-release patterns [213]. Such permeation profiles are common for other highly water-soluble drugs, such as calcein ($\log P = -5.02$). However, as observed in chapter 3 that relatively lipophilic drugs (e.g., rhodamine B, $\log P = 2.43$) do not show a burst in permeation and their absorption is somewhat limited by interaction with stratum corneum lipids [117].

The A_{215}–A_{225} method has been previously used in determining the BSA concentration in *in vitro* permeation studies [169]. The concentration of BSA is a linear function of the difference between extinction at 215 nm and 225 nm [224]. The method is sensitive for protein concentrations as low as 5 ng/mL, which are usually expected in *in vitro* permeation studies.

Conventional skin permeation where steady state can be established is based on the fact that the donor concentration is constant throughout the diffusion process. This can be proven by Fick's first law for membrane diffusion [42]. However, in this study, the donor concentration decreased during the permeation process. Moreover, it is not a pure membrane diffusion process because micropassages were created by these microneedles, making the process a combination of diffusion through the skin membrane and mass transport through micron-sized channels across skin.

Human dermal fibroblasts and HaCaT keratinocytes are representative of skin cells and hence were used to assess the toxicity of the polymeric microdevice on the skin. These cells have been used previously to study the toxicity of transdermal polymeric dosage forms [225, 226]. HEK293 cells were used because they are representative of healthy human cells. HEK293 cells have been used in numerous *in vitro* toxicity studies as being representative of human cells since they offer a convenient model to evaluate toxicity at the cellular level [227]. They have also been previously reported with regard to transdermal toxicity from topical gels [212]. Overall, the low *in vitro* toxicity observed from both MTT and LDH assays showed promising biocompatibility of the polymeric microneedles, both transdermally and systemically.

4.4. Summary

The amenability of a simple photolithographic technique to encapsulate protein drugs was demonstrated in this chapter. Drug distribution was found to be uniform across the microneedle arrays. Moreover, the process was proven to maintain protein stability and is hence expected to retain the biological activity of the encapsulated proteins. The encapsulated protein was released and permeated through the skin in much larger amounts as compared with passive diffusion. *In vitro* biocompatibility of the polymeric microneedles has

been demonstrated by the low cytotoxicity of the polymeric extracts on different cell lines, indicating the safety of these microneedles. The prepared microneedles are expected to serve as a potentially useful drug delivery system to deliver biological drugs.

CHAPTER 5

Microneedle Integrated Transdermal Patch (MITP) for Fast Onset and Sustained Delivery of Lidocaine

(Adapted from *Molecular Pharmaceutics*. 2013, 10 (11):4272–4280)

5.1. Overview

The occurrence of pain is common among all age groups, with about 1.5 billion people suffering from it around the globe. On the basis of duration, pain may be classified as acute or chronic pain. Acute pain is defined as 'pain of recent onset and probable limited duration'. It usually has an identifiable temporal and causal relationship to injury or disease [228]. On the other hand, chronic pain is a 'pain without apparent biological value that has persisted beyond the normal tissue healing time" [229, 230]. Chronic pain is the most prevalent disorder in the United States, with more people affected by it than diabetes, coronary heart disease and cancer combined [231]. Chronic pain of moderate to severe intensity affects 19% of adult Europeans as well [232]. Approximately 3 – 4.5% of world's population suffers from chronic neuropathic pain, with incidence commensurating with increasing age [233, 234].

Lidocaine, also known as lignocaine or xylocaine, has been of special interest for its analgesic properties apart from its known role as a local anesthetic, being used in the management of both acute and chronic pain conditions. For the management of acute pain, perioperative infusion of lidocaine has been used to prevent dose escalation of opioids, reducing pain scores, nausea, vomiting and other related symptoms associated with abdominal surgery [228]. In addition, topical formulations of lidocaine and its combination with prilocaine and tetracaine have been widely used to provide superficial skin anesthesia in prophylactic pain management, especially in children before intravenous administration [235]. It has also been used in minor dermatological surgery procedures [235]. On the other hand, for chronic pain management, lidocaine finds its most prominent analgesic application in the

management of peripheral neuropathic pain, being recommended as a first line therapy. Lidocaine 5% transdermal patch is licensed in many countries for the management of postherpetic neuralgia; it is used off-label in most cases of neuropathic pain [236]. Many randomized controlled trials support the use of transdermal lidocaine patches in the management of peripheral neuropathic pain [237, 238].

Despite their regnant use, their lack of efficacy and rapid action, primarily due to skin's barrier properties is a major concern with patch-wear times up to 60 minutes required, which may be unacceptable to some pediatric patients [239]. In randomized controlled trials, a maximum of 420 cm^2 of patch area was applied to the skin for 4 hours before any significant reduction in pain could be observed [240, 241]. For chronic pain, a maximum of 3-4 patches/day are recommended for a period of 12-18 hours a day. Such a long patch wear time has been reported with incidents of skin rash and erythema, and discomfort [242].

Recently, microneedle arrays have been shown to enhance delivery of drugs like naltrexone [243], lidocaine [244] and insulin [245] in humans. Lidocaine delivery using microneedles has been demonstrated using hollow microneedles coupled to liquid formulation containing syringe to deliver large amounts of lidocaine. However, the complicated multi-component application system is bulky and is not ideal for self administration and long wear times [244]. Coated microneedles using 3M's solid microstructured transdermal system (sMTS) were reported to deliver lidocaine tissue concentrations comparable to commercial EMLA® cream (applied for 1 hour) in 1 - 5 minutes of wear time. However, the drug loading on these microneedles was limited due to small surface area and only 225 µg of lidocaine could be coated [246]. While these hollow and solid microneedles, pose the additional risk of breakage in the skin, polymeric microneedles present a viable alternative.

Drugs could be encapsulated within the polymeric matrix in higher doses than surface coating of solid microneedles and do not require an additional source of drug delivery as needed with hollow microneedles. Lee et al. first demonstrated the utility of polymeric microneedle backings as drug reservoirs

for higher drug loading and sustained release of small molecular weight drugs [92]. Albeit this advantage, drug amounts in the range of 1- 3 mg have been encapsulated at the maximum using polymeric microneedles and their usability in clinical applications requiring higher doses is limited. Ito et al. recently demonstrated the attachment of drug loaded chip fabricated by pouring a drug-polymer glue in the molds of a tabletting machine, to a microneedle array fabricated by conventional mold based process [247]. The process is a multiple step technique and requires several ancillary equipments to increase the drug loading capacity of polymeric microneedle arrays and drug encapsulation of only about 12 mg was achieved. As demonstrated in previous chapters, a simple photolithographical approach was developed to fabricate polymeric microneedle structures [117]. Microneedle arrays, supported on flat backing layer were formed in a solvent- and mold- free, single step process and drug loading capacity of 3 – 4 mg was achieved.

In this chapter, ultraviolet curing was used to fabricate a microneedle integrated transdermal patch (MITP) that could be tuned in size to encapsulate drugs several times higher than the previously reported methods, in a simple process. Mechanical properties of the microneedles attached to the MITP were studied in order to gain an insight into axial loading properties of the newly developed integrated patch system. *In vitro* permeation from MITP was compared to a commercial lidocaine patch, Lignopad®. The integrated patch system is intended to provide a reservoir system with high drug loading, to deliver the drugs the initial drug load rapidly and also sustaining the release of the active ingredient, with potential applications for management of both acute and chronic pain conditions.

In addition, a novel approach to deliver drugs by keeping microneedles in skin was demonstrated, providing the opportunity for longer application time of microneedles where, microneedle shafts act as channels for drugs encapsulated in backing layers. This circumvents the premature closure of miniaturized pores created by microneedles, possibly due to removal of microneedles, aiding in continued drug permeation.

5.2. Results

5.2.1. Geometric properties of MITP

Governed primarily by the photomask dimensions, an array of 8 × 8 microneedles covering an area of ~1.44 cm^2 was fabricated. The fabricated microneedles had an average length of 889 ± 48 μm, base diameter of 334 ± 43 μm and centre-to-centre spacing of 1474 ± 39μm. The thin backing layer fabricated in phase I was 212 ± 22 μm in height while the integrated patch fabricated in the phase II was 1054 ± 34 μm thick. An image of the fabricated MITP containing rhodamine B is shown in **Figure 25 A** and various layers of MITP in **Figure 25 B**.

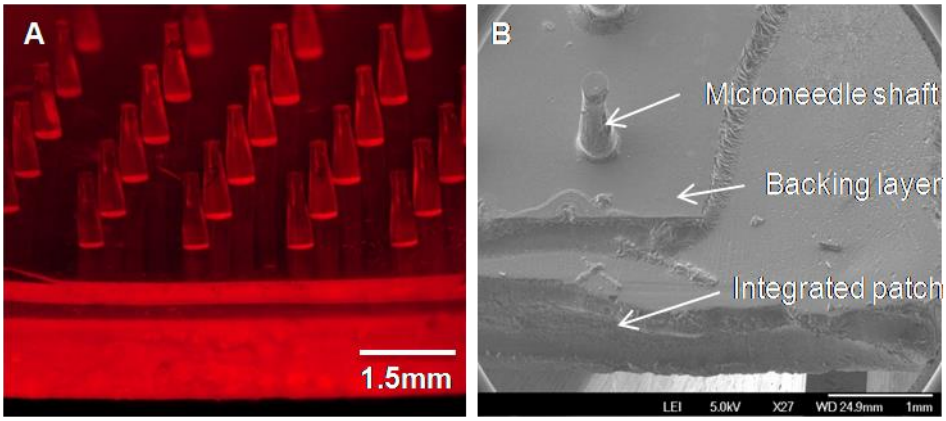

Figure 25 Images of MITP formed during fabrication. (A) With encapsulated rhodamine B imaged using the Nikon AZ100 Multipurpose Zoom Microscope (B) Scanning electron microscope (SEM) image of a single needle with a thin backing layer and the integrated patch.

5.2.2. Drug encapsulation in MITP

As the integrated patch encapsulating lidocaine appeared colorless, rhodamine B (0.075% w/v in prepolymer solution) was encapsulated as a model drug into the array to observe the uniformity of drug distribution. Rhodamine B, a fluorescent dye, was dissolved in the pre-polymer solution prior to UV exposure and was observed to be uniformly distributed in all layers of the fabricated MITP (**Figure 25 A**). Rhodamine B has log P value of 2.43 and serves a good substitute for lidocaine (log P 2.84) for imaging purposes. Lidocaine was encapsulated in different concentrations (2.2%, 15% and 21% w/w), leading to fabrication of MITP containing 7.917 ± 0.739 mg, 50.592 ± 1.855 mg and 70.940 ± 2.189 mg, respectively.

5.2.3. Mechanical strength of MITP

Fracture force of the microneedles supported on the integrated patch was evaluated by application of axial force upon the microneedles held against a stationary aluminium block. The fracture force of the microneedles on the integrated patch against the block was recorded 91.28 ± 9.2 N, as compared to the force of a thumb (10.72 ± 0.9 N) obtained from 5 individuals, which was significantly lower than the fracture force.

MITP application on excised cadaver rat skin was carried out at successively increasing forces to evaluate the extent of penetration and strength of microneedles when applied to a skin model. With successive increase in the force applied between 10- 70 N, an increasing amount of microneedles penetrated the skin (**Figure 26 A**). **Figure 27** shows no apparent change in microneedle structures when applied to rat skin for a period of 1 minute at different forces (10 – 70 N). Insignificant decrease in the average length of a microneedle was observed with length decreasing from 865 ± 22 μm at 10 N to 848 ± 23 μm at 70 N ($p > 0.05$) (**Figure 28**). The microneedle arrays appear sharp even after a single administration and removal from rat skin (**Figure 27 A-D**). While microneedle shafts were robust enough to penetrate the skin, at higher forces beyond 50 N, 2 – 4 needles broke on the surface of the skin (**Figure 26 B**).

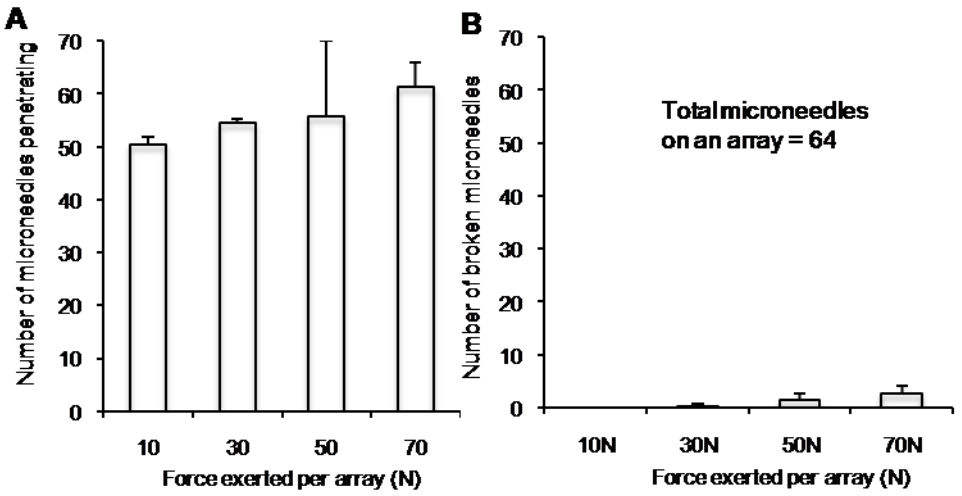

Figure 26 Number of microneedles (A) penetrating and (B) broken on the rat skin, with exertion of different forces between (10 - 70 N).

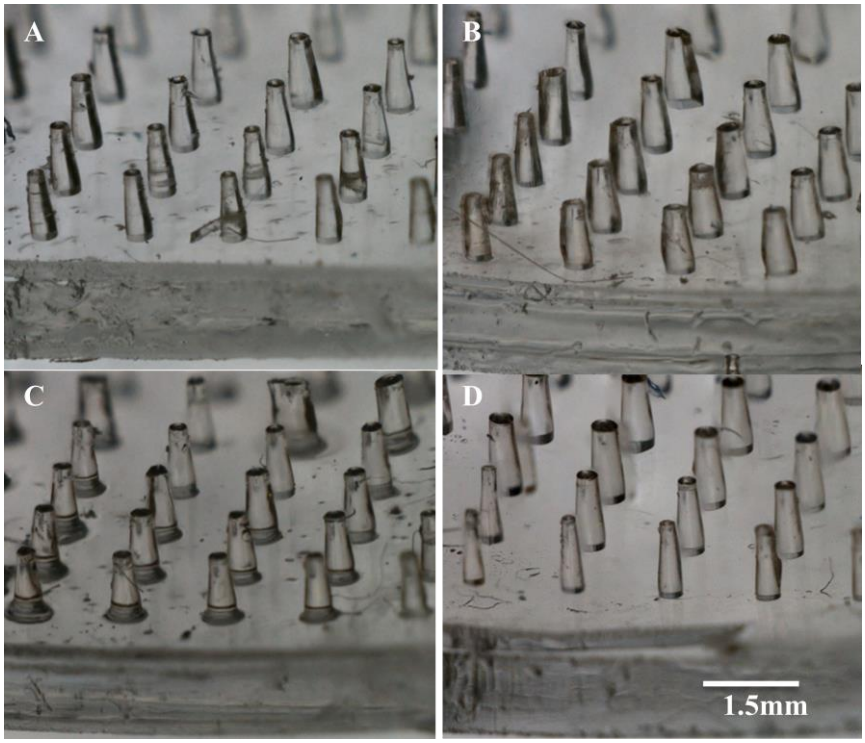

Figure 27 Microneedle arrays after the exertion of different forces (A) 10 N (B) 30 N (C) 50 N (D) 70 N on the skin model were also taken, with the sharpness of the needles maintained.

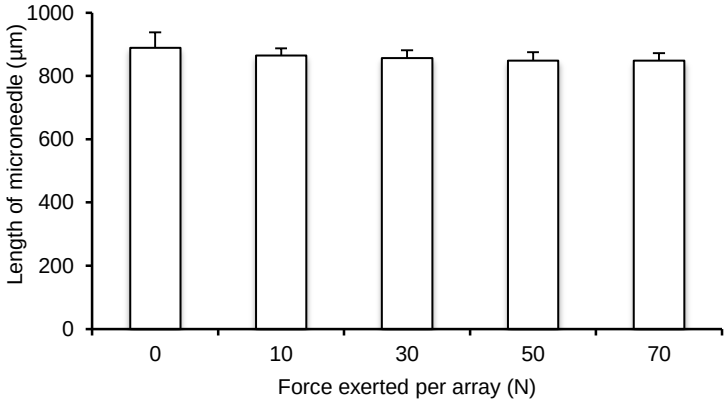

Figure 28 Decrease in the length of microneedles after varying forces were applied on the array.

An increased force of application also increased the percentage of microneedles penetrating through the skin as ascertained by increase in the number of spots stained by trypan blue. Even at the lowest penetration force of 10 N, which closely resembles force of a human thumb, more than 75 % of microneedles penetrate, with this number increasing to nearly 95% at 70 N (**Figure 29**). However, since a force of a thumb would be more ideal and practical in microneedle applications in humans, a force of 10 N using a force gauge was used for application of MITP for subsequent *in vitro* permeation studies.

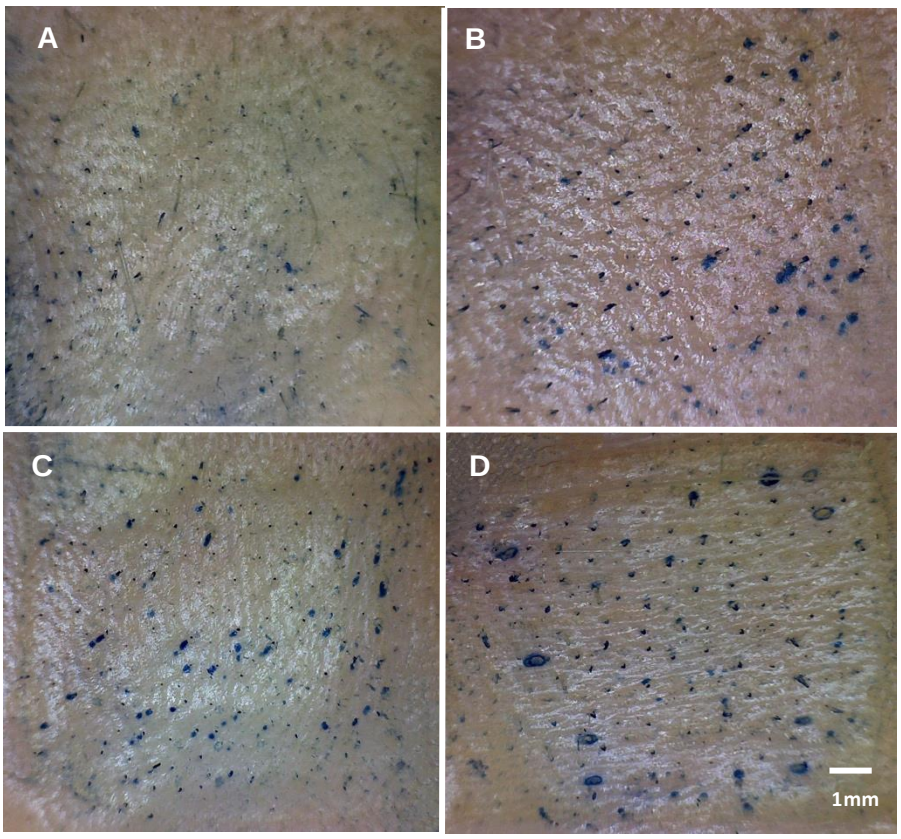

Figure 29 Penetration of microneedles in rat skin by exerting varying amounts of forces on the skin: (A) 10N (B) 30N (C) 50N (D) 70N, as shown by trypan blue staining.

5.2.4. In vitro release of lidocaine from MITP

It is interesting to note that with higher drug concentration, MITP surface exhibits a rougher and corrugated surface, as observed in **Figure 30 A, B** and **C**. With lower (2.2% w/w) lidocaine in MITP, a tightly packed polymer

structure is observed as seen in **Figure 30 A**, while with an increase in concentration to 15% polymer surface appears to be rougher (**Figure 30 B**) and at highest drug loading of 21% w/w, a highly rough and irregular structure is seen (**Figure 30 C**). This rough surface morphology potentially allows for better interaction with the release medium and hence higher drug release. As observed from SEM images post drug release, most of the drug was released from the microneedle shafts, resulting in smooth surface across all tested concentrations (**Figure 30 D, E** and **F**).

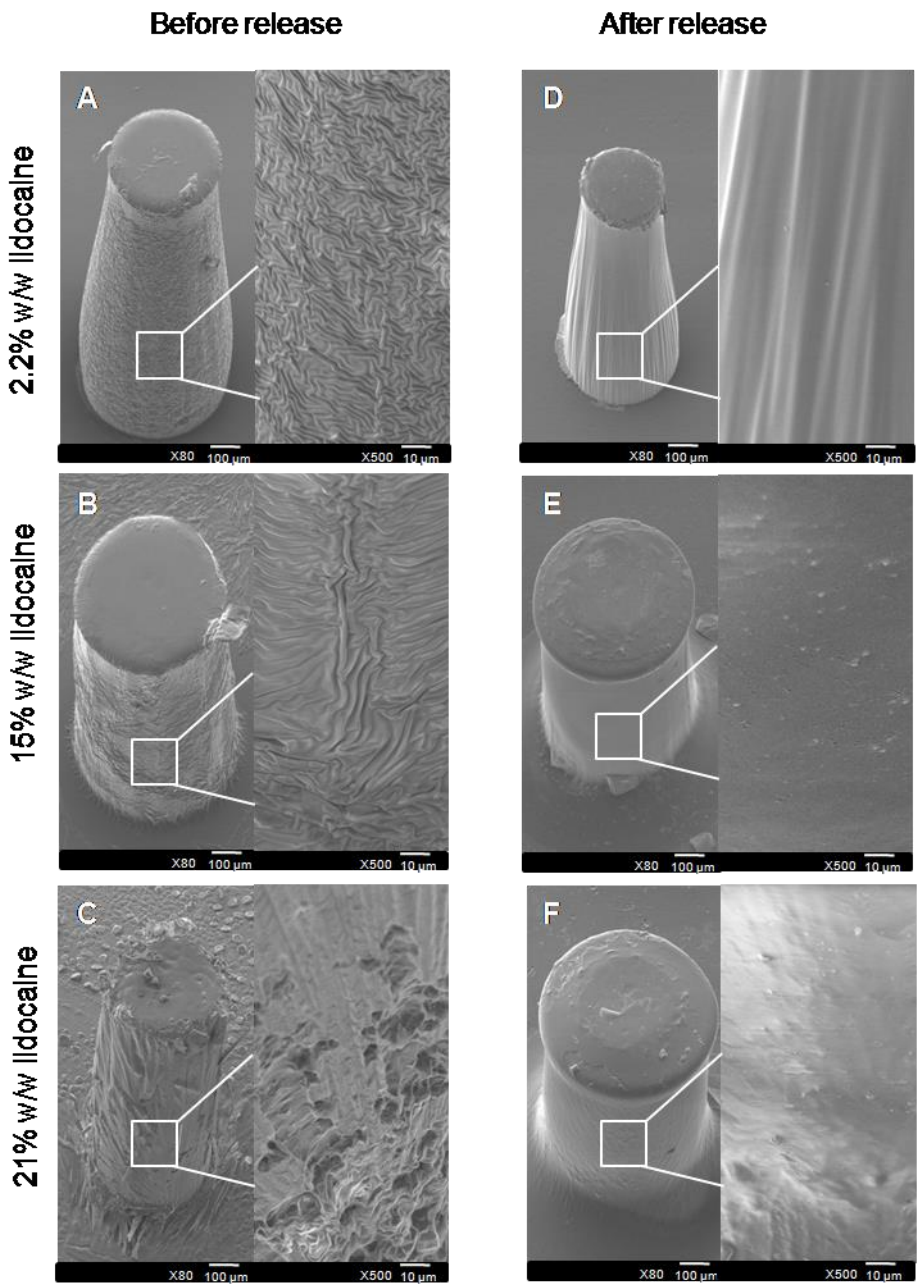

Figure 30 SEM images of MITP before and after the release test. (A) Microneedle containing 2.2% w/w lidocaine shows a smooth surface and tightly packed arrangement of polymer. (B) Microneedle containing 15% w/w lidocaine shows a rougher surface. (C) Microneedle containing 21% w/w lidocaine shows a rough, corrugated surface with a large surface area for interaction with release medium. (D, E and F) SEM images for 2.2%, 15% and 21% w/w lidocaine MITP show a smooth surface indicating almost complete drug release.

The release of lidocaine from the integrated patches encapsulating different concentrations of drug was studied over a period of 24 hours. For all samples, lidocaine was released with an initial rapid burst followed by a gradual release

after about 6 hours (**Figure 31 A** and **B**). A total of 0.20 ± 0.01 mg of lidocaine was released from the MITP containing 2.2% w/w lidocaine, which constituted 15.1% of total lidocaine encapsulated. A larger amount of lidocaine (86.24 ± 11.61 mg) was released from the MITP containing 21% w/w of lidocaine, which made most of the lidocaine encapsulated in the patch (**Figure 31 A**). The difference between the amounts of lidocaine released from the different drug concentrations encapsulated was significant (ANOVA, $p <$ 0.001). The commercial patch released higher amount of lidocaine as compared to all three concentrations of lidocaine-laden MITP.

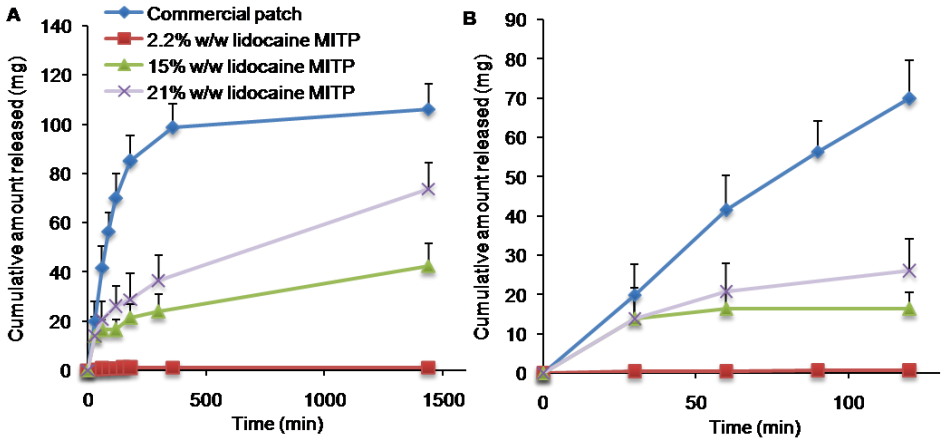

Figure 31 Results from *in vitro* release test of lidocaine encapsulated integrated patch (A) over 24 hours (B) over the first two hours. The cumulative amount of lidocaine released increased as encapsulation concentration increases, with higher concentration showing a sustained release over a period of 24 hours (ANOVA, $p <$, whereas the commercial patch showed an initial burst release followed by a plateau, due to possible drug depletion.

5.2.5. In vitro skin permeation of lidocaine test

With significant amounts of lidocaine released from the fabricated patch, an *in vitro* skin permeation test was conducted over a similar period of 24 hours to determine the practical applications of MITP with respect to a commercial patch, in carrying a higher load of the drug and delivering it at a faster rate.

The MITP was compared with Lignopad® placed on intact rat skin to compare the permeation of lidocaine from both patches.

Although a lower amount of lidocaine permeated when using a 2.2% w/w lidocaine MITP as compared to 5% lidocaine commercial patch, it was observed that when 21% w/w MITP was used more lidocaine permeated through the skin as compared to the commercially available patch (**Figure 32 A**). For the MITP, a total of 25.21 ± 3.41 mg/cm^2 of lidocaine permeated through skin. In contrast, a total of 19.49 ± 8.01 mg/cm^2 of lidocaine from Lignopad® permeated through skin over a period of 24 hours. While a higher amount of drug permeation is desirable, in conditions such as pain a rapid absorption is equally essential. Using the MITP to create microchannels in the skin, lidocaine could be detected in the receptor solution within 5 minutes of placing the MITP on the skin, as compared to Lignopad® in which lidocaine was first detected in the receptor solution only after 45 minutes (**Figure 32 B**). This faster initial rate of drug release could potentially allow for a more rapid rate of pain relief as lidocaine can be delivered to the pain sites faster.

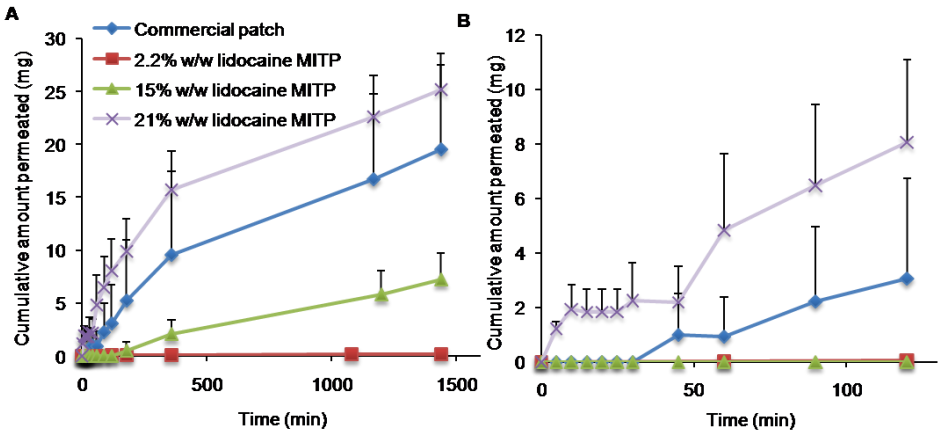

Figure 32 Permeation of lidocaine through rat skin was determined (A) over 24 hours (B) over the first two hours. The amount of lidocaine permeated from the 21% w/w lidocaine patch was higher than that of Lignopad®. Higher initial rates of permeation were also observed for the 21% w/w patch, potentially providing rapid pain relief.

5.2.6. Interaction between polymer and lidocaine: FTIR-ATR spectroscopy

As observed in the *in vitro* release study, particularly for lower concentrations of lidocaine in MITP, a lower amount of lidocaine was released, prompting us to explore any possible chemical interaction between PEGDA and lidocaine. FTIR-ATR spectra revealed the N-H peak shifted from ~3271 cm^{-1} in pure lidocaine powder to ~3258 cm^{-1} in lidocaine in polymerized PEGDA film and broadening of the peak was observed. Also, there was an obvious broadening of the peak at ~1660 cm^{-1}, which could possibly indicate the amide C=O stretch (**Figure 33**). As these observations correlate to those reported in Cui et al.'s characterization of lidocaine in polymers, possible hydrogen bonding might be present in the lidocaine integrated patch, which limits the release of lidocaine from the polymer and some lidocaine to remain in the fabricated patch even after 24 hours of application [248], necessitating a higher initial drug loading required in the MITP. In addition, the spectroscopic peaks at 1635, 1621, 1409 and 810 cm^{-1} corresponding to the main C=C bond signals of acryl groups in liquid PEGDA (**Figure 33 A**) are no longer present upon polymerization of PEGDA into the solid film (**Figure 33 D**) [249], indicating crosslinking between PEGDA molecules to form interpenetrating polymeric networks.

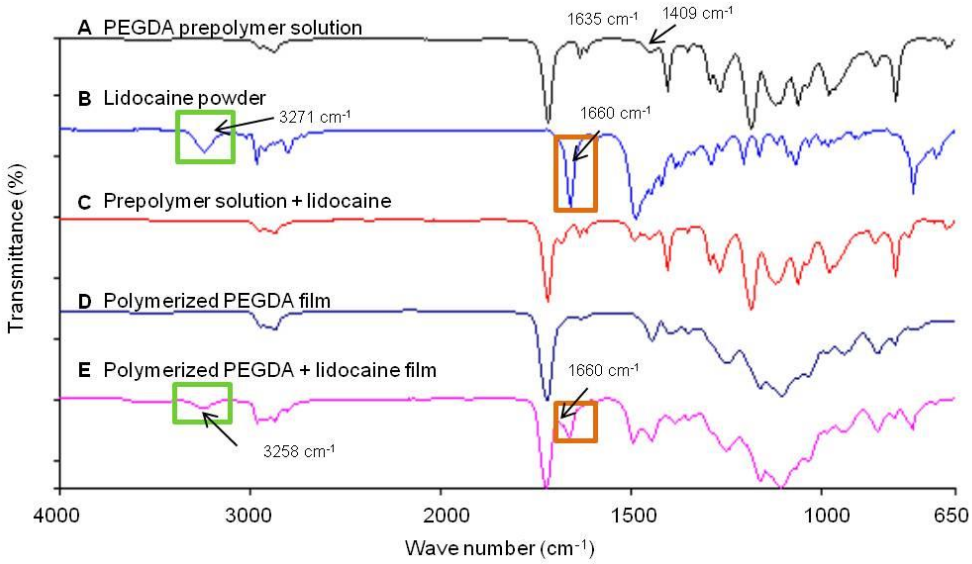

Figure 33 FTIR-ATR spectroscopy of (A) Pre-polymer solution (B) Lidocaine powder (C) Pre-polymer solution with 21% w/w lidocaine dissolved (D) Polymerized pre-polymer film (E) Polymerized pre-polymer with 21% w/w lidocaine film.

5.3. Discussion

The microneedle integrated transdermal patch is a promising approach to improve lidocaine delivery across the skin, providing a suitable alternative to painful injections as well as passive, slow and unreliable diffusion of transdermal creams and patches. Fabrication of the MITP by the photolithographic approach is rapid and simple as encapsulated drugs are not exposed to high heat or drastic temperature changes seen in the micromolding process where the moulds are filled with molten or softened thermoplastics at elevated temperatures [93]. Integration of high loading efficiency backing layer to the microneedle shafts does not require any ancillary equipments as has been reported previously [247]. Fabrication of the whole integrated patch system can be achieved within 1 - 2 minutes, thus commercial scaling up and production of these microneedles is feasible. With more than 1.5 billion people around the world suffering from chronic pain and the pain management market projected to grow to about USD$60 billion by 2015, this microneedle integrated transdermal patch can possibly serve as a viable source for the transdermal delivery of lidocaine with a faster rate of pain relief as compared to the commercially available patch and creams [250].

The applicability of MITP spans the therapeutic and prophylactic domains of acute and chronic pain. The microneedle system aids in creating microchannels on the skin, rapidly delivering the initial analgesic load to cause dermal analgesia. This is particularly important, especially in pediatric patients prior to drug/vaccine injection administration. Also, it would provide clinicians and nurses in emergency and traumatic surgery cases, where it is often difficult to locate the vascular tissues and nerve damage has been a common phenomenon due to inadvertent and accidental injection injury.

At the same time, the transdermal patch integrated to the microneedle array acts as a reservoir of the drug and continues to deliver the analgesic dose through the pores created by the microneedles over a longer period of time, as is desired in the cases of neuropathic pain. This microneedle array has a distinct mechanism of delivering drugs, from the four common ways of drug delivery proposed for microneedle systems by Kim et al. [93]. The

microneedle although being polymeric, are made using poly (ethylene glycol) diacrylate, which doesn't readily dissolve, hence providing an opportunity for provision of channels in the skin, through which the drug stored in the patch could be delivered for prolonged period of time. Since, different layers of the integrated patch were also fabricated independently; hence the drug of interest can possibly be incorporated into the microneedle shafts, the thin or the thick backing layers, to allow for a rapid or sustained drug release as well as the MITP could be used to encapsulate potent drugs in the microneedles to provide rapid analgesia, followed by maintenance analgesia by a less potent drug encapsulated in the integrated transdermal patch.

MITP containing a thicker backing is also amenable to application of larger forces aiding more efficient microneedle penetration and at the same time microneedle shafts more resistant to breakage as compared to microneedles supported on a thin film. Although UV light has been shown to cause photodegradation of light sensitive drugs, short exposure process did not cause lidocaine degradation, as was highlighted from the FTIR-ATR spectra as well (**Figure 33**).

Lidocaine was successfully shown to be released from the MITP and permeated through rat skin (**Figure 31 and 32**). Thus, the MITP serves as a potential drug delivery system, which is able to overcome the limitations of a conventional transdermal patch. Even though Lignopad® released more drug than the microneedle integrated patches, it showed an initial burst release profile followed by a plateau indicating drug depletion in the patch. On the other hand 21% w/w lidocaine showed a consistent increase and sustained release of lidocaine over a period of 24 hours. With lower concentration (2.2% w/w) of drug loading, microneedles structures were formed with tight polymer structure packing as shown from SEM images in **Figure 30 A**, while with higher concentrations (15 and 21% w/w), a more porous structure was observed, explaining the higher drug release from the microneedles containing higher amounts of lidocaine (**Figure 30 B** and **C**). This potentially provides an ideal delivery system, with rapid release of drugs from the polymeric core and a sustained release due from the reservoir patch.

Permeation of lidocaine was greater from the integrated patch due to the presence of microneedles that penetrate the stratum corneum. This highlights the utility of having a combination of active and passive drug delivery system, integrated into one device to have benefits of both. The lag time for lidocaine permeation was reduced from 45 minutes in Lignopad® to 5 minutes when the MITP was used. This is favorable to achieve almost instantaneous pain relief (within 0-15 min) from the use of microneedles, similar to the effects achieved by a hypodermic injection [244]. Maximum pain relief from transdermal patches were shown to be obtained after 4 hours of patch application with three transdermal patches were applied onto the skin [241], with the patch application requiring a larger area for drug absorption. This problem could be potentially alleviated with MITP application as larger amount of drug could diffuse through a smaller area in a shorter period of time, providing higher patient compliance and quality of life. Hence, MITP could provide a more efficient delivery of lidocaine for faster pain relief in patients with peripheral neuropathic pain.

Although lidocaine delivery using microneedles has been studied previously [244, 246], the MITP offers the advantage of having a simple fabrication process and high encapsulation efficiency of more than 70 mg of drug. This is particularly relevant as small molecular weight drugs are required in higher amounts to achieve clinically relevant concentrations. In addition, the use of MITP does not require any additional gel or lidocaine containing solution to be applied onto the skin, as lidocaine can be easily incorporated and released from the cross-linked polymer matrix. For hydrophilic drugs insoluble in PEGDA, they can be first dissolved in very small amounts of water and mixed with PEGDA to form a uniform dispersion [251]. Preferential incorporation of drugs could be achieved in the MITP. Drugs incorporated into microneedle shafts allow for bolus and rapid release while that in the backing layers allow for sustained release as it acts as a drug reservoir. Dissolving lidocaine in PEGDA assures a uniformed distribution of drug and retains the geometry of microneedle shafts, a feature largely lost during coating of microneedles.

Despite the higher permeability achieved with MITP as compared to Lignopad®, a higher amount of drug loading was required to achieve this

effect. This is probably due to chemical interactions between lidocaine and PEGDA, forming hydrogen bonds as was revealed in the FTIR-ATR spectrum (**Figure 33**), where enhanced affinity between lidocaine and the polymer matrix and preventing drug release. A similar effect was also observed in the release test, where lower amounts of lidocaine were released from MITP as compared to Lignopad®, where an MITP patch containing 2.2% w/w of lidocaine contains similar amounts of lidocaine as compared to the same area of Lignopad®. However, the amount of lidocaine released and permeated from the 2.2% w/w lidocaine integrated patch is much lower than that from Lignopad®. This effect was observed to a lower extent, with higher drug loading amounts of 15 and 21% w/w, possibly due to the reason that more diffusion passages were created at higher drug-loading microneedles.

5.3. Summary

The lidocaine encapsulated microneedle integrated transdermal patch was shown to be an ideal alternative to injections and passive transdermal systems like gels and creams for the management of acute and chronic pain. MITP was shown to deliver lidocaine at a faster initial rate than Lignopad®, with lidocaine permeating rat skin within 5 minutes of MITP application, whereas Lignopad® had a delay of 45 minutes before lidocaine permeated. This faster permeation enables a possibly faster rate of pain relief for patients. Having a larger amount of lidocaine permeating through the skin can also potentially reduce the patch application time which decreases the likelihood of developing skin irritation. Thus, the integrated patch could be a good clinical tool for pediatric applications, management of perioperative pain and chronic pain in patients suffering from diabetes, cancer and herpes zoster infection, and can be used in home care settings due to its ease of application.

CHAPTER 6

Direct Microneedle Array Fabrication off a Photomask to Deliver Collagen through Skin

(Adapted from a manuscript submitted to *Pharmaceutical Research*, 2013, In press)

6.1. Overview

Various fabrication methods have been used to form polymeric microneedles. One of the common methods employed by researchers is micromolding in which molds of the desired microneedle geometry are constructed using high-aspect-ratio SU-8 epoxy photoresist or polyurethane master structures to form PDMS (polydimethylsiloxane) molds from which biodegradable polymer microneedle replicates are formed [252, 253]. However, this approach involves numerous steps and the use of toxic SU-8 epoxy in the intermediate processes [254].

In the previously developed method described in chapter 3, photolithography using photomasks was used as an alternative to fabricate polymeric microneedles in a single step, mould free process [117]. Polymer was exposed to high intensity ultraviolet (UV) light through a patterned film in the presence of a photo initiator to form crosslinked polymeric rods. Free radicals formed by the photoinitiator propagate the polymerization reaction. This method offers the advantage of a short fabrication time and a greater suitability of scaling up commercially for industrial purposes. However, as no mechanism to optically modify the light path was involved, the formed microneedles had bigger tip diameter which potentially affects the efficiency of penetration through the skin.

To overcome this problem, in this chapter, a simple photolithographical process using microlenses to fabricate polymeric microneedles of increased sharpness was developed. Instead of planar photomask films, specific convex microlenses were etched on to a glass substrate to guide the light path, resulting in sharper microneedles as compared to previously developed

method. Although some previous studies have involved the use of microlenses to fabricate polymeric microneedles, those methods were limited by involvement of multiple complicated steps [252]. Mechanical properties of microneedles were characterized to ensure their suitability for efficient penetration through excised rat skin. Previous studies have showed that reducing the tip diameter and increasing the base width may improve the mechanical properties of the polymer microneedles [117, 254].

Finally, evaluation of usability of the resultant microneedles in the transdermal delivery of biopharmaceutical cosmetic products like collagen was performed on rat skin.

6.2. Results

6.2.1. Fabrication of photomask

The characteristics of the photomask and the embedded microlenses affect the geometry of the microneedles significantly as the path of the UV rays are dependent on the degree of refraction on the convex surface of microlenses (**Figure 34 A**). All photomasks consisted of an array of microlenses (7 × 7) with a constant center-to-center spacing of 1000 µm. Analysis of microlenses revealed that each microlens has a diameter of 350 µm with a flattened convex surface of diameter 130 µm, and a depth of 62.3 µm as shown in **Figure 34 B - D**. To evaluate the estimated focal length (f) of the microlens, radius of curvature of the first surface was calculated to be 272.89 µm using Pythagoras theorem. Considering these parameters and the refractive index of both glass (1.53627) and air (1.000) at a wavelength of 365 nm, the focal length was estimated to be 509.28 µm via the Lens maker's equation as stated below:

$$1/f = (n_1/n_m - 1) * (1/r_1 - 1/r_2)$$

Where,

n_1 - Refractive Index of Lens Material
n_m - Refractive Index of Ambient Medium
r_1 - Radius of Curvature of the First Surface
r_2 - Radius of Curvature of the Second Surface

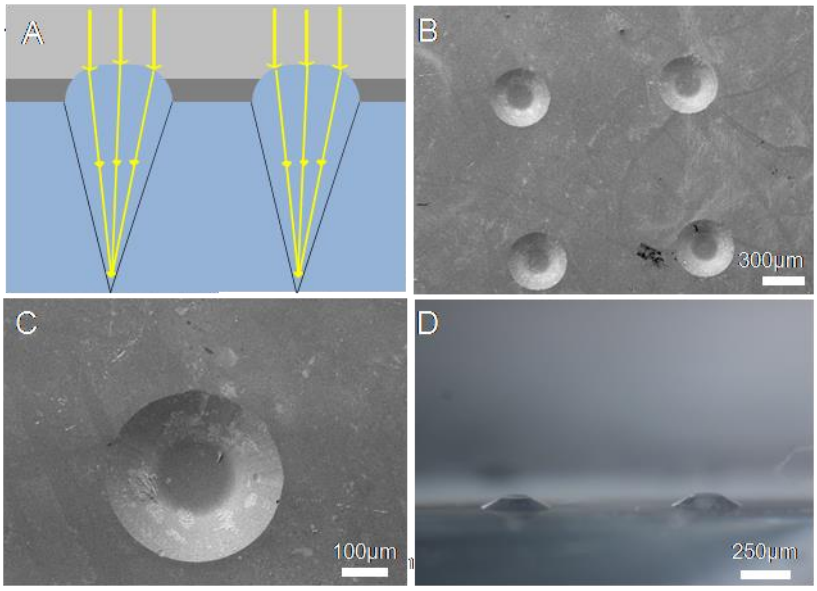

Figure 34 Characterization of photomask. (A) A SEM image of a portion of an array of microlenses etched into a glass substrate. (C) A SEM image of a microlens. (E) A portion of an array of PDMS mold replicas copied from the microlenses, showing the flattened convex surface, under a stereomicroscope. (F) UV (365nm) exposure focuses light into a conical path, producing tapered microneedles.

6.2.2. Fabrication of polymeric microneedles

a) Effect of intensity of UV light

The intensity of UV light was varied between 3.14 to 15.1 W/cm^2 maintaining the spacer thickness (5 mm) and distance from UV light source (3.5 cm) constant. Average microneedle length was found to increase from 2358 ± 144 µm to 3347 ± 156 µm when intensity was increased from 3.14 to 9.58 W/cm^2 ($p < 0.05$) (**Figure 35 A**). However, the difference in average length measured for the needles formed for the intensities 9.58 to 15.1 W/cm^2 was found to be insignificant ($p > 0.05$). The minimum length obtained is more than three times the estimated microneedle length quantified by the focal length.

Sharpness, quantified by tip diameter of microneedles, reduced as intensity was increased. Average tip diameter increased from 41.5 ± 8.4 µm to 49.0 ± 5.8 µm for the intensities of 3.14 to 6.44 W/cm^2 ($p < 0.05$) as shown is **Figure 35 B**. However, no significant change in the tip diameter was observed from 6.44 to 12.4 W/cm^2, with a maximum tip diameter of 71.6 ± 13.7 µm obtained

when an intensity of 15.1 W/cm^2 was used. Interestingly, greater level of deformation on the needles was observed as higher intensities were used. It was noted that the microneedles' upper half became wider and more cylindrical with the lower half acquiring a more tapered formation as intensities increased. In addition, the tips of the microneedles also underwent deformations leading to more irregular structures as shown in **Figure 36 A, C** and **D**. The microneedles fabricated at 6.44 W/cm^2 were observed to be more regular in shape (**Figure 36 B**), than that of higher intensities, without significant structural deformation thus preserving the sharpness. Hence, this intensity was chosen for fabrication of microneedles for subsequent experiments.

b) Effect of spacer thickness

The spacer thickness was varied between 1050 µm to 5000 µm maintaining the intensity (6.44 W/cm^2), and distance from UV light source (3.5 cm) constant. An expected increase in average length was observed for the spacer thivkness of 1050 to 2525 µm ($p < 0.05$). Insignificant difference in average length was recorded for the needles formed for the spacer thickness of 2525 µm to 3000 µm ($p > 0.05$). The longest microneedle length of 3347 ± 156 µm was observed for the needles formed using a spacer thickness of 5000 µm ($p < 0.05$) (**Figure 35 C**). Average tip diameter decreased as the spacer thickness was increased from 1050 µm to 3000 µm ($p < 0.05$), with a constant tip diameter reached beyond the spacer thickness of 3000 µm ($p > 0.05$) (**Figure 35 D**).

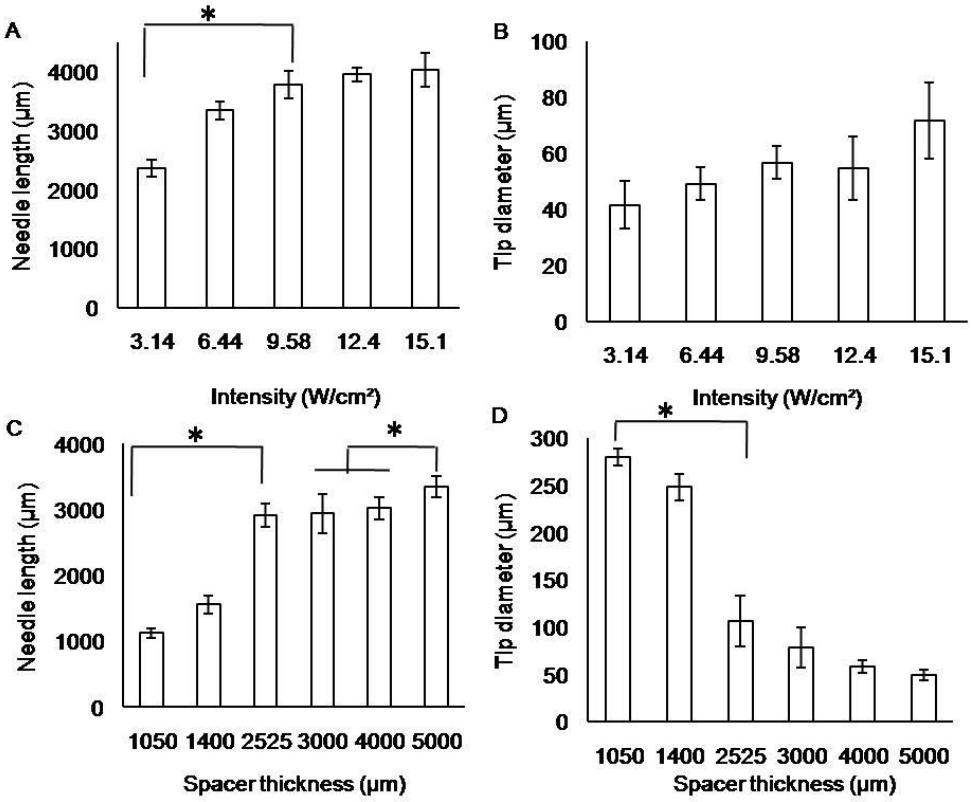

Figure 35 Effect of UV parameters on microneedle geometry. Effect of (A) intensity and (C) spacer thickness on microneedle length. Effect of (B) intensity and (D) spacer thickness on microneedle tip diameter.

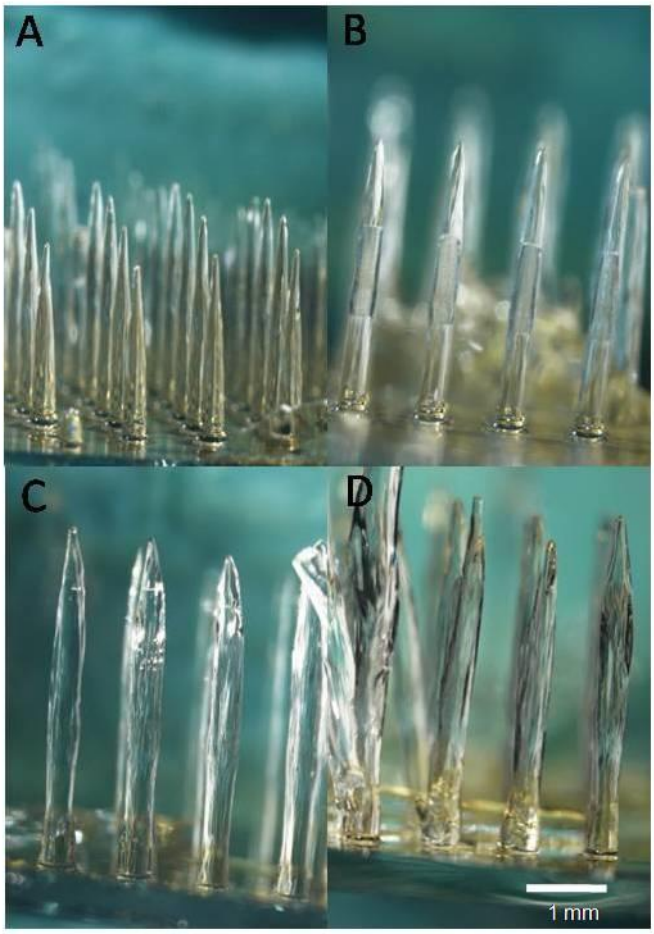

Figure 36 Effect of increasing intensity on geometry of microneedles. (A-D) images showing increasing level of deformations at intensities 3.14, 6.44, 9.58 and 12.4 W/cm² respectively.

6.2.3. Effect of backing layer volume

Formation of a backing layer is crucial to enhance the strength of the microneedle shafts and to enable the removal of the microneedles from the photomasks, making them reusable. The thickness of the backing layer was manipulated by varying the volume of prepolymer solution. Two different volumes (300 µL and 400 µL) were used for this purpose. Due to the affinity between the polymerized microneedles and the prepolymer solution together with the small center-to-center spacing between microneedles, capillary action was evident. Subsequent exposure to UV light led to formation of each patch of microneedle acquiring a range of length, with the tip diameter being unaffected as shown in **Figure 37 A** and **B**. It was observed that the average microneedle length decreased from 1336 ± 193 µm to 957 ± 171 µm as

volume used to form the backing layer, was increased from 300 µL to 400 µL (**Figure 37 E**). Similarly, base diameter reduced from 233 ± 20 µm to 156 ± 21 µm ($p < 0.05$).

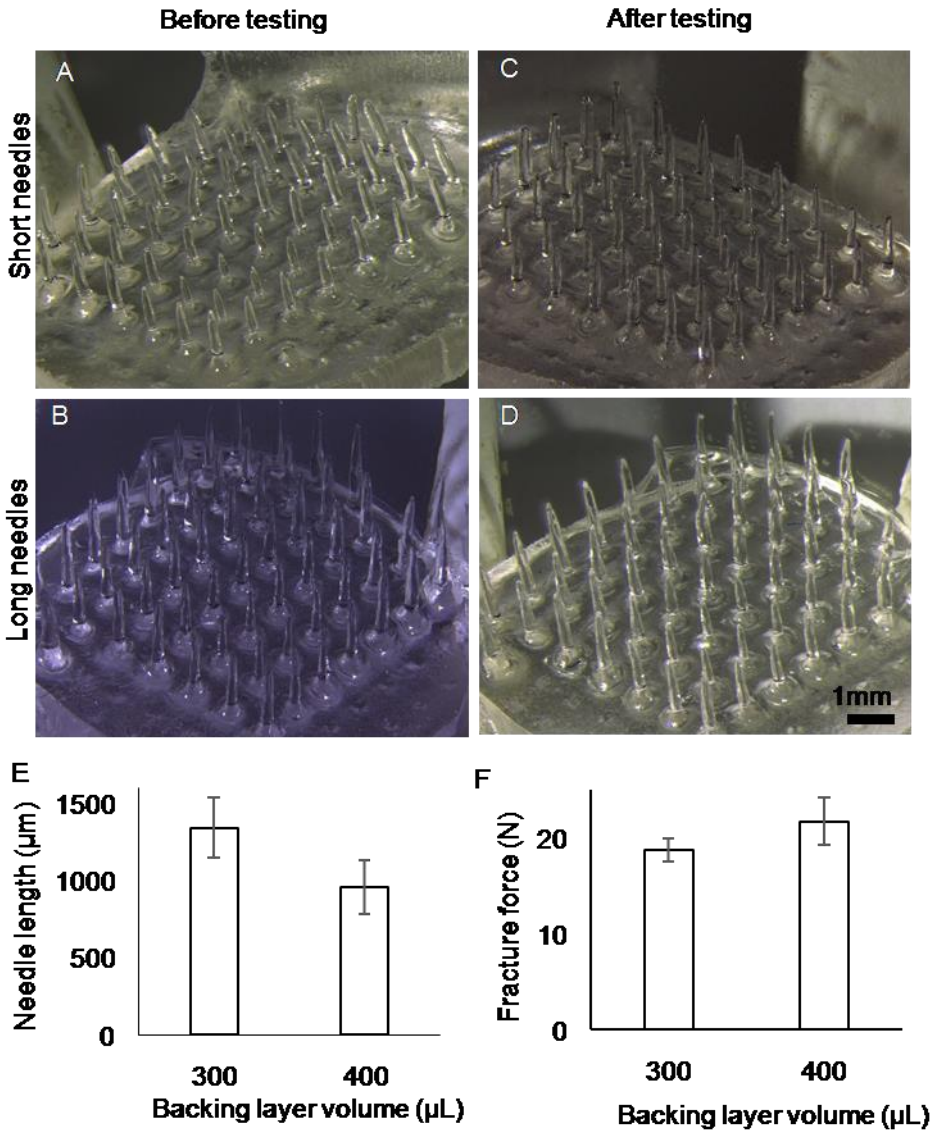

Figure 37 Effect of varying pre-polymer volume used for backing layer fabrication.(A-B) images at various pre-polymer volume, with average microneedle length for short (957 µm) and long (1336 µm) microneedles respectively. (C-D) Images corresponding to (A-B) after fracture force testing. (E) Decrease in microneedle length with increase in pre-polymer volume used for backing layer fabrication. (F) Microneedle fracture force across the two pre-polymer volumes used to fabricate backing layer.

6.2.4. Microneedle fracture force testing

Evaluation of the effect of the thickness of the patch on the strength of microneedles is essential for the selection of the appropriate type of patch for maximum penetration through the skin. After subjecting each class of microneedle array to an increasing force against a flat surface, it was observed that the fracture force was consistent for both classes of patches with a similar negligible degree of breakage for both microneedle arrays as depicted in **Figure 37 C, D** and **F**.

6.2.5. Microneedle penetration in human skin

Microneedles of average length 957 (short) and 1336 (long) μm were inserted in cadaver human skin. Trypan blue staining method was used to demonstrate the extent of penetration by each type of microneedle shaft as shown in **Figure 38 A** and **B**. Negligible staining on the control skin proved that trypan blue only stains the sites of corneum perforation.

The extent of penetration by the shorter microneedle shafts was found to be higher (72.7 ± 5.1%) as compared to longer shafts (52.3 ± 3.1%), ($p < 0.05$) (**Figure 38 C** and **D**). Fracture of microneedle was not observed in any of the microneedle shafts tested.

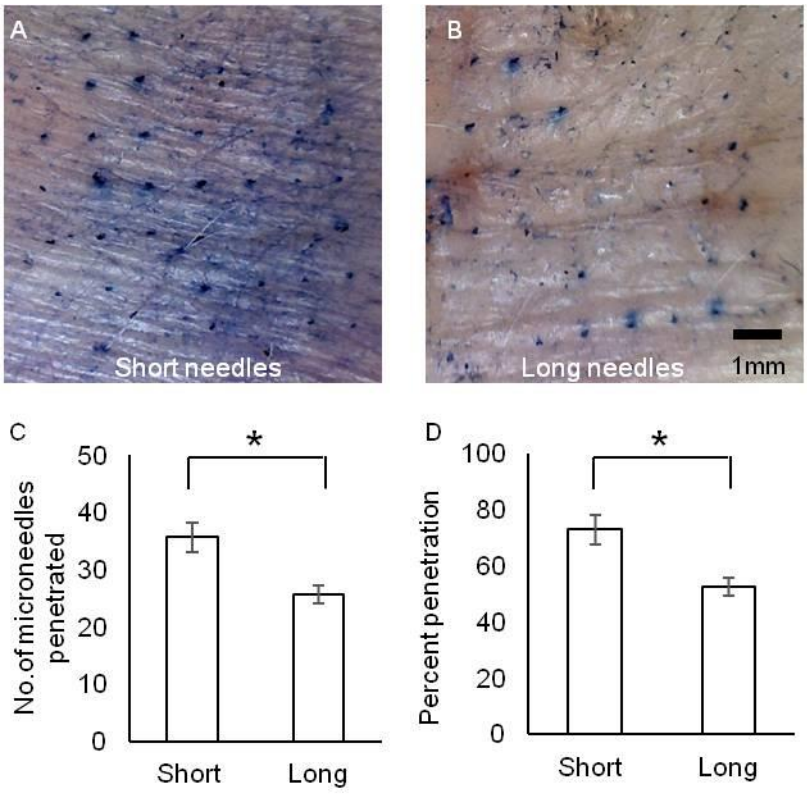

Figure 38 Penetration of microneedles in rat abdominal skin. (A-B) Images of penetration by microneedles of average length 1336 and 957 µm respectively, with the force of a thumb. (C) Number of successfully penetrated microneedles of average length 1336 and 957 µm. (F) Percentage of penetration by microneedles of average length 1336 and 957 µm.

6.2.6. In vitro collagen permeation through rat skin

The ability of microneedles to increase skin permeation of bovine collagen type 1, FITC conjugate (MW = 300 kDa) was assessed. The control skin (without collagen treatment) was found to possess a significant level of auto fluorescence which was visible up to a depth of 150 µm (**Figure 39 A**), while application of collagen solution on intact skin did not lead to any significant absorption (**Figure 39 B**).This phenomenon could be due to the presence of fluorescent biomolecules such as lipofuscin and riboflavin [255-257] on the rat skin which are able to emit light at similar wavelengths used in the experiment. However, this did not hinder the analysis of the increase degree of collagen permeation by the microneedles. With the shorter microneedle of 957 µm, three concentrations of collagen revealed a penetration to a depth of 250

to 300 µm confirming the increased extent of diffusion of collagen molecules through the skin up to the dermis layer as shown in **Figure 39 C - E**.

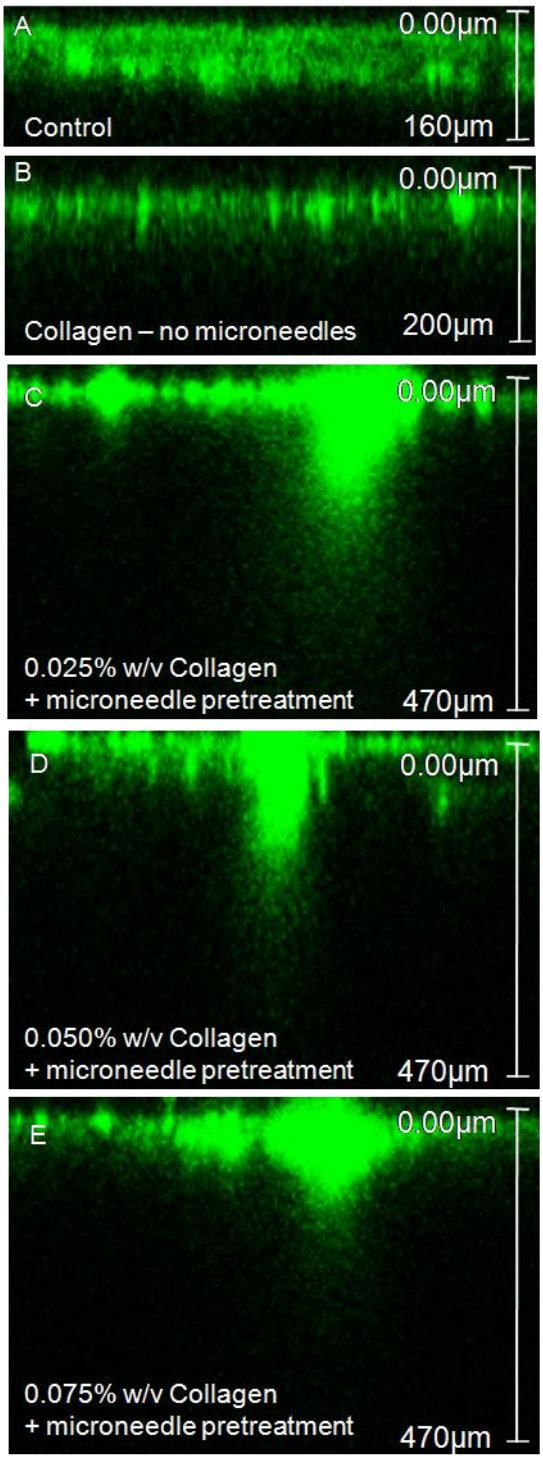

Figure 39 Collagen permeation in rat skin. (A) Auto-fluorescence of cadaver rat skin. (B) Fluorescence of bovine collagen type 1, FITC conjugate together with auto-fluorescence of control rat skin without microneedle treatment. (C-E) Fluorescence of bovine collagen type 1, FITC conjugate together with auto-fluorescence of rat skin for collagen concentrations 0.025, 0.05 and 0.075% w/v respectively.

6.3. Discussion

Many groups have successfully developed polymeric microneedles using photolithographical methods. Previous studies to develop sharp polymeric microneedles have used multi-step methods involving development of SU–8 master structures to create PDMS molds and the use of lasers [252, 258]. Long processing time and requirement for sophisticated equipments are certain limitations of these methods. Development of a simple photolithographical process by us previously involved the use of a planar patterned photomask showed a simple alternative to mould based methods. However, with the use of planar photomasks, UV light passed through straight with little deviation resulting in microneedles with a more cylindrical and less sharp tips.

In this chapter, a one-step lithographical method utilizing a photomask with integrated convex lenses was developed. Ultraviolet rays undergo refraction at the surface of the lens, allowing the rays to converge at a focal point. Polymerization reaction in the presence of UV only occurs in the converged path. This results in sharp- tipped microneedles with improved skin penetration capability than previously fabricated microneedles. While thermal and annealing processes were recently reported for fabrication of microneedles on a curved surface [259], this photolithographical approach is amenable for production of microneedles of any desired shape and geometry.

This new approach to fabrication involved first optimizing fabrication conditions to form sharp microneedles. Lens geometry, UV light intensity and spacer thickness were considered as factors influencing microneedle fabrication and geometry.

Characteristics of the thin lens in the photomask determine the degree of refraction of the UV light rays at the convex surface. The Lens makers' equation, which is used to approximate the focal length of a thin lens, was evaluated for its suitability as a predictive model for microneedle length in the fabrication process. Microneedle length measured was at least three times more than the calculated focal length regardless of UV light intensity. This indicates that the Lens makers' equation may not be an accurate predictive model. This could be due to the presence of the flattened convex surface of the

microlens. The irregular convex surface could have caused spherical aberration of light rays causing the path of light rays to be significantly different from that of a conventional convex thin lens [260]. Spherical aberration allows parallel light rays that pass through the central region of the lens to focus farther away than light rays that pass through the edges of the lens leading to differential microneedle lengths. However, it was found that the lack of a perfectly curved lens did not hinder the formation of sharp-tipped microneedles after optimization of other parameters.

The intensity of UV light used for the polymerization process is another important with respect to the microneedle geometric properties. In the new approach, an intensity of 6.44 W/cm^2 allowed microneedles to reach a high vertical length, with minimal structural deformation, and a desirable sharp tip diameter. Although sharper microstructures without any observable deformation were obtained at lower intensities as well, the microneedles may not possess sufficient strength and a higher intensity leads to formation of more rigid microneedles which improves the penetration efficacy.

Another phenomenon observed was that the length of microneedles increased significantly with the microneedles acquiring a more cylindrical shape, compared to the hypothesized conical shape, as intensity increased. The optical nature of light may rationalize this occurrence. Due to the flat top surface of the microlens, some light rays travel beyond the focal point in a collimated manner [261, 262]. In addition, converged light rays may also extrapolate beyond the focal point. These particular optical movements of light rays could have led to the formation of the more cylindrical portions of the needle. However, as degree of polymerization has a limit and based on the inverse-square law of light, UV light loses energy as the distance away from the surface of the lens increases [263]. This explains the tapered appearance of the microneedles observed beyond the focal point. As intensity was increased, more photons were transmitted to a further distance leading to greater uneven polymerization, evidenced by the non-uniform tapered structures and deformations formed at higher intensities in **Figure 36**.

The formation of the backing layer is important to strengthen the array as a whole and to ensure reusability of the photomask. Emphasizing the importance of the backing layer, effect of the thickness of the backing layer on the strength of the microneedle shafts and extent of penetration was studied. In both different lengths of microneedle shafts, a significant fraction of the microneedles was intact after a force of more than 60 N was applied.

The ability for the polymeric microneedles to bend causes the actual compressive stress at the tip of the microneedle to be much lesser than the total compressive force applied by the thumb. It has been reported in literature that to avoid sudden failure of a microneedle by buckling, and to insert the microneedle into the skin successfully, a 12:1 aspect ratio of length-to-equivalent diameter or lesser is recommended [264]. However, it was observed that for two lengths of microneedles had an aspect ratio lower than 12:1. The shaft with the longer microneedle length (1336 μm) obtained the aspect ratio of 11:1, while the other shorter microneedle shaft obtained an aspect ratio of 8:1. While some microneedle bending when applied on human skin was seen, shorter microneedles with aspect ratio 8:1 penetrated better, indicating that microneedle tip diameter is a more critical determinant of microneedle penetration, irrespective of its base diameter.

As a model for microneedle mediated enhancement of permeation of macromolecules, bovine skin collagen type 1, FITC conjugate was used. While FITC collagen is not a substitute for collagen and its cosmetic properties, fluorescence from FITC tagged collagen enabled easy analysis and visualization of depth of permeation. Diffusion of collagen molecules was greatly enhanced by the treatment of skin with the fabricated microneedles. Microneedles enhance the permeation by creating micro channels allowing macromolecules to pass through the skin. In this particular study, FITC tagged collagen molecules with a molecular weight of approx 300 kDa + 400 Da could permeate the skin, and hence it is expected that native collagen will be able to permeate the skin as well.

Collagen molecules were able to diffuse past the epidermis and reach the dermal layer. This enables exogenous collagen to express its pharmacological

function effectively which includes activating keratinocytes in the dermis layer for reepithelialisation [265]. While collagen has been extensively used as a cosmetic product to retard skin degradation in chronologically aged skin [265, 266], its efficacy from topical preparations is questionable as stratum corneum is impermeable to collagen [267]. With microneedle pretreatment, collagen could permeate in significantly higher amounts and to greater depths in the skin, potentially providing a gateway for its enhanced efficacy.

The fact that higher concentrations of collagen did not significantly increase the diffusion rate, can be explained by the fact that epidermis and dermis layer offer a significant permeability barrier to both small molecules and macromolecules [268] thus becoming the rate limiting step upon sufficient permeabilization of the stratum corneum. This implies that higher doses of collagen may not warrant an increased pharmacological effect when delivered transdermally. Moreover at higher concentrations, collagen is more susceptible to gel formation and hence may actually result in less amount of permeation as compared to lower concentrations which remain in solution and hence more easily available to pass through the micro channels created microneedles.

Another issue with collagen molecules is their stability and maintenance of native confirmation. We also observed that primary structural properties of collagen type 1 when applied to skin post microneedle application were similar to freshly prepared solution of collagen indication stability of collagen post microneedle application and delivery into the skin.

In a recent patented technology [269], collagen type VII was modified by recombinant production in host cells having higher expression of prolyl 4-hydroxlase resulting in collagen having more proline residues. This collagen with increased proline residues has higher in vivo stability and a longer half life. The said collagen was then encapsulated in polymeric microneedles made from chitosan or alginate in pre formed micromolds. These microneedles are then used to deliver collagen VII to epidermis-dermis basement membrane in patients of dystrophic epidermolysis bullosa, a genetic disease where there is lack of functional collagen VII and leads to formation of painful blisters on

the skin. Apart from these, there are some reports in literature and numerous on the internet, whereby microneedles are used to activate the normal healing cascade of the skin, causing temporary injury and initiating collagen synthesis to rejuvenate the skin.

6.4. Summary

A simple photolithographical method to fabricate polymeric microneedles, whose geometry could be controlled by modifying the photomask parameters in a mould free manner, was developed in this study. The microneedles were able to penetrate excised rat skin effectively when inserted with the force of a thumb. Microneedle shafts were also able to withstand high levels of compressive force due to the increased elasticity and shock-absorbing property of the backing layer. Irrespective of the length of the microneedle shafts, this method provides the capability to produce microneedles with similar tip diameters. In addition, it was proven that collagen can be delivered transdermally up to the dermis layer for its cosmetic/pharmacological effect. The approach may be useful for the transdermal delivery of proteins and other macromolecules for localized effect within the skin layers. Finally, the new fabrication process has the potential for scaling up for mass production.

CHAPTER 7

A Miniaturized Flow-through Cell (MFtC) for Testing the Permeation of Drugs across Biological Membranes

(Adapted from *International Journal of Pharmaceutics*. 2013; 441 (1-2): 433-440)

7.1. Overview

Conventionally, a variety of transdermal diffusion cells were developed for the evaluation of *in vitro* permeation characteristics of transdermally delivered drugs. In principle, some are based on the static, non flowing cells [270] in which the donor and receptor compartments may be placed either vertically (Franz type) [271] or horizontally (side-by-side) [272, 273] and others are the in-line, flow through cells, that offer the advantage of continual replenishment of receptor fluid and hence aid in maintaining a condition similar to microcirculation in the *in vivo* setting [274, 275].

Several modified versions of these diffusion cells have also been fabricated and validated against the conventional apparatus. Sanghvi and Collins compared the permeation characteristics of hydrocortisone using the "enhancer cell", which is a modified version of USP type II dissolution apparatus to serve as a diffusion cell [276]. Modified automatic sampling apparatus have been developed [277-280]. These static and flow-through cells have been compared and validated [281-283]

However, a major drawback of these cells is the requirement of relatively large amounts of drug owing to their inherent designs. Investigational new drug entities, such as anticancer drug endoxifen, are prohibitively expensive for such studies. This was the motivation to develop a miniaturized testing system that utilizes minimum amount of the drug.

Microfluidic platforms which are miniaturized fluid flow systems have recently received significant attention in the drug discovery and development horizon, due to their abilities to reduce the amount of reagents necessary for

assays and pre-clinical development [284]. These microscale systems fabricated with biomaterials such as polydimethylsiloxane (PDMS), may provide a useful model to develop miniaturized flow-through cells. A PDMS-based, miniaturized flow-through cell to minimize the consumption of candidate drugs was envisaged. With the economic environment in pharmaceutical firms becoming more tenuous and pharmaceutical cost containment being the main focus, the need to develop pre-formulation testing systems that utilize minimum amount of the drug is the need of the hour.

In this chapter, fabrication of a miniaturized flow-through cell for *in vitro* skin permeation studies is described. The system was compared and validated against a static, horizontal diffusion cell (HDC) using two model drugs, namely, rhodamine B and α-mangostin. Histological sectioning of the skin 24 – 48 hour post-application in both diffusion cells was conducted to test for skin damage. Subsequently, the skin permeation of endoxifen was assessed with several skin permeation enhancers (PEs). One of the enhancers was found to be able to deliver enough endoxifen for its clinical applications.

7.2. Results

7.2.1. Validation of MFtC against horizontal diffusion cell

For the receptor liquid, an average flow rate of 0.18 ± 0.01 mL/hr was measured (**Table 6**). The choice of low flow rate was selected to achieve adequate drug to be present in the samples for detection and quantification. This is particularly important in the case of low flux. It was reported that flow rate of the receptor solution does not affect the numerical value of the flux of drug but the time to achieve steady state instead [281]. Therefore, any small fluctuations in the flow rate would not influence the flux significantly.

Table 6 Flow rate (mL/hr) of the receptor solutions (mean ± S.D.) N = 9.

Flow rate (mL/hr)			Accuracy (%)	RSD (%)
Run 1	Run 2	Mean		
0.17 ± 0.01	0.19 ± 0.01	0.18 ± 0.01	88.50	7.94

The different nature of the two model substances (rhodamine B and mangostin) and varied concentrations were chosen to ensure the reproducibility of permeation parameters in the presence of different test substances. No significant difference in J_{ss} ($p > 0.05$) was found between the horizontal diffusion cell and the MFtC for the three different donor solutions (**Figure 40** and **Table 7**). While the design of the MFtC varies significantly from that of the horizontal diffusion cell, the results obtained confirmed that permeation profiles from both the set-ups were comparable, thereby confirming that the MFtC fabricated is a suitable platform for reproducible results for scaled-down permeation studies.

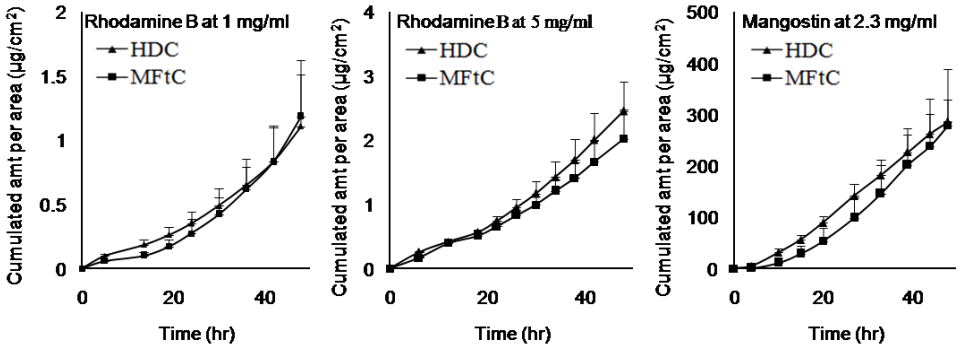

Figure 40 Time course of cumulative amount permeated through rat abdominal skin for rhodamine B at 1 mg/mL, rhodamine B at 5 mg/mL and mangostin at 2.3 mg/mL. Each point represents mean ± S.D.

Histological examination of the skin from both diffusion cells revealed that there were no apparent changes in the skin structure over a period of 48 h

(**Figure 41**). The structure of stratum corneum obliterated minimally, particularly for the first 24 hr of the permeation study. However, shrinkage of the skin thickness was observed in both the diffusion set-ups. This may be attributed to the continuous shredding of the skin as it is in contact with the donor and receptor fluids. Also, the excised skin loses its inherent water content, leading to transepidermal water loss and the resultant shrinkage.

Table 7 Comparison of lag time and fluxes between HDC and MFtC across rat abdominal skin using rhodamine B at 1 mg/mL, rhodamine B at 5 mg/mL and mangostin at 2.3 mg/mL. n denotes number of replicates. Error bars denote S.D. between replicates. Flux comparisons between the setups showed no statistical difference.

	Rhodamine B (1 mg/mL)			Rhodamine B (5 mg/mL)			Mangostin (2.3 mg/mL)		
	n	Lag time (hr)	Flux ($\mu g/cm^2/hr$)	n	Lag time (hr)	Flux ($\mu g/cm^2/hr$)	n	Lag time (hr)	Flux ($\mu g/cm^2/hr$)
HDC	5	17.7 ± 3.47	0.04 ± 0.03	4	11.4 ± 3.31	0.07 ± 0.01	5	7.19 ± 0.47	7.06 ± 1.06
MFtC	3	22.1 ± 4.07	0.05 ± 0.02	5	8.35 ± 4.75	0.05 ± 0.02	7	14.5 ± 2.71	8.34 ± 3.40

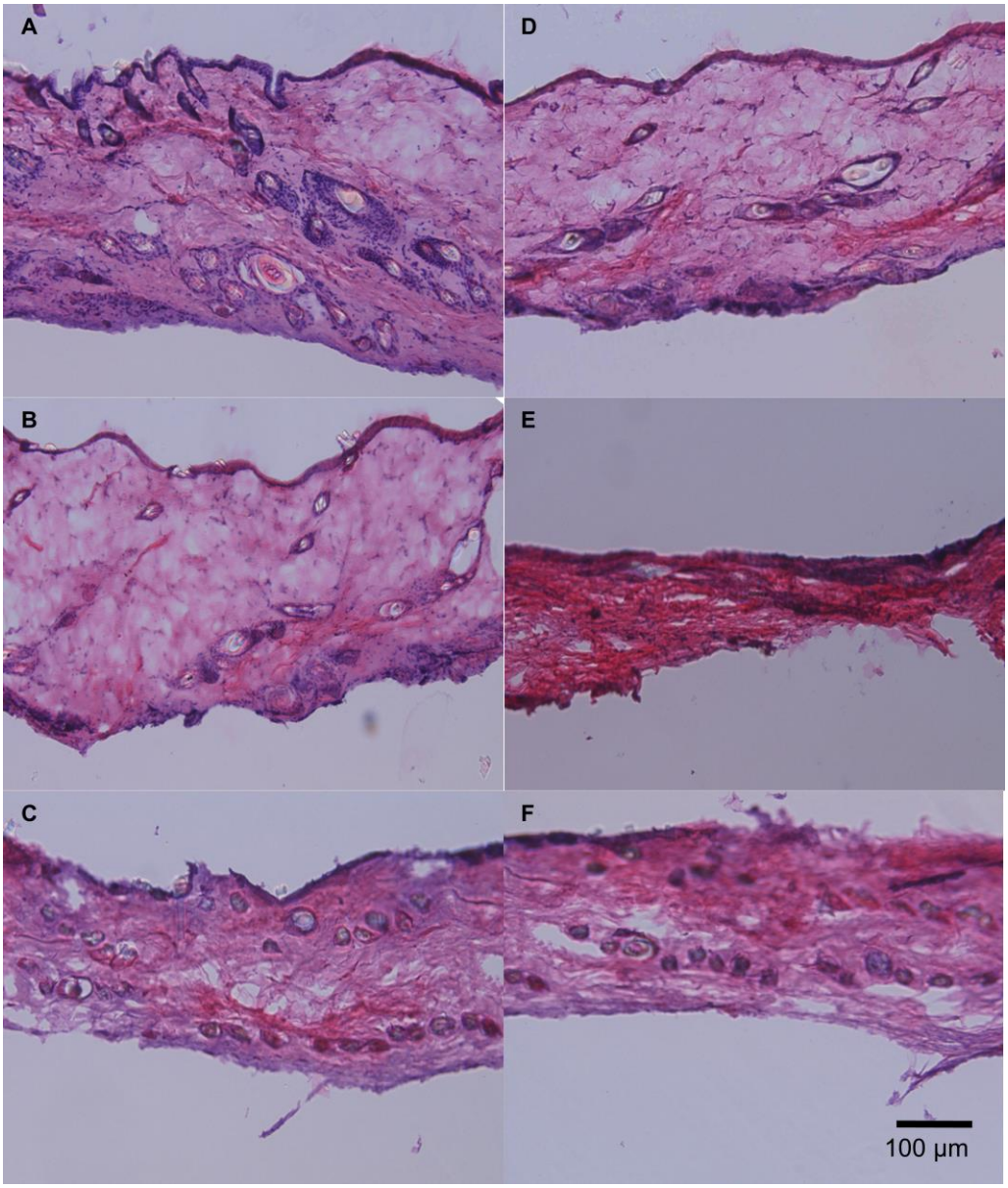

Figure 41 Histological images of the skin mounted on MFtC (A) at 0 hour, (B) at 24 hours, (C) at 48 hours, as well as horizontal diffusion cell (D) at 0 hour, (E) at 24 hours and (F) at 48 hours. The images demonstrate no apparent damage to the skin was caused by MFtC and skin exhibited similar properties as compared to horizontal diffusion cells.

7.2.2. Endoxifen fluorescence assay

Endoxifen (ENX), without irradiation, emits minimal fluorescence. Following UV irradiation, the phenanthrene derivatives of endoxifen emitted fluorescence, which is dependent on the amount of UV exposure [185]. The

optimum duration of UV irradiation of 15 min, which correspond to maximum fluorescence value, was used for all subsequent experiments (**Figure 42**).

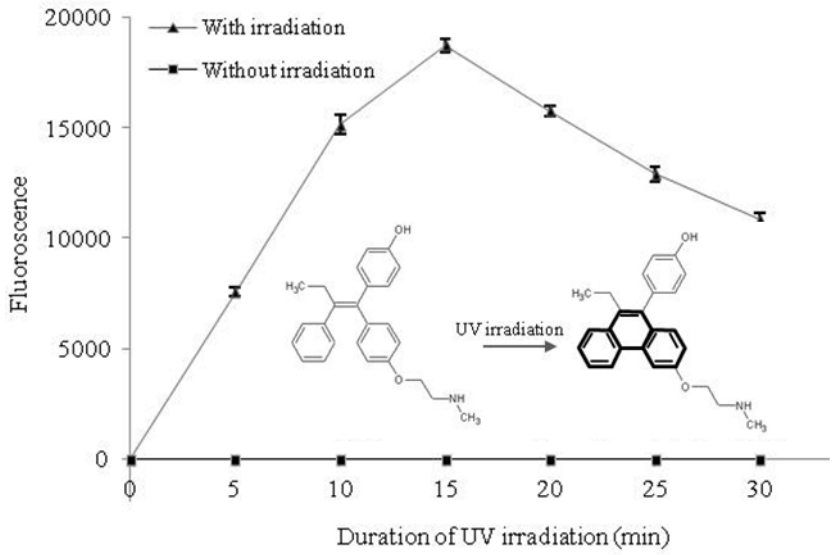

Figure 42 Plot of the fluorescence emitted for ENX in ultrapure water (10 µg/mL) against the duration of UV irradiation. Each point represents mean ± S.D. n = 3. (Inset) Photocyclization of ENX into a product with phenanthrene core.

In order to ensure accurate quantification of endoxifen, the linearity and sensitivity of the fluorescence based assay was determined using calibration experiments. The regression curve was obtained and the limits were:

Range: 0.78–3.13 µg/mL, A = (510.7 ± 90.7) [endoxifen] – (422.4 ± 93.4),

$r^2 = 0.97$

Range: 3.13–25.00 µg/mL, A = (1226.5 ± 38.8) [endoxifen] – (2663.4 ± 149.1), $r^2 = 0.98$.

N = 4, LOD = 0.31 g/mL, LOQ = 0.78 µg/mL, where A is in arbitrary units and the concentration is in µg/ml. Accuracy and precision were assessed using four concentrations, i.e., 1.56 µg/mL, 3.13 µg/mL, 6.25 µg/mL and 12.50 µg/mL. An accuracy of +2.05%, +18.86%, +11.41% and +19.06% with an intra-day CV of 2.99%, 5.21%, 1.68% and 4.82% was respectively observed (**Table 8**).

Table 8 Intra-day precision and accuracy. n = 3.

Actual concentration (µg/mL)	Recovered concentration (mean ± SD) (µg/mL)	Accuracy (%)	Intra-day CV (%)
12.50	14.88 ± 0.72	+19.06	4.82
6.25	6.96 ± 0.12	+11.41	1.68
3.13	3.71 ± 0.19	+18.86	5.21
1.56	1.59 ± 0.04	+2.05	2.99

7.2.3. Endoxifen permeation studies

Cumulative permeation plots and permeation parameters of endoxifen in PG with and without PEs are shown in **Figure 43** and **Table 9**. All PEs significantly increased ($p < 0.05$) the endoxifen flux in comparison with the PG alone. Endoxifen in PG with 0.5% w/v oleic acid, myristyl lactate and limonene achieved an EI of 6.26, 8.17 and 9.99 respectively, when compared to endoxifen in PG alone. The highest J_{ss} was achieved using limonene as a PE, with an EI of about ten times more than PG alone. Lag time of permeation for endoxifen in PG alone was however lower than those achieved with the use of PEs.

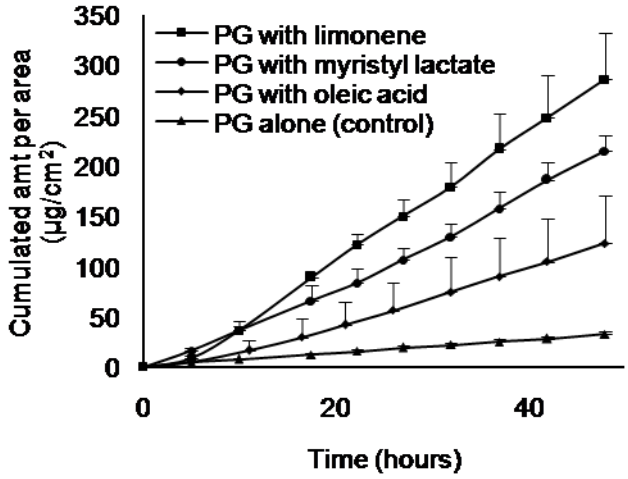

Figure 43 Time course of cumulative ENX permeated through 0.283 cm^2 of rat abdominal skin with or without enhancers using MFtC. ENX donor concentration = 2 mg/mL. Each point represents mean ± S.D.

Table 9 Permeation parameters of ENX in various donor solutions. Data was expressed as mean ± S.D. PE concentration = 0.5% w/v. (n= 3). Enhancement index (EI) = J_{ss} (with enhancer) / J_{ss} (without enhancer).

Donor solution	Lag time (hr)	Flux (µg/cm^2/h)	EI
PG alone (control)	1.03 ± 1.40	0.65 ± 0.01	-
PG with oleic acid	7.58 ± 4.04	4.09 ± 1.07*	6.26
PG with myristyl lactate	7.62 ± 2.18	5.33 ± 0.13*	8.17
PG with limonene	3.75 ± 2.37	6.52 ± 1.41*	9.99

** $p < 0.05$ compared to control.*

7.3. Discussion

Previous attempts at fabricating miniaturized platforms for transdermal testing have been based on metallic cells or glass vials, both of which are not easily customizable and are expensive. These include devices fabricated by Mak VHW[285] and Shockley Jr HD [286]. The multi-compartment bulky device fabricated by Mak VHW was chalked out of a block of steel, aluminium or

glass. The device could be directly attached to a 96-well plate for analysis. Clips are needed to seal donor with the receptor. Donor volume is 350 µL, receptor volume is 1mL. The other one fabricated by Shockley Jr, consists of frame like continuous flow apparatus, with very complicated design. Sensor slots are provided for in-line monitoring of flowing receptor. Clamps are required to secure the skin, making this complex device unsuitable for economic systems.

Another spiral shaped donor and receptor device was developed by Tanojo et al. with area of diffusion 55.2 mm^2, flow rate 5 mL/h, receptor volume 66.2 µL. The cells were mechanically engineered [287]. An interesting innovation was the development of diffusion cells within an HPLC vial by Moody RP. HPLC vial made as a permeation apparatus with two chambers separated by a filter which supports the skin. The skin is immersed in donor solution containing drug which diffuses to the receptor compartment where the HPLC injector can collect the sample for analysis [288]. Despite the development of these innovative models for permeation testing, a simplistic, easy to fabricate and customize, disposable and cost effective permeation testing apparatus was still lacking. Moreover some of these cells still suffer from the drawback of consumption of higher volume of reagents or skin or being static diffusion cells. This provided the impetus to develop miniaturized flow through cell using PDMS.

PDMS was selected for the fabrication of MFtC because of its advantageous properties. Firstly, the total cost of such a device was reduced substantially, thereby making such a setup readily affordable. The fabrication process is simple and can be easily adapted by individual research labs to customize their diffusion cells as per their specific requirements. A single diffusion cell made of PDMS approximately costs 1 USD (material cost) as compared to commercial equivalent that costs around 440 USD.

Secondly, the rheological properties of PDMS allow shaping of any desired design due to its flowability into any pre-formed mold. Owing to the flexible nature of PDMS, miniaturization of the whole assembly could be made possible. MFtC had significantly lower donor area, donor and receptor volumes

as compared to the current flow-through cells (**Table 10**) [42, 281, 289]. The low receptor flow rate of 0.20 mL/hr is in accordance with the general rule that flow rate should be at least ten times the receptor volume (10 µL) [290].

Table 10 Comparison between MFtC and commercial flow-through cell models.

Mechanical elements	MFtC	Commercial
Donor area	0.283 cm^2	0.785 cm^2
Donor volume	70-200 µL	100-1000 µL
Receptor volume	10 µL	230-855 µL

In addition, the optical clarity of PDMS allows a clear view of the area below the skin. This in turn facilitates the ascertainment of the absence of air bubbles which is especially important as these air bubbles can adversely affect the accuracy of permeation results [291]. Lastly, PDMS being an inert material, allows for prolonged shelf life of the diffusion cell, making them reusable.

Moreover, it has been reported that adsorption of PDMS is comparable to glass, especially for hydrophilic compounds while it is four times higher than glass for hydrophobic compounds [292]. While most of the compounds used in this study were relatively hydrophobic, insignificant loss of drug due to adsorption was observed. The diffusion cells made of PDMS were made reusable by washing with acetone and isopropanol. If needed, the surface of PDMS may be modified physically or chemically, to reduce the adsorption of hydrophobic drug molecules [293].

While validating the newly fabricated MFtC against the established permeation equipment, horizontal diffusion cells, two factors, namely, the varied concentrations and the log P of the compounds were considered. First, two different concentrations of rhodamine B were used to investigate the validity of flux at low and high concentrations of the donor solution. Rhodamine B is a fluorescent molecule, with a suitable log P (2.43) and molecular weight (479.02) for skin permeation testing. Its pink colour aids in easy detection of leakage of the donor solution. It was observed that the flux achieved was

comparable for both the concentrations between MFtC and the horizontal diffusion cells.

Second, the permeation profiles of rhodamine B and mangostin, a molecule similar to rhodamine B, in terms of molecular structures and molecular weights (**Figure 44**), but with a higher log P value (6.64) than rhodamine B, were compared. log P is an important parameter to consider for skin permeation, as it will affect the partition of the drug inside stratum corneum and viable layers of epidermis.

It was observed that the permeation parameters of MFtC and the horizontal diffusion cell were in close correlation to each other, signifying the validity of the newly fabricated diffusion cells.

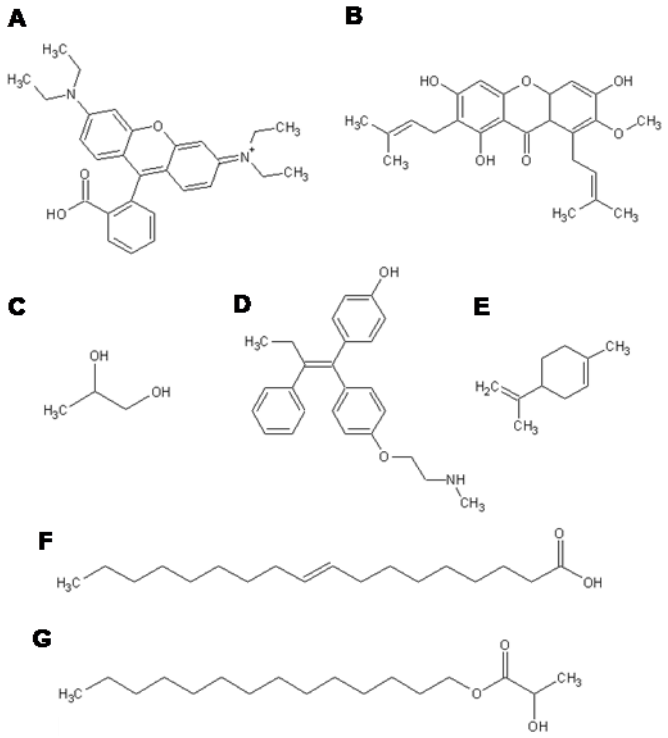

Figure 44 Chemical structures of (A) mangostin (MW = 410.46, Log P = 6.64), (B) rhodamine B (MW = 479.02, Log P = 2.43), (C) PG (MW = 76.09, Log P = -1.00), (D) ENX (MW = 373.49, Log P = 4.94), (E) limonene (MW = 136.2, Log P = 4.83), (F) oleic acid (MW = 282.46, Log P = 7.42) and (G) myristyl lactate (MW = 286.45, Log P = 6.08).

The device was also adaptable for thicker skin samples, such as those from pig cadaver, which closely resemble human skin. Pig skin could be supported on

the MFtC set-up, with the application of vacuum grease and no leakage was detected from the donor compartment when a rhodamine B solution in PG was applied (**Figure 45**).

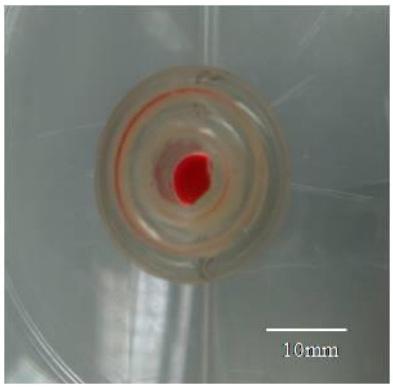

Figure 45 MFtC setup with pig skin showing the ability to be used with thicker skin samples, without any leakage problem.

To achieve a plasma concentration of endoxifen that is comparable to those achieved on administration of an oral daily dose of 2–4 mg [294], an ideal flux of 2.0–4.0 μg/cm^2/hr, assuming an application area of 40 cm^2 would be required from endoxifen transdermal drug delivery system. The reported transdermal endoxifen study was not able to achieve this flux [295]. In this study, the highest flux reported was 0.22 μg/cm^2/hr for endoxifen dissolved in 60% (v/v) ethanol – phosphate buffer with 0.5% (w/v) oleic acid.

In the search of a suitable vehicle and PEs for endoxifen in transdermal drug delivery system, three different permeation enhancers were used. It has been reported that high skin flux of tamoxifen can be achieved by using limonene as a PE with PG as the vehicle [296]. Because of the molecular structural similarities between tamoxifen and endoxifen, in this study, endoxifen was incorporated in PG while limonene was selected as one of the PEs. In addition to limonene, oleic acid and myristyl lactate were also selected as PEs in this study.

It was found that oleic acid, myristyl lactate and limonene in PG enhanced the permeation of endoxifen by 6.26, 8.17 and 9.99 folds respectively as compared to PG alone (**Table 10**). Oleic acid has been reported to increase drug transport

by coexisting as pools in the stratum corneum lipids structure [31]. Myristyl lactate may act by disrupting ceramide – cholesterol or cholesterol - cholesterol interaction and increase permeation of endoxifen [297]. As myristyl lactate (log P = 6.08) has a shorter carbon chain than oleic acid (log P = 7.42), the higher flux achieved by myristyl lactate can be explained by lower partitioning of drugs into stratum corneum as compared to oleic acid.

Results showed that limonene delivered the highest flux among the three PEs tested. Limonene belongs to the class of terpenes which are constituents of essential oils [42]. Their ability to enhance drug flux could have been attributed to partial extraction of stratum corneum lipids, [298] phase separation within the SC lipid lamellae [299] and limonene - PG synergy [300].

Besides, results using oleic acid as a PE in PG has shown significantly better endoxifen delivery with a J_{ss} of 4.09 ± 1.07 μg/cm^2/hr compared with the J_{ss} of 0.22 μg/cm^2/hr as reported by using ethanol–phosphate buffer as the vehicle [295]. A plausible explanation for this observation is the different effects of various vehicles on the skin. It has been reported that PG can affect the transdermal permeability by altering thermodynamic activity of drug and/or barrier nature of skin [301]. Moreover, it is also been known that activity of PEs can be significantly increased when applied in combination with PG [302]. Overall, all three PEs chosen in this study were able to achieve higher flux than control. The best one was limonene, which attained a flux of 6.52 μg/cm^2/hr through rat skin, which can be translated to 2.17 μg/cm^2/hr through human skin [303]. Therefore, the target flux of 2–4 μg/cm^2/hr through human skin can be achieved with this limonene formulation.

7.4. Summary

This chapter dealt with the development and validation of a miniaturized flow-through cell. The developed MFtC utilizes a small amount of donor solution (70–200 μL) and membrane (0.283 cm^2) for skin permeation studies. The device had no damaging effect on the skin as compared to the established models like horizontal diffusion cell. A novel fluorescent spectroscopic method was also developed to quantify endoxifen in a fast and convenient manner. Permeation studies of endoxifen attained the targeted flux. The miniaturized

diffusion cell is demonstrated to be useful for investigative drugs with limited supply during the pre-formulation studies.

CHAPTER 8

Conclusions and Future Directions

8.1. Conclusions

This thesis presents novel strategies to address issues with transdermal drug/cosmetic delivery as well as pre-formulation testing of transdermal dosage forms. As such, this thesis describes a novel method to fabricate polymeric microneedle arrays for transdermal delivery of drugs and cosmetics as well as designing of a novel transdermal formulation testing platform and development work towards the same. Both innovative devices are in the process of being patented and are on their path towards commercialization. Brief conclusion from the development of both devices is summarized below:

The microneedles:

- were fabricated by a simple photolithographical process within seconds, without the need for reverse molds, the method could be potentially scaled up for mass production.
- the geometrical properties of microneedles were controlled spacer thickness and photomask geometry and microneedle arrays of any shape could potentially be fabricated.
- penetrated the skin (rat, pig and human) with little force of a thumb with high penetration efficiencies.
- were able to encapsulate a wide range of drugs (chemical and biological), with exposure process demonstrated to be mild for retention of protein stability.
- were integrated to a transdermal patch and achieve drug loading up to 70 mg, which has not been achieved by any previously developed microneedle system.
- were shown to enable permeation of large amounts of both chemical as well as biological drugs in a faster manner than passive diffusion and to greater depths in the skin.

- were shown to be non toxic to different skin and embryonic kidney cell lines.

The miniaturized flow-through cell:

- was fabricated using simple micromolding process with PDMS.
- utilizes minimal amounts of formulation as well as skin samples.
- could be tuned to low receptor flow rates resulting in lesser dilution of the permeated compound across the skin, making analysis easier.
- was shown to be a good platform for testing permeation of investigational new drug entities like endoxifen.

8.2. Future Directions

This thesis described the development of prototypes for polymeric microneedles as well as a miniaturized flow through cell, with both showing promising results in preliminary studies highlighted previously. Future work pertaining to both devices is mentioned below.

The microneedles:

- could be further optimized for geometry and mechanical strength. Microneedles fabricated using microlens embedded photomasks could be optimized further by fine tuning the lens geometries and hence leading to an array of different geometries, shapes and sizes. Moreover, microneedles could be made in different shapes and sizes to suit the need of the disease, as may be required in skin conditions like psoriasis, melasma and other topical skin disorders.
- could be integrated to microneedle applicators and uniform force ejectors to minimize variation on application by subjects. Microneedle injectors can be optimized to deliver particular force which will lead to uniform delivery of dose to required depths in the skin.
- are to be tested *in vivo* in pig model for delivering both chemical and biological drugs, including enzymes like phenylalanine ammonia lyase for management of phenylketonuria, nucleic acids like shRNA for chikungunya virus. Current understanding and expertise gained with

transdermal diffusion testing as well as development of MFtC will aid in cost efficient analysis of expensive proteins and nucleic acids.

- are to be tested *in vivo* for first-in-human trials for drug and cosmetic compounds to gather data for regulatory approval and commercial launch. Consumer research and physician/cosmetologist feedback is currently being sought and will pave the path for human trials with cosmetic microneedles as well as initial small scale trial in healthy volunteers.
- active permeation could be studied by development of a mathematical model. With considerable amount of data available from various classes of drugs, both hydrophilic and hydrophobic, it will be beneficial to develop a mathematical model for active transport of molecules across stratum corneum. This will enable suitable prediction of permeation of drug and cosmetic compounds, as well as to analyze delivery to local skin sites or systemic delivery based on the predicted extent of permeation.
- could be miniaturized further to nanoneedles with optimization of photomask geometry, which could be then used for cell manipulation studies. This will enable to deliver nucleic acids directly to cells for their action. Even with the current knowledge on optimization of photomasks and ultraviolet curing, nanoneedle fabrication is still a significant challenge, in particular the nanoneedle strength. This will need to be tested and may necessitate the need for alternative materials to achieve needles of sufficient strength.

The miniaturized flow-through cell:

- has to be integrated to a syringe pump and water bath to make a wholly integrated device. A multichannel syringe pump will enable consistent flow rates across several MFtC coupled together and similarly a water bath immersing all the cells together will help ensure consistent temperature distribution throughout the whole system enabling, results which can be more reproducible.
- could be attached to an autosampler for ease of sample collection. Commercial models from Permegear and other such companies come

with the options of autosampler to reduce manual sampling requirements and make the system more user-friendly. This will also enable us to look for potential customers and investors to commercialize the device.

- improvement in design of the cells could be achieved using 3D printing. 3D printing technology has grown leaps and bounces in the past few years and enables easy and precise designing of miniaturized platforms. With the help of experts in this area, MFtC design could be further optimized as per the needs of a particular study and hence making these cells easily customizable and highly adaptable to specific needs.
- could be customized for microneedle permeation studies. So far microneedle mediated skin permeation studies have been carried out in conventional horizontal or vertical type Franz cells which are suitable for semisolid or liquid dosage forms. Microneedles are to be adjusted and clamped between the cells and hence the situation is not very ideal. Design of MFtC platforms that support microneedles in place for the length of the study without hampering the skin/microneedle geometry would be an ideal choice and will be suitable as microneedle is a growing field.
- could be made disposable, which is then expected to revolutionize the *in vitro* testing, significantly reducing cross-batch contamination and lead times between experiments. This could be further made possible by looking for other cheaper raw materials and scaling up of production will further bring down the cost.

Bibliography

1. FDA, *Approved Drug Products with Therapeutic Equivalence Evaluations*. 33rd ed. 2013, Rockville, MD: U.S. Department of Health and Human Services.
2. Marieb, E.N. and Hoehn, K. *Human anatomy and physiology*. 7th ed. 2007, San Francisco: Pearson Education
3. Rein, H., *Zeitschrift Fur Biologie*, 1924. **81**(3/4): p. 125-140.
4. Blank, I.H., *J Invest Dermatol*, 1964. **43**: p. 415-20.
5. Scheuplein, R.J., *J Invest Dermatol*, 1965. **45**(5): p. 334-46.
6. Scheuplein, R.J. and Blank, I.H., *Physiol Rev*, 1971. **51**(4): p. 702-47.
7. Cevc, G., *Expert Opinion on Investigational Drugs*, 1997. **6**(12): p. 1887-1937.
8. Brown, M.B., *Transdermal drug delivery*, in *Drug Delivery Systems*, 2nd ed. 2003, Basel: CRC Press.
9. Henzel, M.R., Loomba, P. K., *J Reprod Med*, 2003. **48**(7): p. 525-40.
10. Kalia, Y.N., Merino, V., and Guy, R.H., *Dermatol Clin*, 1998. **16**(2): p. 289-99.
11. Varvel, J.R., et al., *Anesthesiology*, 1989. **70**(6): p. 928-34.
12. Kormick, C.A., et al., *Drug Saf*, 2003. **26**(13): p. 951-73.
13. Payne, R., et al., *J Clin Oncol*, 1998. **16**(4): p. 1588-93.
14. Jarupanich, T., Lamlertkittikul, S., and Chandeying, V., *J Med Assoc Thai*, 2003. **86**(9): p. 836-45.
15. Archer, D.F., et al., *Contraception*, 2004. **69**(3): p. 189-95.
16. Long, C., *Common skin disorders and their topical treatment*, in *Dermatological and transdermal formulations*, 2002, New York: Marcel Dekker.
17. Frei, A., et al., *J Pain Palliat Care Pharmacother*, 2003. **17**(2): p. 5-26.
18. Bos, J.D. and Meinardi, M.M., *Exp Dermatol*, 2000. **9**(3): p. 165-9.
19. Yano, T., et al., *Life Sci*, 1986. **39**(12): p. 1043-50.
20. Southwell, D., Barry, B.W., and Woodford, R. *Int J Pharm*, 1984. **18**(3): p. 299-309.
21. Steinstrasser, I. and Merkle, H.P., *Pharm Acta Helv*, 1995. **70**(1): p. 3-24.
22. Hogan, D.J. and Maibach, H.I., *J Am Acad Dermatol*, 1990. **22**(5 Pt 1): p. 811-4.
23. Carmichael, A.J., *Drug Saf*, 1994. **10**(2): p. 151-9.
24. Toole, J., et al., *Maturitas*, 2002. **43**(4): p. 257-63.
25. Murphy, M. and Carmichael, A.J., *Am J Clin Dermatol*, 2000. **1**(6): p. 361-8.
26. Prausnitz, M.R., Mitragotri, S., and Langer, R., *Nat Rev Drug Discov*, 2004. **3**(2): p. 115-24.
27. Prausnitz, M.R. and Langer, R., *Nat Biotechnol*, 2008. **26**(11): p. 1261-8.
28. Michaels, A.S., Chandrasekaran, S.K., and Shaw, J.E., *AIChE Journal*, 1975. **21**(5): p. 985-996.
29. Daugherty, A.L. and Mrsny, R.J., *Exp Opin Biol Ther*, 2003. **3**(7): p. 1071-1081.
30. Ahad, A., et al., *Expert Opin Ther Pat*, 2009. **19**(7): p. 969-88.

31. Williams, A.C. and Barry, B.W., *Crit Rev Ther Drug Carrier Syst*, 1992. **9**(3-4): p. 305-53.
32. Finnin, B.C. and Morgan, T.M., *J Pharm Sci*, 1999. **88**(10): p. 955-8.
33. Wright, I.A., et al., *Domest Anim Endocrinol*, 1992. **9**(4): p. 305-12.
34. Pohorecky, L.A., et al., *Alcohol*, 1992. **9**(4): p. 305-9.
35. Barrett, A. and Jiang, Y.Z., *Bone Marrow Transplant*, 1992. **9**(5): p. 305-11.
36. Ferrera, J.M., et al., *Aten Primaria*, 1992. **9**(6): p. 305-6, 308-10.
37. Anonymous, *J Clin Neurophysiol*, 1992. **9**(2): p. 305-13.
38. Kamboh, M.I., Hamman, R.F., and Ferrell, R.E., *Genet Epidemiol*, 1992. **9**(5): p. 305-15.
39. Nigam, R., Schottenfeld, R. and Kosten, T.R., *J Subst Abuse Treat*, 1992. **9**(4): p. 305-9.
40. Lopez, A., et al., *Int J Pharm*, 2000. **202**(1-2): p. 133-40.
41. Kanikkannan, N., et al., *Curr Med Chem*, 2000. **7**(6): p. 593-608.
42. Kang, L., et al., *J Control Release*, 2007. **120**(3): p. 211-9.
43. Kang, L., et al., *Eur J Pharm Biopharm*, 2007. **67**(1): p. 149-55.
44. Kanikkannan, N. and Singh, M., *Int J Pharm*, 2002. **248**(1-2): p. 219-28.
45. Takanashi, Y., et al., *Drug Dev Ind Pharm*, 1999. **25**(1): p. 89-94.
46. Akimoto, T. and Nagase, Y., *J Control Release*, 2003. **88**(2): p. 243-52.
47. McVary, K.T., et al., *J Urol*, 1999. **162**(3 Pt 1): p. 726-30; discussion 730-1.
48. Kalia, Y.N., et al., *Adv Drug Deliv Rev*, 2004. **56**(5): p. 619-58.
49. Helmstadter, A., *Pharmazie*, 2001. **56**(7): p. 583-7.
50. Costello, C.T. and Jeske, A.H., *Phys Ther*, 1995. **75**(6): p. 554-63.
51. Warwick, W.J., et al., *Clin Chem*, 1986. **32**(5): p. 850-3.
52. Holzle, E. and Alberti, N., *Dermatologica*, 1987. **175**(3): p. 126-35.
53. Miller, K.A., et al., *AANA J*, 2001. **69**(3): p. 185-7.
54. Tamada, J.A., et al., *JAMA*, 1999. **282**(19): p. 1839-44.
55. Prausnitz, M.R., *Adv Drug Deliv Rev*, 1996. **18**(3): p. 395-425.
56. Kanikkannan, N., *BioDrugs*, 2002. **16**(5): p. 339-47.
57. Mitragotri, S., Blankschtein, D., and Langer, R., *Pharm Res*, 1996. **13**(3): p. 411-20.
58. Denet, A.R., Vanbever, R. and Preat, V., *Adv Drug Deliv Rev*, 2004. **56**(5): p. 659-74.
59. Prausnitz, M.R., et al., *Biotechnology*, 1995. **13**(11): p. 1205-9.
60. Sen, A., Daly, M.E., and Hui, S.W., *Biochim Biophys Acta*, 2002. **1564**(1): p. 5-8.
61. Misra, A., Ganga, S., and Upadhyay, P., *Vaccine*, 1999. **18**(5-6): p. 517-23.
62. Zhao, Y.L., et al., *Vaccine*, 2006. **24**(9): p. 1282-90.
63. Zewert, T.E., et al., *Biochem Biophys Res Commun*, 1995. **212**(2): p. 286-92.
64. Ogura, M., Paliwal, S., and Mitragotri, S., *Adv Drug Deliv Rev*, 2008. **60**(10): p. 1218-23.
65. Paliwal, S., Menon, G.K., and Mitragotri, S., *J Invest Dermatol*, 2006. **126**(5): p. 1095-101.
66. Becker, B.M., et al., *Acad Emerg Med*, 2005. **12**(4): p. 289-95.
67. Clarys, P., et al., *Eur J Pharm Biopharm*, 1998. **46**(3): p. 279-83.

68. Akomeah, F., et al., *Eur J Pharm Sci*, 2004. **21**(2-3): p. 337-45.
69. Klemsdal, T.O., Gjesdal, K., and Bredesen, J.E., *Eur J Clin Pharmacol*, 1992. **43**(6): p. 625-8.
70. Park, J.H., et al., *Int J Pharm*, 2008. **359**(1-2): p. 94-103.
71. Levin, G., et al., *Pharm Res*, 2005. **22**(4): p. 550-5.
72. Herndon, T.O., et al., *BMC Med*, 2004. **2**: p. 12.
73. Glenn, G.M., et al., *Expert Rev Vaccines*, 2007. **6**(5): p. 809-19.
74. Lee, W.R., et al., *J Invest Dermatol*, 2003. **121**(5): p. 1118-25.
75. Andrews, S.N., Jeong, E., and Prausnitz, M.R., *Pharm Res*, 2013. **30**(4): p. 1099-1109.
76. Lee, W.R., et al., *J Control Release*, 2001. **75**(1-2): p. 155-66.
77. Jacques, S.L., et al., 1988, *US Patent* 06/851,117
78. Lee, S., et al., *J Invest Dermatol*, 1998. **111**(6): p. 925-9.
79. Lee, S., et al., *Pharm Res*, 1999. **16**(11): p. 1717-21.
80. Doukas, A.G. and Kollias, N., *Adv Drug Deliv Rev*, 2004. **56**(5): p. 559-79.
81. Sintov, A.C., et al., *J Control Release*, 2003. **89**(2): p. 311-20.
82. Murthy, S.N., *Pharmazie*, 1999. **54**(5): p. 377-9.
83. Murthy, S.N. and Hiremath, S.R., *AAPS PharmSciTech*, 2001. **2**(1): p. E-TN1.
84. Svedman, P., et al., *Pharm Res*, 1996. **13**(9): p. 1354-9.
85. Giudice, E.L. and Campbell, J.D., *Adv Drug Deliv Rev*, 2006. **58**(1): p. 68-89.
86. Gerstel, M.S. and V.A. Place, 1976, *US Patent* 05/144,061.
87. Henry, S., et al., *J Pharm Sci*, 1998. **87**(8): p. 922-5.
88. Kaushik, S., et al., *Anesth Analg*, 2001. **92**(2): p. 502-4.
89. Belshe, R.B., et al., *N Engl J Med*, 2004. **351**(22): p. 2286-94.
90. Wilke, N., et al., *Microelectronics Journal*, 2005. **36**(7): p. 650-656.
91. Alarcon, J.B., et al., *Clin Vaccine Immunol*, 2007. **14**(4): p. 375-81.
92. Lee, J.W., Park, J.H., and Prausnitz, M.R., *Biomaterials*, 2008. **29**(13): p. 2113-24.
93. Kim, Y.C., Park, J.H., and Prausnitz, M.R., *Adv Drug Deliv Rev*, 2012. **64**(14): p. 1547-68.
94. Broderick, K.E., *Ther Deliv*, 2012. **3**(8): p. 937-9.
95. Ji, J., et al., *J Micromech Microeng*, 2006. **16**(5): p. 958.
96. Donnelly, R.F., Singh, T.R.R., and Woolfson, A.D., *Drug Deliv*, 2010. **17**(4): p. 187-207.
97. Paik, S.J., et al., *Sens Actuators A-Phys*, 2004. **114**(2-3): p. 276-284.
98. Wei-Ze, L., et al., *Int J Pharm*, 2010. **389**(1-2): p. 122-129.
99. Shikida, M., Hasada, T., and Sato, K., *J Micromech Microeng*, 2006. **16**(10): p. 2230-2239.
100. Shikida, M., et al., *Sens Actuators A Phy*, 2004. **116**(2): p. 264-271.
101. Wilke, N., et al., *Sens Actuators A Phys*, 2005. **123-24**: p. 319-325.
102. Ma, B., et al., *Microfluid Nanofluidics*, 2006. **2**(5): p. 417-423.
103. Baron, N., et al., *Microsyst Technol*, 2008. **14**(9-11): p. 1475-1480.
104. Chen, B., Wei, J., and Iliescu, C., *Sens Actuators B Chem*, 2010. **145**(1): p. 54-60.
105. Han, T. and Das, D.B., *J Pharm Sci*, 2013. **102**(10): p. 3614-3622.
106. Gill, H.S. and Prausnitz, M.R., *J Control Release*, 2007. **117**(2): p. 227-37.

107. Martanto, W., et al., *Pharm Res*, 2004. **21**(6): p. 947-952.
108. Chandrasekaran, S., Brazzle, J.D., and Frazier, A.B., *J Microelectromech Sys*, 2003. **12**(3): p. 281-288.
109. Parker, E.R., et al., *J Microelectromech Syst*, 2007. **16**(2): p. 289-295.
110. Jung, P.G., et al., *Sensors and Materials*, 2008. **20**(1): p. 45-53.
111. Gill, H.S. and Prausnitz, M.R., *J Phys Chem Solids*. **69**(5-6): p. 1537-1541.
112. Wang, P.M., et al., *J Invest Dermatol*, 2006. **126**(5): p. 1080-1087.
113. Bystrova, S. and R. Luttge, *Microelectron Eng*, 2011. **88**(8): p. 1681-1684.
114. Gittard, S.D., et al., *Biofabrication*, 2009. **1**(4).
115. Gill, H.S. and Prausnitz, M.R., *Pharm Res*, 2007. **24**(7): p. 1369-80.
116. Sullivan, S.P., Murthy, N., and Prausnitz, M.R., *Adv Materials*, 2008. **20**(5): p. 933-38.
117. Kochhar, J.S., et al., *Drug Dev Ind Pharm*, 2013. **39**(2): p. 299-309.
118. Park, J.H., Allen, M.G., and Prausnitz, M.R., *Pharm Res*, 2006. **23**(5): p. 1008-1019.
119. Ito, Y., et al., *Int J Pharm*, 2008. **349**(1-2): p. 124-9.
120. Li, G., et al., *Int J Pharm*, 2009. **368**(1-2): p. 109-115.
121. Miyano, T., et al., *Biomed Microdevices*, 2005. **7**(3): p. 185-188.
122. Park, J.H., Allen, M.G., and Prausnitz, M.R., *J Control Release*, 2005. **104**(1): p. 51-66.
123. Moon, S.J. and Lee, S.S., *J Micromech Microeng*, 2005. **15**(5): p. 903-911.
124. Perennes, F., et al., *J Micromech Microeng*, 2006. **16**(3): p. 473-479.
125. Aoyagi, S., et al., *Sens Actuators A Phys*, 2007. **139**(1-2): p. 293-302.
126. Ito, Y., et al., *Eur J Pharm Sci*, 2006. **29**(1): p. 82-8.
127. Kolli, C.S. and Banga, A.K., *Pharm Res*, 2008. **25**(1): p. 104-113.
128. Miyano, T., et al., *Biomed Microdevices*, 2005. **7**(3): p. 185-188.
129. Donnelly, R.F., et al., *Drug Dev Ind Pharm*, 2009. **35**(10): p. 1242-1254.
130. Ito, Y., et al., *J Drug Target*, 2006. **14**(5): p. 255-61.
131. Park, J.H., et al., *Eur J Pharm Biopharm*, 2010. **76**(2): p. 282-9.
132. Donnelly, R.F., et al., *Pharm Res*, 2011. **28**(1): p. 41-57.
133. http://www.clinicaltrials.gov/ct2/show/NCT00539084?term=Microneedles&rank=5. Accessed 22 April, 2013.
134. http://www.clinicaltrials.gov/ct2/show/NCT00602914?term=Microneedle&rank=13. Accessed 22 April, 2013.
135. http://www.clinicaltrials.gov/ct2/show/NCT01049490?term=Microneedle&rank=9. Accessed 22 April, 2013.
136. http://www.clinicaltrials.gov/ct2/show/NCT01145326?term=Microneedle&rank=8. Accessed 22 April, 2013.
137. http://www.clinicaltrials.gov/ct2/show/NCT01611844?term=Microneedle&rank=6. Accessed 22 April, 2013.
138. http://www.clinicaltrials.gov/ct2/show/study/NCT01257763?term=Microneedle&rank=23. Accessed 22 April, 2013.
139. Shah, V.P., et al., *Pharm Dev Technol*, 2003. **8**(1): p. 97-102.
140. Friend, D.R., *J Control Release*, 1992. **18**(3): p. 235-248.
141. Williams, A.C., *Transdermal and Topical Drug Delivery*. 2003, London, UK: Pharmaceutical Press.

142. Stehle, R.G. and Higuchi, W.I., *J Pharm Sci*, 1972. **61**(12): p. 1931-5.
143. Diembeck, W., et al., *Food Chem Toxicol*, 1999. **37**(2-3): p. 191-205.
144. Washitake, M., et al., *Chem Pharm Bull*, 1980. **28**(10): p. 2855-61.
145. Chien, Y.W. and Valia, K.H., *Drug Dev Ind Pharm*, 1984. **10**(4): p. 575-599.
146. Saydek, M.E., et al., 1989, *US Patent* 4863696.
147. Higuchi, T. and Kans, L., 1988, US Patent 4740309.
148. Flynn, G.L. and Smith, E.W., *J Pharm Sci*, 1971. **60**(11): p. 1713-7.
149. Wurster, D.E., Ostrenga, J.A., and Matheson, L.E., *J Pharm Sci*, 1979. **68**(11): p. 1406-9.
150. Southwell, D., Barry, B.W., and Woodford, R., *Int J Pharm*, 1984. **18**(3): p. 299-309.
151. Coldman, M.F., Poulsen, B.J., and Higuchi, T., *J Pharm Sci*, 1969. **58**(9): p. 1098-1102.
152. Franz, T.J., *J Invest Dermatol*, 1975. **64**(3): p. 190-195.
153. Gummer, C.L., Hinz, R.S., and Maibach, H.I., *Int J Pharm*, 1987. **40**(1-2): p. 101-104.
154. Smith, E.W. and Haigh, J.M., *Acta Pharm Nord*, 1992. **4**(3): p. 171-8.
155. Marzulli, F.N., *J Invest Dermatol*, 1962. **39**(5): p. 387-393.
156. Hawkins, G.S. and Reifenrath, W.G., *J Pharm Sci*, 1986. **75**(4): p. 378-81.
157. Addicks, W.J., Flynn, G.L., and Weiner, N., *Pharm Res*, 1987. **4**(4): p. 337-341.
158. Clowes, H.M., Scott, R.C., and Heylings, J.R., *Toxicol In Vitro*, 1994. **8**(4): p. 827-30.
159. Astley, J.P. and Levine, M., *J Pharm Sci*, 1976. **65**(2): p. 210-5.
160. Kazmierska, K.A. and Ciach, T., *Recent Pat Biomed Eng*, 2009. **2**(1): p. 1-14.
161. Ahn, D., et al., *Opt. Express*, 2009. **17**(19): p. 16603-16612.
162. Varshney, M., Khanna, T., and Changez, M., *Colloids and Surf B Biointerfaces*, 1999. **13**(1): p. 1-11.
163. Laemmli, U.K., *Nature*, 1970. **227**(5259): p. 680-5.
164. Murayama, K. and Tomida, M., *Biochemistry*, 2004. **43**(36): p. 11526-32.
165. Estey, T., et al., *J Pharm Sci*, 2006. **95**(7): p. 1626-39.
166. Andrade, M.A., et al., *Protein Eng*, 1993. **6**(4): p. 383-90.
167. Whitmore, L. and Wallace, B.A., *Nucleic Acids Res*, 2004. **32**(Web Server issue): p. W668-73.
168. Whitmore, L. and Wallace, B.A., *Biopolymers*, 2008. **89**(5): p. 392-400.
169. Xie, Y., Xu, B., and Gao, Y., *Nanomedicine*, 2005. **1**(2): p. 184-90.
170. Mosmann, T., *J Immunol Methods*, 1983. **65**(1-2): p. 55-63.
171. Berckmans, P., et al., *Toxicol In Vitro*, 2007. **21**(7): p. 1262-7.
172. Davis, S.P., et al., *J Biomech*, 2004. **37**(8): p. 1155-63.
173. Chaudhri, B.P., et al., *Conf Proc IEEE Eng Med Biol Soc*, 2011. **2011**: p. 3680-3.
174. Huang, L., et al., *Free Radic Biol Med*, 2012. **53**(11): p. 2062-71.
175. Liawruangrath, S., Liawruangrath, B., and Pibool, P., *J Pharm Biomed Anal*, 2001. **26**(5-6): p. 865-72.
176. Tay, F.E.H., et al., *Microsyst Technologies*, 2006. **12**(10-11): p. 935-939.

177. Iliescu, C., Chen, B., and Miao, J., *Sensors Actuators A Phys*, 2008. **143**(1): p. 154-161.
178. Iliescu, C., et al., *Surf Coat Technol*, 2005. **198**(1-3 SPEC. ISS.): p. 314-318.
179. Peebles, L. and Norris, B., *Appl Ergon*, 2003. **34**(1): p. 73-88.
180. Sugiyama, K., et al., *Kurume Med J*, 1980. **27**(2): p. 63-9.
181. Zhou, C.P., et al., *Int J Pharm*, 2010. **392**(1-2): p. 127-33.
182. Park, J.H., Allen, M.G., and Prausnitz, M.R., *J Control Release*, 2005. **104**(1): p. 51-66.
183. Tokumoto, S., et al., *J Control Release*, 2005. **105**(3): p. 296-304.
184. Lakowicz, J.R., et al., *J Phys Chem*, 1994. **98**(1): p. 334-342.
185. Aranda, E.O., et al., *Talanta*, 2011. **84**(2): p. 314-8.
186. Šalamoun, J., et al., *J Chromatogr A*, 1990. **514**(0): p. 179-187.
187. http://www.ich.org/products/guidelines/quality/quality-single/article/validation-of-analytical-procedures-text-and-methodology.html. Accessed 20 February, 2012.
188. Ito, Y., et al., *Drug Dev Ind Pharm*, 2010. **36**(7): p. 845-51.
189. Sun, G. and Chu, C.C., *Carbohydrate Polymers*, 2006. **65**(3): p. 273-287.
190. Pasut, G. and Veronese, F.M., *Prog Polym Sci*, 2007. **32**(8-9): p. 933-961.
191. Mellott, M.B., Searcy, K., and Pishko, M.V., *Biomaterials*, 2001. **22**(9): p. 929-41.
192. Sullivan, S.P., et al., *Nat Med*, 2010. **16**(8): p. 915 - 20.
193. Chan, V., et al., *Lab on a Chip*, 2010. **10**(16): p. 2062-2070.
194. Kang, L., et al., *J Biomed Mater Res A*, 2010. **93**(2): p. 547-57.
195. Khademhosseini, A., et al., *Lab on a Chip*, 2004. **4**(5): p. 425-430.
196. Phillips, A.J., ed. *Contact Lenses*. 5 ed. 2007, Elsevier: London. 548-549.
197. Kerwin, B.A. and Remmele, R.L.,, *J Pharm Sci*, 2007. **96**(6): p. 1468-79.
198. Kindernay, J., et al., *J Photochem Photobiol A Chem*, 2002. **151**(1-3): p. 229-236.
199. Donnelly, R.F., et al., *Pharm Res*, 2009. **26**(11): p. 2513-22.
200. Jiang, J., et al., *Invest Ophthalmol Vis Sci*, 2007. **48**(9): p. 4038-43.
201. Koutsonanos, D.G., et al., *PLoS One*, 2009. **4**(3): p. e4773.
202. Kumar, A., et al., *Int J Nanomedicine*, 2011. **6**: p. 1253-64.
203. Baek, C., et al., *J Control Release*, 2011. **154**(2): p. 138-47.
204. Panyam, J., et al., *J Control Release*, 2003. **92**(1-2): p. 173-87.
205. Xie, J. and Wang, C.H., *Biotechnol Bioeng*, 2007. **97**(5): p. 1278-90.
206. Angelova, A., et al., *Acc Chem Res*, 2011. **44**(2): p. 147-56.
207. Pan, J., et al., *Biotechnol J*, 2011. **6**(12): p. 1477-87.
208. Angelova, A., et al., *Langmuir*, 2003. **19**(17): p. 6928-6935.
209. Yang, S., et al., *Int J Nanomedicine*, 2012. **7**: p. 1415-22.
210. Zhuang, W., et al., *J Lumin*, 2012. **132**(2): p. 350-356.
211. Tan, L., et al., *Anal Sci*, 2004. **20**(3): p. 441-4.
212. Rozman, B., et al., *AAPS PharmSciTech*, 2009. **10**(1): p. 54-61.
213. Garland, M.J., et al., *J Control Release*, 2012. **159**(1): p. 52-9.
214. Gonzalez-Gonzalez, E., et al., *Mol Ther*, 2010. **18**(9): p. 1667-74.
215. Titus, J.A., et al., *J Immunol Methods*, 1982. **50**(2): p. 193-204.

216. He, Y. and Yeung, E.S., *J Proteome Res*, 2002. **1**(3): p. 273-7.
217. Weber, K. and Osborn, M., *J Biol Chem*, 1969. **244**(16): p. 4406-12.
218. Çetin, M., et al., *F J Pharm Sci*, 2007. **32**(3): p. 103-107.
219. Husband, F.A., et al., *J Agric Food Chem*, 2001. **49**(2): p. 859-66.
220. Hu, X., Cui, S., and Liu, J., *Spectrochim Acta A Mol Biomol Spectrosc*, 2010. **77**(2): p. 548-53.
221. Price, N.C., *Biotechnol Appl Biochem*, 2000. **31 (Pt 1)**: p. 29-40.
222. Lakowicz, J.R., *Protein Fluorescence*, in *Principles of Fluorescence Spectroscopy*, 2006, New York : Springer.
223. Harvey, A.J., et al., *Pharm Res*, 2011. **28**(1): p. 107-16.
224. Aitken, A. and Learmonth, M.P., *Protein Determination by UV Absorption*, in *The Protein Protocols Handbook*, 2002, New Jersey : Humana Press Inc
225. Mangalathillam, S., et al., *Nanoscale*, 2011.
226. Maupas, C., et al., *Int J Pharm*, 2011. **411**(1-2): p. 136-41.
227. Goncharuk, V., Nezheradze, K., and Datskevich, E., *J Water Chem Technol*, 2010. **32**(1): p. 50-55.
228. Koneti, K.K. and Jones, M., *Surgery*, 2013. **31**(2): p. 77-83.
229. Anonymous, *Anesthesiology*, 2010. **112**(4): p. 810-33.
230. Reimer-Kent, J., *Nurs BC*, 2004. **36**(4): p. 20-4.
231. http://www.painmed.org/patient/facts.html#chronic. Accessed 29 April, 2013.
232. Breivik, H., et al., *Eur J Pain*, 2006. **10**(4): p. 287-333.
233. http://www.prweb.com/pdfdownload/8052240.pdf. Accessed 29 April, 2013.
234. Evans, S.R., et al., *AIDS*, 2011. **25**(7): p. 919-28.
235. Herberger, K., et al., *J Dermatol Treat*, 2012. **23**(6): p. 437-442.
236. Mick, G. and Correa-Illanes, G., *Curr Med Res Opin*, 2012. **28**(6): p. 937-51.
237. Meier, T., et al., *Pain*, 2003. **106**(1-2): p. 151-8.
238. Galer, B.S., et al., *Pain*, 1999. **80**(3): p. 533-8.
239. http://www.emla.com.au/. Accessed 29 April, 2013.
240. Comer, A.M. and Lamb, H.M., *Drugs*, 2000. **59**(2): p. 245-9; discussion 250-1.
241. Rowbotham, M.C., et al., *Pain*, 1996. **65**(1): p. 39-44.
242. Fleming, J.A. and O'Connor, B.D., *Pain Res Manag*, 2009. **14**(5): p. 381-388.
243. Wermeling, D.P., et al., *Proc Natl Acad Sci U S A*, 2008. **105**(6): p. 2058-63.
244. Gupta, J., et al., *Clin J Pain*, 2012. **28**(2): p. 129-135.
245. Gupta, J., Felner, E.I., and Prausnitz, M.R., *Diabetes Technol Therap*, 2011. **13**(4): p. 451-456.
246. Zhang, Y., et al., *Pharm Res*, 2012. **29**(1): p. 170-7.
247. Ito, Y., et al., *Chem Pharm Bull*, 2013. **61**(1): p. 8-15.
248. Cui, Y. and Frank, S.G., *J Pharm Sci*, 2006. **95**(3): p. 701-13.
249. Kaihara, S., Matsumura, S., and Fisher, J.P., *Eur J Pharm Biopharm*, 2008. **68**(1): p. 67-73.
250. Baker, S. Pharmaceutical and Medical Packaging News, 2011.
251. Kochhar, J.S., et al., *Int J Nanomedicine*, 2012. **7**: p. 3143-54.
252. Park, J.H., et al., *IEEE Trans Biomed Eng*, 2007. **54**(5): p. 903-13.

253. Zhang, Y., Lin, C.T., and Yang, S., *Small*, 2010. **6**(6): p. 768-75.
254. Arora, A., Prausnitz, M.R., and Mitragotri, S., *Int J Pharm*, 2008. **364**(2): p. 227-36.
255. Walsh, A.J., et al., *Lasers Surg Med*, 2012. **44**(9): p. 712-8.
256. Zipfel, W.R., et al., *Proc Natl Acad Sci U S A*, 2003. **100**(12): p. 7075-80.
257. Schonenbrucher, H., et al., *J Agric Food Chem*, 2008. **56**(15): p. 6220-6.
258. Gittard, S.D., et al., *Expert Opin Drug Deliv*, 2010. **7**(4): p. 513-33.
259. Choi, C.K., et al., *Small*, 2012. **8**(16): p. 2483-8.
260. Friedman, G.B., and Sandhu, H.S., *Am J Phys*, 1967. **35**(7): p. 628-&.
261. Xu, Q.A., Li, J., and Zhang, W., *Semiconductor Lasers and Applications* , 2010. **7844**.
262. Lin, T.W., et al., *J Micromech Microeng*, 2008. **18**(9).
263. Dunne, S.M. and Millar, B.J., *Prim Dent Care*, 2008. **15**(4): p. 147-52.
264. Park, J.H. and Prausnitz, M.R., *J Korean Phys Soc*, 2010. **56**(4): p. 1223-1227.
265. Pilcher, B.K., et al., *Arch Dermatol Res*, 1998. **290 Suppl**: p. S37-46.
266. Varani, J., et al., *Am J Pathol*, 2006. **168**(6): p. 1861-1868.
267. Anonymous, *Health News*, 2006. **12**(1): p. 14-5.
268. Yamaguchi, K., et al., *J Pharm Sci*, 2008. **97**(10): p. 4391-403.
269. Marinkovich, M.P., et al., 2012, WIPO Patent WO/2012/149136
270. Bartosova, L. and Bajgar, J., *Curr Med Chem*, 2012. **19**(27): p. 4671-4677.
271. Windheuser, J.J., et al., *J Pharm Sci*, 1982. **71**(11): p. 1211-3.
272. Bellantone, N.H., et al., *Int J Pharm*, 1986. **30**(1): p. 63-72.
273. Tojo, K., Chiang, C.C., and Chien, Y.W., *J Pharm Sci*, 1987. **76**(2): p. 123-6.
274. Bronaugh, R.L. and Stewart, R.F., *J Pharm Sci*, 1985. **74**(1): p. 64-7.
275. Selzer, D., et al., *Adv Drug Deliv Rev*, 2013. **65**(2): p. 278-94.
276. Sanghvi, P.P. and Collins, C.C., *Drug Dev Ind Pharm*, 1993. **19**(13): p. 1573-1585.
277. Akazawa, M., et al., *Int J Pharm*, 1989. **50**(1): p. 53-60.
278. http://www.hansonresearch.com/. Accessed 26 June, 2012
279. Martin, B., et al., *Int J Pharm*, 1989. **49**(1): p. 63-68.
280. http://www.permegear.com/ilc14.htm. Accessed 26 June, 2012.
281. Córdoba-Díaz, M., et al., *J Control Release*, 2000. **69**(3): p. 357-367.
282. Ng, S.F., et al., *AAPS PharmSciTech*, 2010. **11**(3): p. 1432-41.
283. Rapedius, M. and Blanchard, J., *Pharm Res*, 2001. **18**(10): p. 1440-1447.
284. Kang, L., et al., *Drug Discov Today*, 2008. **13**(1-2): p. 1-13.
285. Mak, V.H.W., and Francoeur, M., 1996, *US Patent* 5490415.
286. Shockley Jr, H. and Wilkinson, W., *US Patent* 5641458.
287. Tanojo, H., et al., *J Control Release*, 1997. **45**(1): p. 41-47.
288. Moody, R.P., *Toxicol in Vitro*, 2000. **14**(5): p. 467-474.
289. Brand, R.M., et al., *Toxicol Ind Health*, 2003. **19**(1): p. 9-16.
290. Bronaugh, R.L., *Diffusion Cell Design* in *Topical drug bioavailability, bioequivalence and penetration*, 1993, New York : Plenum Press.

291. http://www.cosmeticseurope.eu/publications-cosmetics-europe-association/guidelines.html?view=item&id=26.Accessed 2 April, 2012.
292. Li, N., Schwartz, M., and Ionescu-Zanetti, C., *J Biomol Screen*, 2009. **14**(2): p. 194-202.
293. Wong, I. and Ho, C.M., *Microfluid Nanofluidics*, 2009. **7**(3): p. 291-306.
294. Ahmad, A., et al., *Breast Cancer Res Treat*, 2010. **122**(2): p. 579-84.
295. Lee, O., et al., *Breast Cancer: Targets and Therapy*, 2011. **3**: p. 61-70.
296. Zhao, K. and Singh, J., *J Pharm Sci*, 2000. **89**(6): p. 771-780.
297. Brain, K.R. and Walters, K.A., *Molecular modeling of skin permeation enhancement by chemical agents* in *Pharmaceutical Skin Penetration Enhancement*, 1993, New York : Marcel Dekker.
298. Krishnaiah, Y.S.R., Satyanarayana, V., and Bhaskar, P., *Pharmazie*, 2002. **57**(12): p. 842-847.
299. Moghimi, H.R., Williams, A.C., and Barry, B.W., *Int J Pharm*, 1997. **146**(1): p. 41-54.
300. Barry, B.W., *J Control Release*, 1991. **15**(3): p. 237-248.
301. Panchagnula, R., et al., *Int J Pharm*, 2001. **219**(1–2): p. 95-105.
302. Aungst, B.J., Rogers, N.J., and Shefter, E., *Int J Pharm*, 1986. **33**(1–3): p. 225-234.
303. Godin, B. and Touitou, E., *Adv Drug Deliv Rev*, 2007. **59**(11): p. 1152-61.
304. Ito, Y., et al., *Chem Pharm Bull*, 2010. **58**(4): p. 458-63.
305. Han, M., et al., *JMicromech Microeng*, 2007. **17**(6): p. 1184-1191.
306. You, S.K., et al., *J Drug Target*, 2010. **18**(1): p. 15-20.

Appendix 1 Major methods of polymeric microneedle fabrication.

Polymer/s or sugar used	**Technique**	**Shape**	**Length (μm)**	**Base diameter (μm)**	**Tip diameter (μm)**	**Center-to-center spacing (μm)**	**Needles on an array**	**Array size**	**References**	**Comments**
Polylactic/ polyglycolic acid	MEMS masking/ etching	Chisel tip, Beveled tip, Tapered cone	570-1500	100-200	10-20	400-1400	120-225	9x9 mm	Park et al. [122]	Lens geometry and refractive index can be changed to control geometry. Complex etching procedures to create master structures. Heating used to melt polymer may not be ideal for drug encapsulation.
Polymethyl methacrylate (PMMA) Polyvinyl alcohol (PVA)	Deep X-ray lithography	Tapered with long shafts	600-1000	190-400	70-100	-	25-60	5-6 mm^2	Moon et al. [123] and Perennes et al. [124]	Complicated multistep x-ray exposure of polymer, creation of master structures of PVA by pouring PVA solution over PMMA coated with metal.

Polymer/s or sugar used	**Technique**	**Shape**	**Length (µm)**	**Base diameter (µm)**	**Tip diameter (µm)**	**Center-to-center spacing (µm)**	**Needles on an array**	**Array size**	**References**	**Comments**
Polylactic acid	Excimer laser	Straight, with jagged sides	1000	230	-	-	-	-	Aoyagi et al. [125]	Laser cutting and heating to high temperatures is required.
Carboxymethylcellulose (CMC), amylopectin, bovine serum albumin	PDMS molding	Conical, Pyramidal	600-800	300	25	-	-	-	Lee et al. [92]	Creation of master structures using toxic SU-8 photoresist. Matrix preparation at high temperatures may not be suitable for thermolabile drugs.
Polyvinyl pyrrolidone	PDMS molding, UV lithography	Conical	650	300	5	-	100	-	Sullivan et al. [116]	Longer exposure to UV light. Similar approach in [192]

Polymer/s or sugar used	**Technique**	**Shape**	**Length (µm)**	**Base diameter (µm)**	**Tip diameter (µm)**	**Center-to-center spacing (µm)**	**Needles on an array**	**Array size**	**References**	**Comments**
Dextrin, Chondroitin sulphate	Dipping method	Conical	-	-	-	-	Single needles	-	Ito et al. [126]	Individual needles restrict drug loading capacity. Similar approach in [119, 130]
Maltose	Metal mold casting	Tetrahedron	150-2000	-	> 5	350 µm for 500 µm needles	28	-	Miyano et al. [128]	Metal molds need to be prepared by etching. Heating of maltose to 140 ° C to melt and pour in mold.
Chondroitin sulphate	Mold casting	Conical	500	300	-	-	100	1 cm^2	Ito et al. [304]	Separate preparation of molds required
Polyetherimide, polycarbonate	Inclined lithography, electroforming, PDMS molding	Square pillar or Microneedle rollers, with square pillars	500-1500	-	2	500-200	17	-	Han et al. [305] You et al. [306]	Complex multistep procedure of inclined UV lithography of SU-8 to create Nickel master structures followed by PDMS molding. Related method used in [131]